ASPECTS OF TRANSITION METAL INTERACTION WITH BACTERIA: IMAGING OF EXTRACELLULAR pH IN BIOFILMS, Hg BINDING TO CURLI, AND DIFFERENTIAL GENE EXPRESSION IN RESPONSE TO Hg

by Gabriela Hidalgo Casanueva

ASPECTS OF TRANSITION METAL INTERACTION WITH BACTERIA: IMAGING OF EXTRACELLULAR pH IN BIOFILMS, Hg BINDING TO CURLI, AND DIFFERENTIAL GENE EXPRESSION IN RESPONSE TO Hg

A Dissertation

Presented to the Faculty of the Graduate School

of Cornell University

In Partial Fulfillment of the Requirements for the Degree of

Doctor of Philosophy

by

Gabriela Hidalgo Casanueva

August 2010

ASPECTS OF TRANSITION METAL INTERACTION WITH BACTERIA: IMAGING OF EXTRACELLULAR pH IN BIOFILMS, Hg BINDING TO CURLI, AND DIFFERENTIAL GENE EXPRESSION IN RESPONSE TO Hg

Gabriela Hidalgo Casanueva, Ph. D.

Cornell University 2010

The fate and transport of transition metals is of great interest because of metal toxicity and bioavailability. The growth of all organisms is dependent on the acquisition of essential metals. However, at higher concentrations heavy metals can inhibit the normal functioning of cells. Overall physiological effects of metals on biological systems are determined by metal speciation, not by their total concentration. Environmental fate and speciation of metals are influenced by interdependent biogeochemical variables such as pH, adsorption, complexation and biological interactions.

Biofilms can generate three-dimensional physicochemical gradients that create microenvironments where local conditions are substantially different from those in the surrounding medium. The use of functional tomographic imaging microscopy of ratiometric core-shell silica nanoparticle sensors was shown to be an effective tool to study the spatial and temporal evolution of pH microenvironments in *Escherichia coli* PHL628 and mixed-culture wastewater biofilms.

Curli are amyloid extracellular fibers expressed by *E. coli* and other bacterial species. The role of curli in the tolerance of *E. coli* PHL628 to Hg(II) was examined. Curli-

producing strains proved to be more resistant than a curli-deficient mutant to Hg(II). Higher fluorescence was measured in a curli-deficient mutant than in the wild type following an addition of Hg(II) to cells harboring the *merR-gfp* reporter. Measurement of Hg(II) adsorption kinetics revealed that curli increases the rate and extent of Hg(II) adsorption. These findings indicate that curli sorb Hg(II) and reduce the amount of Hg(II) that reaches the cytoplasm.

Microarray analysis of *E. coli* MG1655 cells grown in Hg(II) revealed upregulation of genes for arginine biosynthesis and transport. Increased resistance of *E. coli* to Hg(II) was not observed when the medium was supplemented with arginine. Induction of transcription of an arginine transport gene, *artJ*, by Hg(II) was confirmed with an *artJ-lux* reporter and exposure of this bioreporter to Zn(II) and Cd(II) revealed that these metals also induce the transcription of *artJ*. Furthermore, a *merR-gfp* bioreporter showed that arginine supplementation did not alter Hg uptake. These results indicate that group 12(IB) elements may act to induce the transport of arginine, but that arginine availability is not a strategy for alleviating their toxicity.

BIOGRAPHICAL SKETCH

Gabriela Hidalgo was born in La Habana, Cuba in July of 1976 to a Mexican mother and a Costa Rican father. When she was less than two years old her family left Cuba and although she has no recollection of this communist past, American Immigration Officers remind her of it every time they get a chance. She was raised in Costa Rica with her siblings Julia and Emiliano and the dogs Cariari, Gypsy and Piranha. As a child Gabriela was interested in science and literature. The striking tropical landscape combined with the poverty of the region and one too many episodes of The Blue Planet led to her to develop a great interest in environmental issues from a young age. After finishing high school she enrolled as a chemical engineering major at the University of Costa Rica but after a three-month-long backpacking trip through Europe she decided to move to Monterrey, Mexico, where she restarted her academic career at the Monterrey Institute of Technology. She was awarded a B.S. degree in Chemical and Environmental Engineering in December of 2001. During those formative years she developed a passion for soccer, eating tacos and her future husband, Jose Moran-Mirabal. In 2002 Gabriela, now a married woman, moved to the beautiful town of Ithaca, NY, where her lovely daughter, Camila, was born in November of that year. She started her PhD in Environmental Engineering in 2003 under the direction of Prof. Leonard Lion and has investigated varied topics such as bacterial heavy metal resistance, imagining of pH gradients in bacterial biofilms, and transcriptomic response to a Hg stress in *Escherichia coli*. After obtaining her degree she will relocate to Montreal, Canada and work as a postdoctoral researcher at McGill University under Prof. Nathalie Tufenkji. Although she is excited about this new enterprise she does not quite understand why she keeps moving to increasingly colder places.

Para José y Camila

ACKNOWLEDGMENTS

First and foremost I want to acknowledge Prof. Len Lion. He has been my mentor and my friend during these trying years and without his focus, support and trust I could not have achieved this. I am also tremendously indebted to Prof. Anthony Hay. In addition to being a remarkable scientist he has shown me that it is effectively possible to live a balanced life and be successful in its different aspects. He always welcomed me in his lab and was extremely generous with his time, knowledge and resources. A very important Thank You goes to my other committee member Prof. Michael Shuler and to all the other people that at one point or another have given me their expert advice, Prof. Bill Ghiorse, Prof. Paul Houston, Prof. Hector Abruña, Prof. Jim Gossett and Prof. Jim Bisogni. I feel privileged to have worked with Prof. Ulrich Wiesner, Andrew Burns and Erik Herz; collaborating with them was an enriching and fruitful enterprise. I am also grateful to all the people at Hollister Hall: Chris Day, Cameron Wilkens, Maureen Letter, Nadine Porter and the rest of the faculty and staff. I would also like to put Hay lab members in a special category, Daniela, Bryan, Andreas, Mitch, Giomar, Kevin, Jennie and the rest of the gang, thank you, thank you, thank you. A special thank you also goes to Dr. Chen with whom it was a pleasure to collaborate. Finally, I would like to thank my fellow CEEs, Annie, Chloe, Wan, Gretchen, Iman, Deborah, Matt, Cresten, Po-Hsun and everyone else that I have met there through the years.

To all my dear friends that have made of Ithaca my home, thank you. Chloe, Annie, Ben and Gretchen, Daniela, my dear friend Jesse and his wonderful family, Luz, Martin and the girls, the Getzins, I cannot put in words how privileged I feel to be your friend. I would also like to thank my family for being how a family should be:

dysfunctional and unconditional. I love you. I also want to thank my adopted sister Carolina, you friendship keeps making me a better person.

Finally, to the people that have accompanied me during this wild journey, Jose and Camila, thank you. It is hard to express how I feel about you. Thank you again to those that I have mentioned and those that I may have forgotten.

TABLE OF CONTENTS

LIST OF FIGURES

Appendix 1

Appendix 2

LIST OF TABLES

Chapter 3

Chapter 4

CHAPTER 1

INTRODUCTION

It is a well documented phenomenon that the bioavailability and toxicity of heavy metals is determined by the chemical species of the metal that is present and not by its total concentration (2, 5). The environmental fate and speciation of metals are influenced by interdependent biogeochemical variables such as pH, adsorption, complexation, redox potential and biological interactions (2, 3). The general goal of my work has been to provide some insight into the interactions between toxic metal speciation, gene regulation in bacteria and the chemical characteristics of the aqueous phase they inhabit. This dissertation describes the specific efforts conducted towards visualizing the development of pH gradients in bacterial biofilms, adsorption of Hg(II) by bacterial curli and the relationship between the presence of Hg(II) in solution and differential regulation of gene expression.

It has been demonstrated that the vast majority (99%) of bacteria in natural habitats aggregate as biofilms (1, 4). These are attached microbial communities that are entrapped in a self-produced matrix of extracellular polymeric substances, and whose abundance impacts our society in both detrimental and beneficial ways. One of the main characteristics of biofilms is that they can generate three-dimensional physicochemical gradients that can create microenvironments where local conditions are substantially different from those just a few micrometers away. Therefore, the development of better tools for the quantitative understanding of biofilms and the gradients they create becomes essential.

Chapter two of this dissertation details research conducted with the purpose of studying the morphology and temporal evolution of pH microenvironments in *Escherichia coli* PHL628 and mixed-culture wastewater biofilms. pH is considered to be a master variable controlling trace metal speciation. For this research a novel methodology was developed that uses three-dimensional imaging, via confocal fluorescence microscopy of ratiometric core-shell silica nanoparticle sensors. This study demonstrated that the combination of 3D functional fluorescence imaging with pH sensors provides a powerful tool for *in situ* characterization of chemical microenvironments in complex biofilms.

Bacteria may cope with heavy metal stress by actively exporting metal cations from the cytoplasm. There are several types of export mechanisms currently known to carry on this efflux; however, other less understood mechanisms of metal tolerance are likely to exist. In the third chapter of this dissertation I describe the research conducted to demonstrate that curli, amyloid extracellular fibers produced by *E. coli* and other bacterial species, temporarily reduce the concentration of Hg(II) that reaches the cytoplasm and, as a result, provide protection to the cell from Hg(II) stress. In addition the upregulation of curli biosynthesis genes in the presence of Hg was evaluated as a part of this project.

In the fourth thesis chapter I present research that was conducted with the objective of enhancing our understanding of bacterial response to Hg(II) stress. For this work, *E. coli* cultures were grown in a defined glucose minimal medium with and without Hg(II) and RNA from the cell suspensions was extracted. Microarray analysis revealed that transcription of arginine biosynthesis and transport genes were induced in the presence of Hg(II). Supplementation of the medium with arginine did not

demonstrate increased resistance to Hg(II) toxicity. Upregulation of *artJ*, a gene that encodes a periplasmic arginine importer, was confirmed with an *artJ-lux* reporter. Furthermore, an increase in the specific luminescence signal was observed upon exposure of the reporter to Zn(II) and Cd(II). A mer-gfp bioreporter for intracellular Hg(II) showed that arginine supplementation did not alter Hg(II) uptake. The main conclusion of this work is that group 12(IB) elements may act to induce the transport of arginine, but arginine availability does not alleviate their toxic effects.

The fifth and final chapter of this dissertation includes general conclusions from each of the above research projects. It also contains recommendations for future research. Additionally there are two appendices located at the end of the dissertation. The first appendix includes preliminary research conducted to elucidate how cysteine alters Hg(II) toxicity to and uptake by *E. coli* bacteria. The second appendix contains the supplementary information for chapter 2.

REFERENCES

1. **Costerton, J. W., Z. Lewandowski, D. E. Caldwell, D. R. Korber, and H. M. Lappin-Scott.** 1995. Microbial biofilms. Annu Rev Microbiol **49:**711-45.
2. **Farrell, R. E., J. J. Germida, and P. M. Huang.** 1993. Effects of chemical speciation in growth media on the toxicity of mercury(II). Appl Environ Microbiol **59:**1507-14.
3. **Nelson, Y. N., and L. W. Lion.** 2003. Formation of Biogenic Manganese Oxides and Their Influence on the Scavenging of Trace Metals *In* M. H. Selim and W. L. Kingery (ed.), Geochemical and Hydrological Reactivity of Heavy Metals in Soils Lewis Publishers, Boca Raton, Florida.
4. **Potera, C.** 1996. Biofilms invade microbiology. Science **273:**1795-7.
5. **Rensing, C., and R. M. Maier.** 2003. Issues underlying use of biosensors to measure metal bioavailability. Ecotoxicology and Environmental Safety **56:**140-147.

CHAPTER 2

FUNCTIONAL TOMOGRAPHIC FLUORESCENCE IMAGING OF pH MICROENVIRONMENTS IN MICROBIAL BIOFILMS WITH SILICA NANOPARTICLE SENSORS[1]

Abstract

Attached bacterial communities can generate three-dimensional (3D) physicochemical gradients that create microenvironments where local conditions are substantially different from those in the surrounding solution. Given their ubiquity in nature and their impacts on issues ranging from water quality to human health, better tools for understanding biofilms and the gradients they create are needed. Here we demonstrate the use of functional tomographic imaging via confocal fluorescence microscopy of ratiometric core-shell silica nanoparticle sensors (C dot sensors) to study the morphology and temporal evolution of pH microenvironments in axenic *Escherichia coli* PHL628 and mixed-culture wastewater biofilms. Testing of 70-, 30-, and 10-nm-diameter sensor particles reveals a critical size for homogeneous biofilm staining, with only the 10-nm-diameter particles capable of successfully generating high-resolution maps of biofilm pH and distinct local heterogeneities. Our measurements revealed pH values that ranged from 5 to >7, confirming the heterogeneity of the pH profiles within these biofilms. pH was also analyzed following glucose addition to both suspended and attached cultures. In both cases, the pH became more acidic, likely due to glucose metabolism causing the release of tricarboxylic acid cycle acids and CO_2.

[1] The contents of this chapter were published in *Applied and Environmental Microbiology* with coauthors Andrew Burns, Erik Herz, Anthony G. Hay, Paul L. Houston, Ulrich Wiesner and Leonard W. Lion. This material is reproduced with permission from *Applied and Environmental Microbiology*.

These studies demonstrate that the combination of 3D functional fluorescence imaging with well-designed nanoparticle sensors provides a powerful tool for in situ characterization of chemical microenvironments in complex biofilms.

Introduction

Biofilms are collections of surface-attached microbes entrapped in a self-produced matrix of extracellular polymeric substances anchored to a surface (17). Their growth is characterized by complex three-dimensional structures including channels, voids, towers and mushroom-like protrusions (9). They are common both in biological systems as well as in near-surface fluid rock systems and may occupy a significant portion of the surface area exposed to fluids in many natural environments including fresh and saline surface waters, ground waters, deep-sea hydrothermal systems and deep sedimentary basins (41, 51). The ubiquity of biofilms has a variety of important implications for modern society. Industrially, biofilms are used in a wide array of engineered systems including treatment of wastewater and hazardous waste, contaminated soils and oil spills (43). Conversely, biofilms can also contaminate water distribution systems, foul the hulls of ships and promote corrosion (30). Medically, biofilms have been implicated in infections in lungs and chronic wounds as well as in catheters and implants, in cystic fibrosis, tuberculosis, and in dental caries and periodontal diseases (12, 17).

One prominent characteristic of biofilms is the development of three-dimensional chemical gradients, from the diffusion of nutrients, metabolic products, and signaling molecules throughout the film. These gradients create microenvironments in which the local physicochemical properties may differ substantially from those in the

surrounding solution (48). This gradation of conditions allows, for example, anaerobic bacteria to flourish within biofilms that are growing in an otherwise aerobic environment (23, 36). Another example of the effects of biofilm-generated chemical gradients is dental caries. Following sugar consumption, the pH within a dental plaque biofilm drops dramatically (<5.5) while the pH of the overlying saliva remains near neutral. This acidification leads to demineralization of the tooth enamel and ultimately caries (33, 34).

Several techniques have been applied to analyzing pH gradients in biofilms, each with its own benefits and limitations. Most recently, Beveridge and Hunter (22) used seminaphtorhodafluor-4F 5-(and -6) carboxylic acid (C-SNARF-4), a ratiometric fluorescent dye to measure pH microenvironments in *Pseudomonas aeruginosa* biofilms and observed pH values that ranged from 5.6 to 7.0. This method minimizes perturbations to the biofilm and its spatial resolution is limited only by that of the microscope in use. Unfortunately, free sensor dyes have been demonstrated to interact with biofilm components, potentially altering their sensitivities and perturbing the resulting images (22). Further, the penetration of any molecular or nanometer-sized probe into the biofilm can be limited by the decreased diffusion rates within the dense microcolony environment (55). Finally, like all free dye molecules, brightness and photostability are limited, and photoexcitation can cause cellular toxicity (4). Microelectrode-based techniques have also been used on a large variety of biological systems (27, 42, 49) but the spatial resolution of microelectrode-based techniques is limited by the tip size and the insertion of the microelectrode into the biofilm inherently perturbs the local surroundings. Each data point obtained with a microsensor is a single measurement integrated over a spatial volume covering approximately twice the tip diameter (14), which limits the ultimate spatial resolution

of the sensors. In addition, a systematic study of a common microelectrode system revealed highly variable accuracy and precision between different electrodes (29).

Finally, fluorescence lifetime imaging (FLIM) can be used to measure chemical concentration through the use of appropriate dye molecules. By imaging a sample with a pulsed laser and analyzing the decay rate of the dyes in the sample as they fluoresce, Vroom et al (55) were able to measure pH in a mixed culture of oral bacteria. One hour after the biofilms were exposed to 14 mM sucrose, pH was measured throughout the biofilm and values ranged from 7.0 to 5.5 were observed. This technique provides great definition and tissue penetration; however, the equipment needed to perform FLIM includes fast detectors and electronics capable of differentiating nanosecond emissions in addition to a pulsed laser excitation source and are not universally available. Detailed reviews on this method may be found elsewhere (2, 6).

We implemented three-dimensional (tomographic) fluorescence imaging with ratiometric silica nanoparticle sensors to study the morphology and temporal evolution of pH microenvironments in *Escherichia coli* PHL628 and mixed-culture wastewater biofilms. Because of the diversity of structure and environments, functional tomographic imaging is of particular interest for investigating biofilms in their native state. Tomographic imaging techniques, such as optical coherence tomography (58), soft X-ray microscopy (25) and confocal fluorescence microscopy (38) enable high resolution structural reconstructions with minimal perturbation to the biofilm. We have chosen the spatial variation of pH within microbial biofilms to test tomographic imaging via confocal fluorescence microscopy as it is an exciting area of research relevant to both the industrial and clinical impacts of biofilms. From a clinical standpoint, non-uniform pH profiles in biofilm infections are important because the

degree of physiological heterogeneity, marked by the establishment of nutrient, dissolved gas and pH gradients, increases with time and is positively correlated with the development of drug resistance (15). Furthermore, it has been well established that the susceptibilities of bacterial cells towards antibiotics and biocides are profoundly affected, among other factors, by their pH (15). The recent emergence of antibiotic-resistant pathogenic bacteria makes this a topic of great interest (11, 15, 17).

We employed ratiometric core-shell silica nanoparticle sensors, referred to as C Dot sensors (5), in order to overcome the limitations of free ratiometric sensor dyes. As shown schematically in Figure 1a, incorporating green-emitting, pH-sensitive dye molecules (Fluorescein) in a thin silica shell surrounding a core rich in red-emitting, pH-insensitive dye molecules (Cy5) (5), permits ratiometric quantification of the local pH by comparison of sensor and reference dye emission intensities (Figure 1b). This internally-standardized design allows the analyte concentration to be measured independent of changes in the sensor concentration, unlike single-color sensor imaging which can only give a qualitative description of the local environment (8, 16, 26). Further, the covalent incorporation of dyes into a core-shell silica matrix significantly enhances both dye brightness and photostability through increases in the radiative and decreases in the non-radiative fluorescence rates (31). Finally, silica is a highly biocompatible and easily functionalized material for diverse biological applications (4, 19, 7). As is demonstrated below, however, only if the C dot sensors are kept below a critical particle size is homogeneous biofilm staining possible. This discovery enabled, to the best of our knowledge, the first functional volumetric imaging of pH in prokaryotic systems using ratiometric nanoparticle sensors.

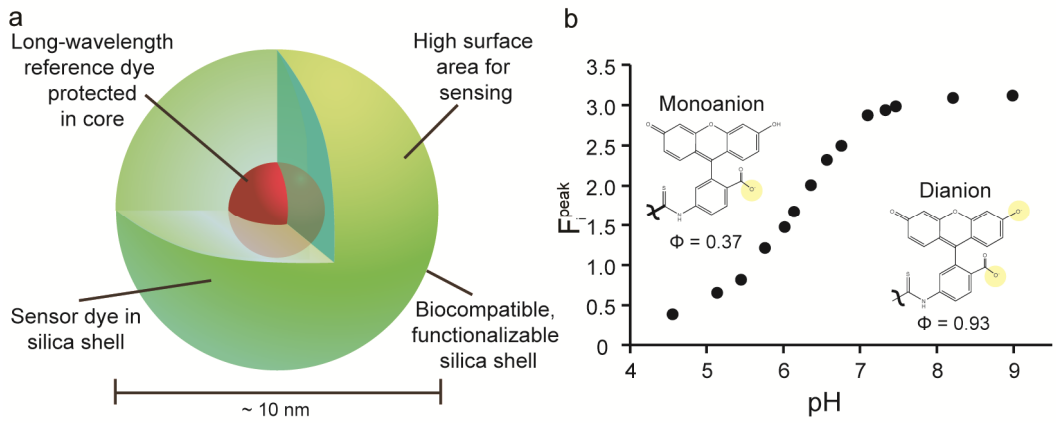

Figure 1. Sensor schematic and calibration. (a) Schematic diagram showing the core/shell architecture of a C dot sensor that highlights the reference dye (Cy5) sequestered in the core and coated by a sensor dye shell (fluorescein). (b) Peak fluorescein emission collected for solutions of known pH value from 4.5 to 9.0. The figure also shows the molecular structure of the dye in its di-anionic charge state where it exhibits a quantum yield of approximately 93% and in its monoanionic state where its quantum yield is of approximately 37%.

Materials and Methods

C Dot Sensors

C dot sensors with 70, 30 and 10 nm diameters were grown via modified Stöber silica nanoparticle syntheses (31, 50). Amination was performed using 3-aminopropyl triethoxysilane (APTS) as a surface-silanizing agent. The 10 nm diameter bare silica particles, which were ultimately used for all of the functional three-dimensional reconstructions shown here, consist of a particle core covalently incorporating Cy5 as an environmentally insensitive reference dye via coupling to a reactive silane, surrounded by a shell covalently incorporating fluorescein dye (FITC) through coupling to a reactive silane. FITC was chosen for its pKa of 6.4, which is within the range of interest for this biological system. At high pH (9 and above), FITC exists in the dianionic charge state and exhibits a quantum yield of approximately 93%, while at low pH (4.5 and below) the dye is protonated to the monoanion state with a quantum yield of approximately 37% (Figure 1b) (18). Cy5 has a quantum yield that is constant within this pH range making it an ideal internal standard. Additional information on the synthesis and characteristics of these particles may be found elsewhere (4, 5, 31). All supplementary information and figures referred to in this chapter are included in the Appendix 2.

Culture and media

E. coli PHL628, an adherent K-12 MG1655 derivative was used as the test bacterium for the pure-culture experiments. This strain has a mutation in the *ompR* gene that results in an overproduction of curli; thin fibrillar pili at the surface of the cells that allow the bacteria to adhere and form sessile communities (54). The cultures were grown in a solution of 1 part Luria-Bertani (LB) medium (which contained, per liter,

10 g NaCl, 10 g tryptone and 5 g yeast extract) and 2 parts water and which was sterilized by autoclaving at 121ºC before use. All experiments performed with *E. coli* PHL628 were supplemented with kanamycin (50 mg/L). Suspended cultures were grown at 37ºC with rotary shaking at 150 rpm. Attached cultures were grown in 35 mm Petri dishes with an untreated 14 mm Microwell No. 1.5 coverglass at the bottom surface (MatTek, Ashland, MA). After inoculation, the cells were kept at 30ºC with rotary shaking at 30 rpm. Every 48 hours the media was discarded and fresh media was added. Biofilms were grown for a period of 7 to 8 days. Approximately 9 hours prior to imaging, the C dot sensors were added (to a concentration of 50 nM) and the cultures were continuously stirred for 4 hours. 5 hours prior to imaging the biofilms were washed twice to remove unbound dots and fresh media was added.

The mixed-culture seed (potentially containing archaea and eukaryotic microorganisms *e.g.* fungi and protozoans, in addition to bacteria) (24) came from a municipal wastewater treatment facility in Ithaca, NY. Biofilms and suspended cultures of the mixed cultures were grown following the same protocols described above.

Growth curves

To investigate the biocompatibility and potential toxicity of the core-shell silica nanoparticles, 10 nm diameter sensor particles and dye-free nanoparticles of the same size were added to diluted LB medium at varying concentrations representative of biofilm growth conditions (18-50 nM). The solutions were then inoculated at 1% volume with either *E. coli* PHL628 cultures or mixed wastewater cultures. 200 μL aliquots of the cultures were placed in sterile, clear 96-well plates and optical density (OD) at 600 nm was recorded until stationary phase was reached. OD was measured

using a Biotek multi-detection microplate reader equipped with Synergy HT and KC4 software. The microplate reader maintained the cultures at 37ºC with shaking prior to each measurement, which were performed at 20 minute intervals. Each condition was analyzed in triplicate. Sterile controls both with and without particles were also analyzed. Reported ODs correspond to the absorbance measured from the bottom of each well through approximately 3 mm of medium; therefore, OD numbers are not comparable to standard OD measurements with 1 cm path-length cuvettes.

pH analysis in suspended cultures

A calibration curve for C dot sensors was generated by mixing the dots with a series of pH-adjusted phosphate buffered saline solutions (pH 4.0 to pH 8.0) and measuring sensor (green) and reference (red) emission spectra upon excitation at 488 and 633 nm, respectively, on a PTI spectrofluorometer (Supp. Fig. 3a-b, respectively). For each measurement, the peak intensity ratio ($F_i = I_{FITC} / I_{Cy5,}$ Supp. Fig. 3c) was plotted versus pH and analyzed by a modified Henderson-Hasselbalch equation (Eq. 1) where F_{min} and F_{max} are the extreme values of F_i at low and high pH, respectively, to determine the pK_a and generate a calibration curve (Supp. Fig. 3d).

$$pH = pK_a + \log\left(\frac{F_i - F_{min}}{F_{max} - F_i}\right) \qquad \text{Eq. 1}$$

100 mL of overnight cultures of *E. coli* PHL628 grown in 1/3 LB were spiked with a concentrated glucose solution to achieve final concentrations of 90 mM glucose or an equal volume of distilled water (control). For the following 12 hours, 700 µL aliquots were retrieved from the spiked flask as well as the 0 mM glucose control and placed in cuvettes where the suspensions were mixed with C dots to a concentration of 180 nM. Fluorescence in the green and red channel was recorded at the excitation and emission

wavelengths described above. pH was simultaneously recorded with a UP-10 Denver Instrument pH meter. The experiment was simultaneously performed with the mixed wastewater culture. Next, the relationship obtained from the calibration curve (r^2= 0.99) was used to calculate the pH of the cell suspensions.

Imaging

All biofilm images were collected using a Leica TCS-SP2 Confocal Laser Scanning Microscope (CLSM) equipped with Argon ion and Helium-Neon lasers. A 40x 0.8 NA water immersion objective was used for all imaging. 512 x 512 pixel TIF images were collected at 12-bit color depth in xy mode. Image stacks were generated by sequential imagining in 1 μm steps through the biofilm.

To determine the spatial distribution of pH microenvironments within the biofilms, both *E. coli* PHL628 and mixed-culture films were grown and mixed with the sensors as described above. The samples were maintained at room temperature and under constant shaking at 30 rpm until imaging. The biofilms were concurrently imaged using transmitted light and fluorescence with excitation at 488 and 633 nm and appropriate emission filter settings. Particle-free biofilms were similarly imaged to control for background fluorescence. In order to record pH variations in biofilms following a glucose spike, an initial series of images was taken as a baseline, followed by a glucose addition that resulted in a final concentration equal to that used for the suspended cultures (90 mM). The same field was imaged every 30 minutes for the next 1.5 hours. For calibration purposes aliquots of phosphate-buffered saline solutions were mixed with particles to a final concentration of 15 μM and imaged in 96-well plates.

Image analysis

Example analysis routines are included in the supplemental information as MATLAB code. Briefly, all image files were loaded into MATLAB 7.4.0 using the *imread* command and background-corrected based on average background images taken at each image setting. For the calibrations, replicates in each channel, at each pH, were median filtered (to remove noise) and averaged prior to pixel-wise division of the green (sensor channel) by the red (reference) channel to determine F_i (I_{FITC}/I_{Cy5}). The mean and standard deviation of this ratio were calculated across each image and used as the F_i values in the modified Henderson-Hasselbalch equation (Eq. 1).

For the biofilm images, each sensor and reference channel image was pixel-wise divided to generate F_i values throughout the imaging field and the pH was calculated at each point which contained sufficient reference intensity to be considered above background. The 512x512 arrays of pH values were scaled for output as 8-bit grayscale TIFs from MATLAB in the order that they were read-in and appended with a pH scale bar. The images were then imported into Osirix DICOM image processing software (44). Originally designed for MRI, CT and PET image analysis, the software creates three-dimensional tomographs from two-dimensional image stacks in a variety of false spectrum colors and allows for manipulation of the data and export to still images (Figures 3-6).

Results

C-dot sensor distribution and toxicity

We assayed biofilms with C dot sensors of varying diameters: 70, 30 and 10 nm and both positively charged (aminated) and negatively charged (bare silica) surfaces. The amination process screened the local pH effects on the particle making sensing difficult and thus was not pursued further.

For 70 and 30 nm diameter bare silica sensors, the particles distributed sparsely and heterogeneously in the biofilms and a majority of the beads were removed during the wash steps. Furthermore, upon imaging, the biofilm did not overlay with the C dots, rather, those dots that remained agglomerated in clusters separate from the bacteria (data not shown). Only when using the smallest, 10 nm diameter bare C dots sensors were we able to reproducibly achieve high and homogeneous biofilm incorporation. The following experiments were all performed with the bare 10 nm particles.

Measurements to determine the kinetics of the integration of the particles into the matrix were not performed. The dots were assumed to be able to diffuse into the biofilm and anchor to cells or EPS in the 4 hours provided between the C dot sensor addition and the wash that eliminated unbound dots. It is reasonable to assume that an active equilibrium was reached within this period of time and that some of the particles may have been detaching and reattaching during and after the wash. However, the fact that the particles may not all have been completely immobilized was not considered an issue of concern because, as mentioned earlier, each C dot sensor has its own internal reference. This implies that each measurement is an

individual determination of the pH in the surroundings of the particle, regardless of the state of the attachment.

The growth curves presented in Figure 2a reveal that the bacterial growth is not affected by the introduction of 10 nm C dot sensor particles or dye-free silica nanoparticles of similar size. The OD reached after 18 hours of growth was, on average, 0.33 for the *E.coli* PHL628 culture and 0.46 for the wastewater culture, with minimal effect of particle type (Figure 2a) or concentration (Suppl. Fig. 2). The OD of sterile controls remained constant at approximately 0.0 OD.

pH measurement in suspended cultures

The pH profiles after glucose addition to *E. coli* PHL628 cultures and to mixed community wastewater cultures are shown in Figure 2b-c and 2d-e, respectively. The pH was tracked both with C dots (Fig. 2b, d) and with a pH meter (Fig. 2c, e). For these samples, the trends in pH as measured over time using C dot sensors and a pH meter are comparable. Naturally, one would expect a pH electrode to provide measurements that are less noisy but also with less spatial localization. Conversely, when using C dots for biofilm pH measurements the values are averaged over much smaller volumes, such that each pixel has a specific spatial location and is assigned a pH value. Hence, anywhere a fluorescent bead may be present within a biofilm, *i.e.* attached to a cell or to EPS or floating inside a pore, the pH corresponding to that location may be quantified. This explains how, within a biofilm, pH microenvironments may be observed with this technique. These results validate our claim that C dots may be used for real time tracking of pH in bacterial environments.

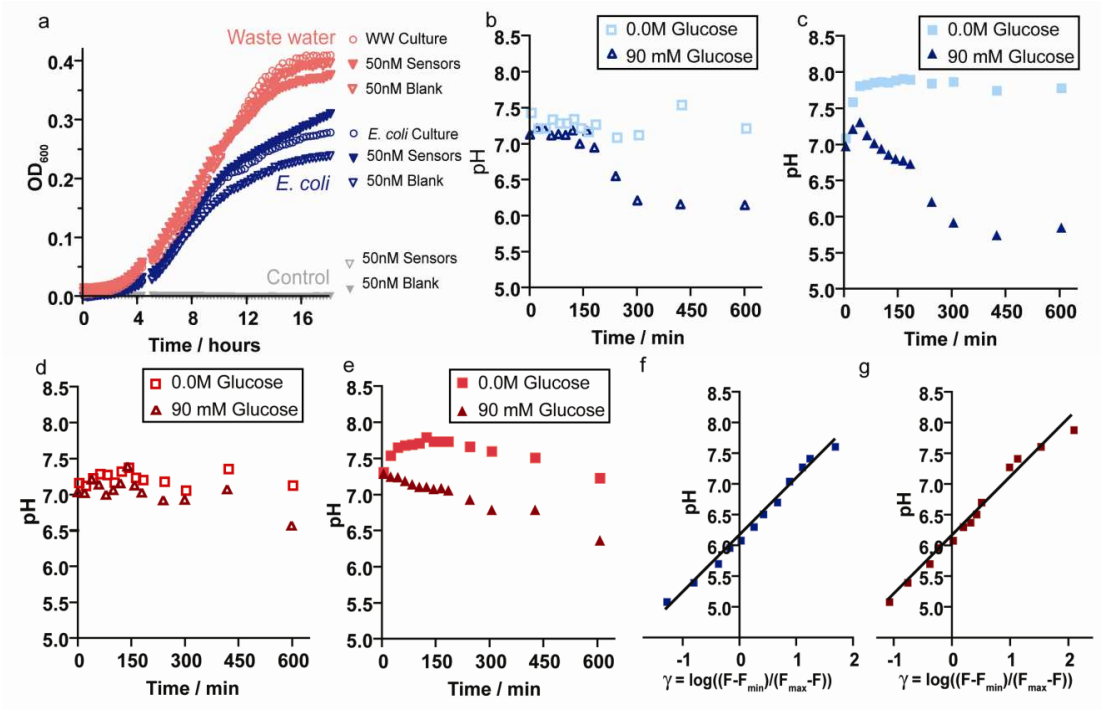

Figure 2. C Dot Sensor Biocompatibility, Solution pH measurements and calibrations. (a) OD at 600 nm for *E. coli* PHL628 (middle curves, shown in blue), mixed wastewater culture (top curves, shown in red) and sterile controls (along x-axis, black) versus time, under normal growth conditions (○), and in the presence of 50 nM C dot sensors (▼) or 50 nM pure silica nanoparticles of the same size (□). (b-e) pH versus time after glucose introduction as measured by silica nanoparticle sensors (b,d) and pH meter (c,e) in planktonic *E. coli* (b,c) and wastewater culture (d,e) suspensions. Square and triangle symbols indicate glucose additions of 0 or 90 mM respectively. (f,g) pH calibration graphs for *E. coli* biofilm imaging, (f) (R^2 = 0.99) and wastewater mixed-culture biofilm imaging, (g) (R^2 = 0.99) based on pixel-wise image analysis of confocal microscopy images of particles suspended in pH calibrated solutions.

Figures 2b and c show that the pH of a suspended *E. coli* PHL628 culture after glucose addition dropped from 7.0 to near 5.5, over ~400 minutes. Over the course of the experiment, the pH did not return to neutral values. We do not believe this acidification to be the result of fermentation, because the cultures were stirred continuously to maintain aerobic conditions.

As shown in Figures 2d and e, the decrease in pH in the 90 mM glucose-exposed mixed-culture over the course of the experiment was minimal. This difference, relative to the behavior of the *E. coli* culture, is reasonable given that glucose is the primary energy source for this enteric bacterium which constitutively expresses the necessary enzymes for glucose metabolism (40). Therefore in *E. coli*, catabolism can begin immediately upon glucose exposure leading to a pH drop as metabolites accumulate in solution. The mixed wastewater culture, however, includes a wide variety of microorganisms, some of which are unable to consume glucose and others that must undergo an induction process to metabolize glucose, resulting in a pH drop that is both of a smaller magnitude and delayed.

Functional Three-dimensional Tomographic Imaging

In Figure 2f and g we show the image-based pH calibration graphs for the (f) *E. coli* PHL628 biofilm ($R^2 = 0.99$) and (g) wastewater biofilm ($R^2 = 0.99$) image settings as calculated by the modified Henderson-Hasselbalch equation shown previously (Eq. 1) where $F_i = I_{FITC} / I_{Cy5}$, and F_{min} and F_{max} are the extreme values of F_i at low and high pH, respectively. F_{min}, F_{max} and F_i were calculated by pixel-wise analysis of confocal microscopy images of C dot sensors suspended in calibration buffers of varying pH as

described in the methods section. Based on these calibration curves, we were able to accurately determine pH from 5.0 to 8.0, which covers the physiological range of this system. The two bacterial systems were analyzed on separate occasions, and thus were analyzed based on different calibration curves to correct for differences in 488 and 633 nm laser intensity, filter settings for optimal imaging and solution conditions (Fig 2f, g).

Figures 3a and b show, respectively, the green (sensor dye) channel and the red (reference dye) channel confocal images of a typical live, hydrated *E. coli* PHL628 biofilm at a focal plane 90 μm from the attachment substratum. Figure 3c depicts the sensor and reference images merged with a brightfield image of the biofilm, demonstrating the incorporation of the particles within the film. The greater depth of field of the brightfield image shows the structure of the film above and below the confocal image plane, which accounts for the apparent mismatch of the fluorescence and brightfield images. Vertical scanning of the sample results in registry of particle fluorescence with the brightfield images of the biofilm over the full z-range of imaging (top maximum intensity projection, Figure 3 e).

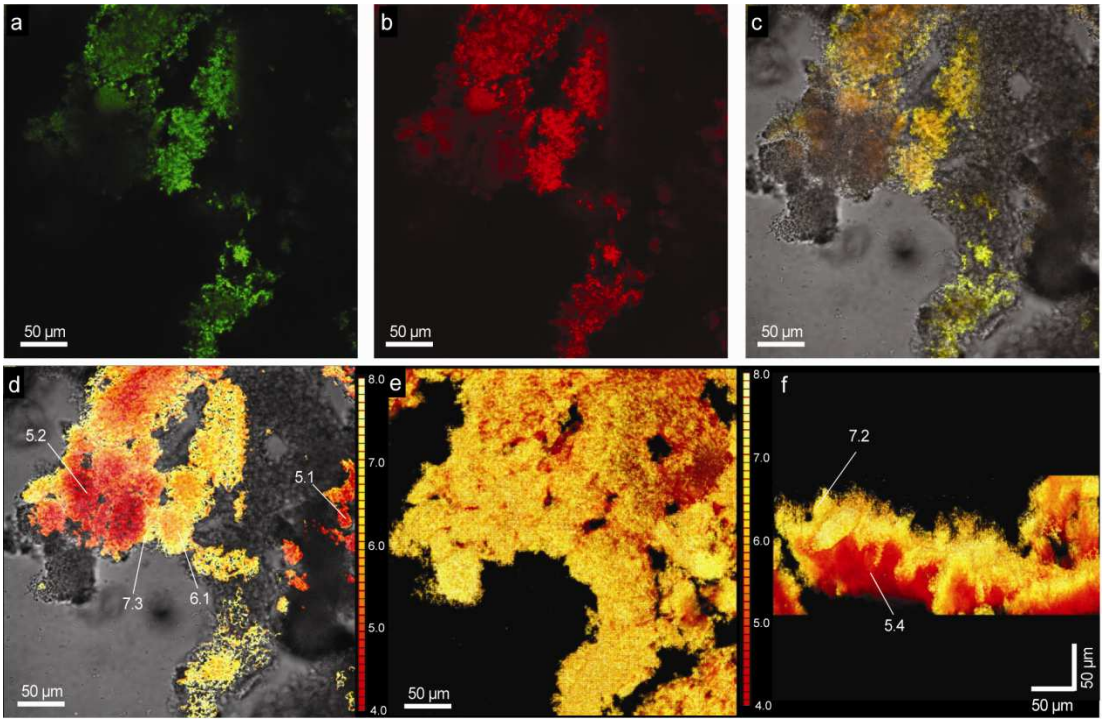

Figure 3. *E. coli* Confocal and Tomographic pH Imaging. (a), Green and (b), red channel confocal images of a typical live, hydrated *E. coli* PHL628 biofilm at a focal plane 90 µm from the substratum. (c) Sensor and reference images superimposed on a brightfield image of the biofilm, showing the co-localization of the particles in the film. The pH was analyzed ratiometrically based on the sensor and reference images and is expressed as a false spectrum (red-yellow) in (d) overlaid on the brightfield image, with the pH scale shown at the right in the image. (e) Top-down and, (f) side volumetric projections (smooth opacity, OsiriX) of the reconstructed biofilm pH map show the local variation of pH from the neutral outside surface of the film to the acidic core, scale in (e,f). pH values are shown at a few sites in (d) and (f) to show the gradients.

The pH was analyzed ratiometrically based on the sensor and reference images and is expressed in pseudocolor (red-yellow) in Figure 3d overlaid on the brightfield image. The pH scale is shown on the right of the image. Specifically, the pH within the core of the biofilm is low (red) and increases (orange/yellow) towards the periphery of the film, potentially due to low diffusion rates of acidic metabolites into solution or the accumulation of fermentation products in oxygen-limited portions of the biofilm. This region of the biofilm was imaged from the attachment substratum up through a depth of 160 μm in 1 μm steps, and volumetrically reconstructed to show the biofilm morphology as well as the pH gradients and microenvironments in the x, y and z directions. Top and side maximum projections are presented in Figures 3e and f, respectively. The vertical gradient from low pH deep in the film to more neutral pH at the upper surface observed in the side-view (Figure 3f) correlates well with the in-plane gradients seen in Figure 3d.

It is worth pointing out that images 3c and 4a show the merged green and red channel images over the brightfield image, as viewed on the microscope. Because, when using C dots, the intensity of the red channel is constant and the green signal increases with pH, the images locally appear red, yellow and green, depending on the local intensity of sensor and reference emission. While these overlaid images provide a qualitative assessment of pH, the on-scope calibrations (Fig 2f, g) convert the green/red intensity ratio to pH for each pixel. This data is represented as the ratiometric pH maps (3d-f, 4b-f, 5a-f and 6b-c) which use a false spectrum to represent the local pH, from red to yellow, as shown in the scale appended to each image or series. These false-color pH maps were generated with Osirix image processing software using a color look-up table.

Figures 4a and 4b depict the overlay and ratiometric pH images of a mixed-culture biofilm 77 μm from the substratum. The pH is more heterogeneous throughout this mixed-culture than the axenic one, both horizontally and vertically, as revealed by the variation in top- and side- maximum intensity projections in Figures 3e and 3f and 4c and 4d. Figures 4e and 4f show the distinct pH microenvironments in the three dimensional pH image of the mixed culture film by presenting projections of the full tomographic reconstruction (500x500x160 μm). Based on the morphological and chemical differences between micro-environments, it is likely that bacteria from different functional groups are coexisting and generating different metabolic by-products.

Investigating specific regions of interest by zooming into the full tomographic reconstructions and providing various views of the *E. coli* and the mixed-culture biofilms (Figure 5) demonstrates the power of nanoparticle sensor–enabled 3D functional imaging. Figures 5 a-c show in detail the low-to neutral pH gradient formed from the core of the biofilm to the periphery, as well as the fine structure with channels and voids of the *E. coli* film. Figures 5 d-f show the voids formed by the interpenetration of the low pH film components and the fibrous neutral regions as well as the different growth habits of the two including a mushroom-like protrusion in the mixed-culture biofilm.

Figure 6a depicts the average pH versus time following a glucose injection (90mM) for *E. coli* PHL628 (red) and wastewater mixed culture (blue) biofilms. Figures 6b and 6c show the corresponding confocal ratiometric pH images at t = 0 and 90 minutes, respectively, after the glucose addition to the *E. coli* PHL628 biofilm at a focal plane

60 μm from the attachment substratum (additional images available in Supplemental Information).

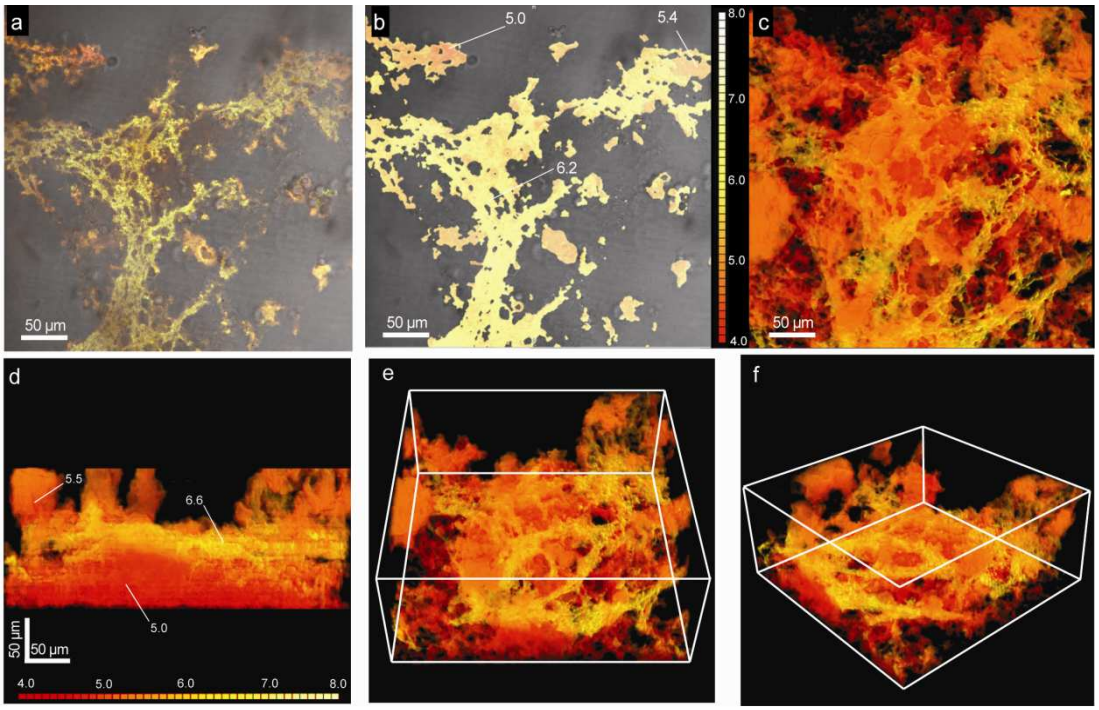

Figure 4. Mixed-Culture Confocal and Tomographic pH Images. (a) Sensor and reference confocal images of a live, hydrated wastewater biofilm at a focal plane 77 mm from the substratum superimposed on a brightfield image of the biofilm showing the colocalization of the particles in the film. The pH was analyzed ratiometrically based on the sensor and reference images and is expressed as a false spectrum (red-yellow) in (b), and overlaid on the brightfield image, with the pH scale shown at the right in the image. Top-down, (c) and side, (d) maximum intensity projections of the biofilm. (e and f) off-axis, maximum intensity projections of the fully reconstructed biofilm pH map (500x500x160 μm) showing the considerable heterogeneity that exists within the mixed-culture film, where a web-like neutral environment exists within the acidic film with tower structures surrounding and penetrating it.

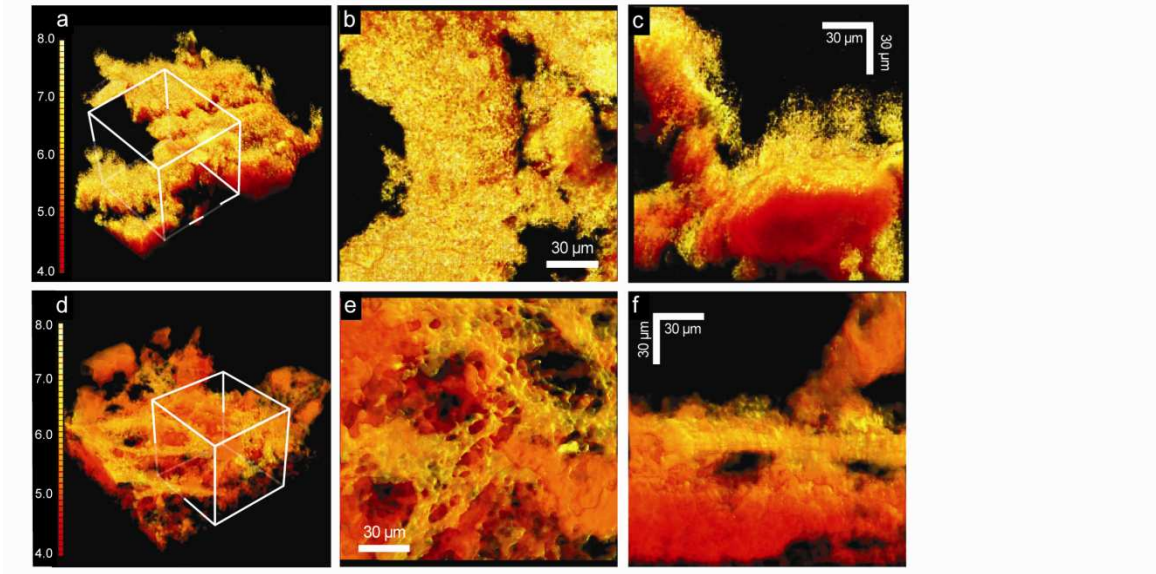

Figure 5. Magnified views of regions of interest in *E. coli* and mixed-culture biofilms. (a) An off-axis maximum projection of the reconstructed *E. coli* PHL628 biofilm and pH map scale at left (pH 4.0-8.0, red-yellow). For images (a) and (d) a region of interest was defined by the white cube (160x160x160 µm). (b) and (c) are top and side views of the region of interest defined by the white cube in (a), showing the pH heterogeneities, as well as the local structure of the biofilm. (d) An off-axis volumetric (smooth table) projection of the reconstructed wastewater mixed-culture biofilm and pH map scale at left (pH 4.0-8.0, red-yellow). (e) and (f), top and side views of cube shown in (d) showing the pH heterogeneities, as well as the local structure of the biofilm including voids, channels and a tower.

The *E. coli* biofilm pH drops sharply from 6.3 to 5.2 in the first 30 minutes and then remains constant for the remainder of the experiment. The wastewater biofilm follows a similar trend, though the magnitude of the pH change is lower (plateau value at 5.6 at 90 minutes, images in Supplementary Information). This result is similar to the behavior observed in the suspended cultures, though the kinetics are much faster in the biofilms. The increased rate of pH change in the biofilm is most likely due to the fact that diffusion is hindered in the biofilm as compared to the stirred suspensions, allowing acidic metabolites to accumulate in the biofilm and change the local pH more quickly.

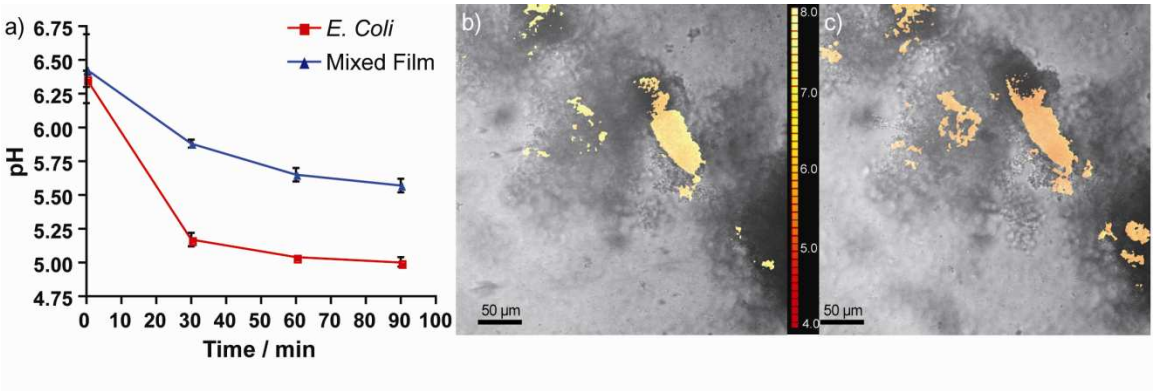

Figure 6. Time-resolved *in situ* pH measurements in biofilms. (a), average pH versus time post injection of 90 mM glucose to biofilms to *E. coli* PHL628 (in red, mean +/- s.d., n = 3) and mixed wastewater culture (in blue, mean +/- s.d. n = 6). Values are significantly different from t = 30 minutes onward, Mann-Whitney U, one-tailed test, p = 0.011. (b)-(c), Imaging of C dots within an *E. coli* PHL628 biofilm corresponding to the initial, (b), and final, (c), timepoints of the graph in (a) (color scale corresponds to pH values from 4 to 8).

All of the biofilm imaging experiments were performed without shaking or perfusion in order to maintain a stable field of view over the course of the experiment. Therefore, the rate of oxygen diffusion was low and anoxic zones may have developed within the biofilms. So, in contrast to the planktonic cultures (Figures 2b-e), it is possible that the drop in pH observed in the biofilms (Figure 6a) is the combined result of limited diffusion and different metabolic processes, *i.e.* aerobic and anaerobic respiration and fermentation. In the case of the wastewater culture biofilm, the presence of glucose fermentors (such as other species of enteric bacteria, *Clostridium*, *Lactobacillus* and even yeasts) might also explain the presence of the low pH microenvironments.

Discussion

In nanobiotechnology, tools of nanotechnology are used to study biology and in particular to further the goals of biotechnology. Over the past two decades, fueled by the discovery of fluorescent semiconductor nanocrystals, an explosion has taken place in the development of fluorescent nanoparticles and nanoparticle systems for imaging, sensing and diagnostic purposes (35, 39). Concurrently, microscale heterogeneities in biofilms, in particular sucrose-induced pH gradients in dental caries have been the subject of much research (13, 21, 27, 28, 34, 37, 42, 45-47, 55). However, despite recent advances, present understanding of the complex processes that occur in biofilms is incomplete. The presence of biofilms at the solid-water interface in virtually all systems allows them to impact the quality of water in the environment, regulate the behavior and fate of pollutants, enhance the resistance of infections to treatment, and, in short, have an effect on all ecosystems and the organisms that inhabit them (41). Concomitant with increasing recognition of the importance of

biofilms is the need for better investigational tools. Development and execution of *in situ* monitoring and characterization of biofilms is expected to be particularly powerful to address present and future needs. Towards this end, the research presented here demonstrates, for the first time, the use of ratiometric fluorescent silica nanoparticle sensors as tools for high resolution three-dimensional and time-domain functional fluorescence imaging of pH gradients in microbial biofilms. These nanoparticle sensors provide a minimally invasive route to quantitative chemical imaging with resolution limited only by the microscopy system in use.

In order for nanoparticle sensor-based functional imaging of biofilms to work, the nanoparticle probes must intimately mix with, and stay in the extracellular matrix of the biofilm. Interestingly, through performing experiments with 70, 30 and 10 nm diameter silica particles, we found only the smallest bare C dot sensors provided the desired effective and homogeneous staining. There are several effects, which, by themselves or in combination could explain these observations. Gels of polysaccharides and fibrous proteins fill the intercellular spaces of biofilms. First, fluid gaps between these elements of the extracellular matrix could simply be too small for the bigger particles to penetrate. Second, it is expected that mixing between nanoparticles and polymer matrices is size dependent for entropic reasons. In fact, such entropic size dependencies have been theoretically predicted and experimentally observed (32, 52, 56). For mixing to occur, polymer chains must wrap around the nanoparticles, a process which becomes more entropically unfavorable as the particle size increases relative to the polymer size.

Because polymer dimensions scale with only the square root of the number (N) of units constituting them (ideal case (10)) particle size quickly outgrows chain size. Plugging in relevant numbers for extracellular matrix polymer sizes (data not included) suggests that it is not unreasonable to expect the critical particle size for demixing to be between 10 and 30 nm. Third, the electrostatic repulsion between the negatively charged particle surfaces and biofilm extracellular matrix could cause a similar size-dependent effect. The electrostatic repulsion energy for particles of uniform surface charge scales approximately with the surface area of the particles (20), such that 70 nm diameter particles would experience a ~50-fold stronger repulsion than 10 nm diameter particles, making their inclusion into the biofilm much less favorable. While repulsive electrostatic effects will be partially screened by the ions in solution (*e.g.* 0.05M NaCl in LB) they may still affect the behavior at small length scales. Irrespective of which of these effects dominates the behavior, particle size becomes a critical design criterion for nanoparticle probes for biofilm interrogation.

The dyes in the C dot sensors are shielded by the silica matrix from interactions with extracellular matrix components that can bias the results, which simultaneously renders the particles biocompatible for use in both prokaryotic and higher biological systems with minimal toxicity. The enhanced photostability of the silica-encapsulated dye molecules also facilitates high-resolution measurements in xyz and xy-time spaces without compromising sensitivity. Although the long wavelength photons used in multiphoton imaging give greater penetration depth than single photon imaging, for this work a dual-excitation, single-photon system was chosen to provide a large spectral separation between sensor and reference emissions. Several recent reviews

further elaborate on the relative merits of single and multiphoton imaging techniques (19, 57).

The sensor/reference dye combination chosen for this work is well suited to the pH values in living biofilms, but other combinations can be synthesized to study environments with more extreme pH gradients such as microbial mats (53), insect midguts (3) and river sediments exposed to acid mine drainage (1). Substituting a fluorophore with a more acidic or basic pKa such as Oregon Green 514 or carboxynaphthofluorescein (4.8 and 7.6 respectively (18)) for fluorescein allows the linear range of the particles to be tailored. Moreover, by changing to other dyes, it is possible to quantitatively measure other variables of interest such as redox potential, oxygen status or concentration of ions such as Ca^{+2} and Mg^{+2} without significantly altering the particle architecture. Such nanoparticle probes, if designed appropriately, should provide powerful tools for future *in situ* monitoring and characterization of complex biofilms.

Future work will explore the potential correlations between heterogeneities in pH (i.e. in mixed-culture biofilms) and the bacterial species present in those locations. This line of research can be carried out by fluorescence *in situ* hybridization (FISH) performed on the biofilms co-labeled with pH sensing C dots. This objective might also be pursued by staining of extracellular products with fluorescent lectins specific for the polysaccharides that are produced by the particular microorganisms which are being tested followed by concurrent imaging of the lectins and the sensor particles. This last approach, although indirect, may provide an interesting and so far unexplored perspective.

Acknowledgements

We appreciate the assistance of Carol Bayles and the Microscopy and Imaging Facility of the Cornell Biotechnology Research Center. Gabriela Hidalgo was funded through a CONACYT graduate fellowship. This work was supported, in part, by NSF grant EAR-4 0311767. Andrew Burns was supported by the Cornell Nanobiotechnology Center (NBTC), an STC center of the NSF under agreement No. ECS-9876771. UW declares a financial role in a start-up company (Hybrid Silica Technologies) in the field of fluorescent nanoparticle development.

REFERENCES

1. **Blothe, M., D. M. Akob, J. E. Kostka, K. Goschel, H. L. Drake, and K. Kusel.** 2008. pH gradient-induced heterogeneity of Fe(III)-reducing microorganisms in coal mining-associated lake sediments. Appl Environ Microbiol **74:**1019-29.

2. **Botvinick, E. L., and J. V. Shah.** 2007. Laser-based measurements in cell biology. Methods Cell Biol **82:**81-109.

3. **Brune, A., D. Emerson, and J. A. Breznak.** 1995. The Termite Gut Microflora as an Oxygen Sink: Microelectrode Determination of Oxygen and pH Gradients in Guts of Lower and Higher Termites. Appl Environ Microbiol **61:**2681-2687.

4. **Burns, A., H. Ow, and U. Wiesner.** 2006. Fluorescent core-shell silica nanoparticles: towards "Lab on a Particle" architectures for nanobiotechnology. Chemical Society Reviews **35:**1028-1042.

5. **Burns, A., P. Sengupta, T. Zedayko, B. Baird, and U. Wiesner**. 2006. Core/shell fluorescent silica nanopartictes for chemical sensing: Towards single particle laboratories. Small **2:**723-726.

6. **Chang, C. W., D. Sud, and M. A. Mycek.** 2007. Fluorescence lifetime imaging microscopy. Methods Cell Biol **81:**495-524.

7. **Choi, J. H., A. A. Burns, R. M. Williams, Z. X. Zhou, A. Flesken-Nikitin, W. R. Zipfel, U. Wiesner, and A. Y. Nikitin.** 2007. Core-shell silica nanoparticles as fluorescent labels for nanomedicine. Journal of Biomedical Optics **12:-**.

8. **Clark, H. A., M. Hoyer, M. A. Philbert, and R. Kopelman.** 1999. Optical nanosensors for chemical analysis inside single living cells. 1. Fabrication, characterization, and methods for intracellular delivery of PEBBLE sensors. Analytical Chemistry **71:**4831-4836.

9. **de Beer, D., P. Stoodley, F. Roe, and Z. Lewandowski.** 1994. Effects of biofilm structures on oxygen distribution and mass transport. Biotechnology and Bioengineering **43:**1131–1138.

10. **De Gennes, P.-G.** 1979. Scaling Concepts in Polymer Physics, Ithaca, NY.

11. **Dethlefsen, L., M. McFall-Ngai, and D. A. Relman.** 2007. An ecological and evolutionary perspective on human-microbe mutualism and disease. Nature **449:** 811-8.

12. **Donlan, R. M.** 2002. Biofilms: microbial life on surfaces. Emerg Infect Dis **8:** 881-90.

13. **Ferris, M. J., T. S. Magnuson, J. A. Fagg, R. Thar, M. Kuhl, K. B. Sheehan, and J. M. Henson.** 2003. Microbially mediated sulphide production in a thermal, acidic algal mat community in Yellowstone National Park. Environ Microbiol **5:**954-60.

14. **Gieseke, A., S. Tarre, M. Green, and D. de Beer.** 2006. Nitrification in a biofilm at low pH values: role of in situ microenvironments and acid tolerance. Appl Environ Microbiol **72:**4283-92.

15. **Gilbert, P., T. Maira-Litran, A. J. McBain, A. H. Rickard, and F. W. Whyte.** 2002. The physiology and collective recalcitrance of microbial biofilm communities. Adv Microb Physiol **46:**202-56.

16. **Gryczynski, Z., I. Gryczynski, and J. R. Lakowicz.** 2003. Fluorescence sensing methods. Methods Enzymol **360:**44-75.

17. **Hall-Stoodley, L., J. W. Costerton, and P. Stoodley.** 2004. Bacterial biofilms: from the natural environment to infectious diseases. Nat Rev Microbiol **2:**95-108.

18. **Haugland, R. P.** 2007. The Handbook—A Guide to Fluorescent Probes and Labeling Technologies, 10 ed. Molecular Probes, Inc., Eugene, OR.

19. **Helmchen, F., and W. Denk.** 2005. Deep tissue two-photon microscopy. Nature Methods **2:**932-940.

20. **Hermansson, M.** 1999. The DLVO theory in microbial adhesion. Colloids and Surfaces B-Biointerfaces **14:**105-119.

21. **Hunter, K. S., Y. Wang, and P. Van Cappellen.** 1998. Kinetic modeling of microbially-driven redox chemistry of subsurface environments: coupling transport, microbial metabolism and geochemistry. Journal of Hydrology **209:**53-80.

22. **Hunter, R. C., and T. J. Beveridge.** 2005. Application of a pH-sensitive fluoroprobe (C-SNARF-4) for pH microenvironment analysis in Pseudomonas aeruginosa biofilms. Appl Environ Microbiol **71:**2501-10.

23. **Ito, T., J. L. Nielsen, S. Okabe, Y. Watanabe, and P. H. Nielsen.** 2002. Phylogenetic identification and substrate uptake patterns of sulfate-reducing bacteria inhabiting an oxic-anoxic sewer biofilm determined by combining microautoradiography and fluorescent in situ hybridization. Appl Environ Microbiol **68:**356-64.

24. **Kaewpipat, K., and C. P. L.** Grady. 2002. Microbial population dynamics in laboratory-scale activated sludge reactors. Water Science and Technology **46:**19-27.

25. **Kemner, K. M., S. D. Kelly, B. Lai, J. Maser, J. O'Loughlin E, D. Sholto-Douglas, Z. Cai, M. A. Schneegurt, C. F. Kulpa, Jr., and K. H. Nealson.** 2004. Elemental and redox analysis of single bacterial cells by x-ray microbeam analysis. Science **306:**686-7.

26. **Koo, Y. E. L., Y. F. Cao, R. Kopelman, S. M. Koo, M. Brasuel, and M. A. Philbert.** 2004. Real-time measurements of dissolved oxygen inside live cells by organically modified silicate fluorescent nanosensors. Analytical Chemistry **76:**2498-2505.

27. **Kuhl, M.** 2005. Optical microsensors for analysis of microbial communities. Methods Enzymol **397:**166-99.

28. **Kuhl, M., and T. Fenchel.** 2000. Bio-optical Characteristics and the Vertical Distribution of Photosynthetic Pigments and Photosynthesis in an Artificial Cyanobacterial Mat. Microb Ecol **40:**94-103.

29. **Kuseler, A., V. Baelum, O. Fejerskov, and J. Heidmann.** 1993. Accuracy and precision in vitro of Beetrode microelectrodes used for intraoral pH measurements. Caries Res **27:**183-90.

30. **Lappin-Scott, H. M., and J. W. Costerton.** 1989. Bacterial biofilms and surface fouling. Biofouling **1:**323 – 342.

31. **Larson, D. R., H. Ow, H. D. Vishwasrao, A. A. Heikal, U. Wiesner, and W. W. Webb.** 2008. Silica nanoparticle architecture determines radiative properties of encapsulated fluorophores. Chemistry of Materials **20:**2677-2684.

32. **Mackay, M. E., A. Tuteja, P. M. Duxbury, C. J. Hawker, B. Van Horn, Z. B. Guan, G. H. Chen, and R. S. Krishnan.** 2006. General strategies for nanoparticle dispersion. Science **311:**1740-1743.

33. **Marquis, R. E.** 1995. Oxygen metabolism, oxidative stress and acid-base physiology of dental plaque biofilms. J Ind Microbiol **15:**198-207.

34. **Marsh, P. D., and D. J. Bradshaw.** 1995. Dental plaque as a biofilm. J Ind Microbiol **15:**169-75.

35. **Michalet, X., F. F. Pinaud, L. A. Bentolila, J.** 1 **M. Tsay, S. Doose, J. J. Li, G. Sundaresan, A. M. Wu, S. S. Gambhir, and S. Weiss.** 2005. Quantum dots for live cells, in vivo imaging, and diagnostics. Science **307:**538-44.

36. **Okabe, S., T. Itoh, H. Satoh, and Y. Watanabe.** 1999. Analyses of spatial distributions of sulfate-reducing bacteria and their activity in aerobic wastewater biofilms. Appl Environ Microbiol **65:**5107-16.

37. **Okabe, S., H. Satoh, and Y. Watanabe.** 1999. In situ analysis of nitrifying biofilms as determined by in situ hybridization and the use of microelectrodes. Appl Environ Microbiol **65:**3182-91.

38. **Palmer, R. J., Jr., and C. Sternberg.** 1999. Modern microscopy in biofilm research: confocal microscopy and other approaches. Curr Opin Biotechnol **10:**263-8.

39. **Piao, Y., A. Burns, J. Kim, U. Wiesner, and T. Hyeon.** 2008. Designed Fabrication of Silica-Based Nanostructured Particle Systems for Nanomedicine Applications. Advanced Functional Materials **18:**3745-3758.

40. **Plumbridge, J.** 1998. Control of the expression of the manXYZ operon in Escherichia coli: Mlc is a negative regulator of the mannose PTS. Mol Microbiol **27:**369-80.

41. **Potera, C.** 1996. Biofilms invade microbiology. Science **273:**1795-7.

42. **Ramsing, N. B., M. Kuhl, and B. B. Jorgensen.** 1993. Distribution of sulfate reducing bacteria, O2, and H2S in photosynthetic biofilms determined by oligonucleotide probes and microelectrodes. Appl Environ Microbiol **59:**3840-9.

43. **Roeselers, G., M. C. M. van Loosdrecht, and G. Muyzer.** 2008. Phototrophic biofilms and their potential applications. Journal of Applied Phycology **20:**227-235.

44. **Rosset, A., L. Spadola, and O. Ratib.** 2004. OsiriX: 1 An Open-Source Software for Navigating in Multidimensional DICOM Images. Journal of Digital Imaging **17:**205-216.

45. **Sissons, C.** 1998. Plaque, plaque model systems and pH. N Z Dent J **94:**56-60.

46. **Sissons, C. H., T. W. Cutress, G. Faulds, and L. Wong.** 1992. pH responses to sucrose and the formation of pH gradients in thick 'artificial mouth' microcosm plaques. Arch Oral Biol **37:**913-22.

47. **Sissons, C. H., L. Wong, E. M. Hancock, and T. W. Cutress.** 1994. pH gradients induced by urea metabolism in 'artificial mouth' microcosm plaques. Arch Oral Biol **39:**507-11.

48. **Stewart, P. S., and M. J. Franklin.** 2008. Physiological heterogeneity in biofilms. Nat Rev Microbiol **6:**199-210.

49. **Stief, P., and G. Eller.** 2006. The gut microenvironment of sediment-dwelling Chironomus plumosus larvae as characterised with O2, pH, and redox microsensors. J Comp Physiol [B] **176:**673-83.

50. **Stober, W., A. Fink, and E. Bohn.** 1968. Controlled Growth of Monodisperse Silica Spheres in Micron Size Range. Journal of Colloid and Interface Science **26:**62-&.

51. **Stoodley, P., K. Sauer, D. G. Davies, and J. W. Costerton.** 2002. Biofilms as complex differentiated communities. Annu Rev Microbiol **56:**187-209.

52. **Thompson, R. B., V. V. Ginzburg, M. W. Matsen, and A. C. Balazs**. 2001. Predicting the mesophases of copolymer-nanoparticle composites. Science **292:**2469-2472.

53. **Vasconcelos, C., R. Warthmann, J. A. McKenzie, P. T. Visscher, A. G. Bittermann, and Y. van Lith.** 2006. Lithifying microbial mats in Lagoa Vermelba, Brazil: Modern Precambrian relics? Sedimentary Geology **185:**175-183.

54. **Vidal, O., R. Longin, C. Prigent-Combaret, C. Dorel, M. Hooreman, and P. Lejeune.** 1998. Isolation of an Escherichia coli K-12 mutant strain able to form biofilms on inert surfaces: involvement of a new ompR allele that increases curli expression. J Bacteriol **180:**2442-9.

55. **Vroom, J. M., K. J. De Graw, H. C. Gerritsen, D. J. Bradshaw, P. D. Marsh, K. G. Watson, J. J. Birmingham, and C. Allison.** 1999. Depth Penetration and

Detection of pH Gradients in Biofilms by Two-Photon Excitation Microscopy. Applied and Environmental Microbiology **65:**3502-3511.

56. **Warren, S. C., F. J. Disalvo, and U. Wiesner.** 2007. Nanoparticle-tuned assembly and disassembly of mesostructured silica hybrids. Nature Materials **6:**156-U23.

57. **Williams, R. M., D. W. Piston, and W. W. Webb.** 1994. 2-Photon Molecular Excitation Provides Intrinsic 3-Dimensional Resolution for Laser-Based Microscopy and Microphotochemistry. Faseb Journal **8:**804-813.

58. **Xi, C., D. Marks, S. Schlachter, W. Luo, and S. A. Boppart.** 2006. High resolution three-dimensional imaging of biofilm development using optical coherence tomography. J Biomed Opt **11:**34001.

CHAPTER 3

CURLI PRODUCED BY *ESCHERICHIA COLI* PHL628 PROVIDE PROTECTION FROM Hg(II)[2]

Abstract

Curli are amyloid extracellular fibers expressed by *Escherichia coli* and other bacterial species, and are involved in the colonization of inert surfaces, biofilm maturation, and mediate binding to a variety of host proteins. In this study we examined the role of curli in the tolerance of *Escherichia coli* PHL628 to Hg(II). The PHL628 strain has a point mutation in the regulatory protein OmpR that results in overproduction of curli. Specifically, we evaluated the effect of curli on the resistance to Hg toxicity and whether Hg alters the induction of curli expression; furthermore, we assessed how the presence of curli altered Hg uptake and adsorption. Viable cell counts revealed that after exposure to Hg(II), curli-producing strains were more resistant than the curli deficient mutant (*csgA*$^-$). Transcription of the genes encoding curli is known to be induced by some heavy metals, but we found no induction of a *csgB-lux* bioreporter after Hg(II) exposure. In cells harboring a *merR-gfp* bioreporter, higher fluorescence was measured in the *csgA*$^-$ mutant than in the wild type after Hg(II) addition, suggesting Hg(II) was more bioavailable. The kinetics of Hg(II) adsorption were also evaluated and revealed that curli increased the rate and extent of Hg(II) adsorption. Based on these findings we conclude that curli sorb Hg(II) and reduce the amount of Hg(II) that reaches the cytoplasm, acting as a temporary protective barrier for the cell.

[2] The contents of this chapter have been submitted for publication in *Applied and Environmental Microbiology* with co-authors X. Chen, A.G. Hay, and L.W Lion.

To our knowledge, this is the first time a protective role of curli against toxic transition metals has been demonstrated.

Introduction

Anthropogenic and natural activities produce elevated levels of heavy metals in the environment (6). The U.S. Environmental Protection Agency's Priority List of Hazardous Substances placed 12 heavy metals among its top 100 compounds and ranked mercury in the third place following arsenic and lead (14). Mercury, to date, has no known biological function because its affinity to thiol compounds is so high that it disrupts protein structure and function. Furthermore, Hg^{+2} is genotoxic because it also binds to nitrogen atoms in nucleic acids (18). It is therefore a highly toxic element to all forms of life (23).

Bacteria are involved in the global environmental cycling of mercury. They both reduce Hg^{2+} to metallic Hg^{0}, which is volatile and relatively inert, and methylate ionic Hg(II) in an enzymatic process that makes Hg more bioavailable and more toxic (24). The most thoroughly studied bacterial transformation of mercury is its reduction through enzymes encoded by the *mer* resistance operons. These operons occur naturally in chromosomes, plasmids and transposable elements and are widely distributed among Gram-negative and Gram-positive bacteria. Hg-resistant microbes are ubiquitous in natural habitats and are enriched in Hg-polluted sites (24). The genes of the *mer* operon encode for proteins that transport the water-soluble, ionic Hg^{2+} into the cytoplasm in an energy-dependent manner. Subsequently, mercuric reductases convert the divalent Hg^{2+} to Hg^{0}, which is less toxic than Hg^{2+} and is also volatile. Hg^{0} is then free to leave the cell by passive diffusion and volatilize from the growth environment (1).

Bacteria may also cope with heavy metal stress by actively exporting metal cations from the cytoplasm (31). There are three types of export mechanisms currently known that carry on this efflux: P-type ATPases, CBA transporters, and the cation diffusion facilitator (CDF) family of transporters (19, 22, 29). However, other less understood mechanisms of tolerance are likely to exist.

Curli are thin, aggregative, extracellular fibers that have been described in enterobacteria, including *Escherichia*, *Salmonella* and *Citrobacter* spp. (16). Interestingly, transcription of the genes encoding curli is induced by exposure to some heavy metals (25). This type of amyloid fiber has also been found to be abundant in natural biofilms, particularly in oligotrophic environments (17, 20). The genes responsible for the production of curli in *E. coli* are clustered in two divergent operons: the *csgBA* operon, which encodes the major structural subunit, CsgA, and the nucleator protein, CsgB; and the *csgDEFG* operon, encoding genes necessary for transcription regulation, export of the curli subunit, and stabilization of the fibers (10). Expression of these promoters is affected by several transcriptional regulators, among them *rpoS*, *crl*, *hns* and *ompR* (27, 28) and is sensitive to cell wall stress (13, 32). Given the recent work of Perrin *et al.* (25) who reported that sub-inhibitory concentrations of nickel can induce the synthesis of curli by *E. coli*, we wondered if curli might play a role in resistance to the deleterious effects of heavy metals. In this report, we describe the role curli play in alleviating Hg(II) stress and the impact of Hg(II) on transcription of the genes encoding curli.

Materials and Methods

Bacterial strains and media

In this study, we used *E. coli* PHL628, a biofilm-forming K12 MG1655 derivative with a single point mutation that results in the replacement of a leucine by an arginine residue at position 43 in the regulatory protein OmpR (34). The omp234 allele enhances curli gene expression and promotes biofilm formation (34). Derivative strains and plasmids are listed in Table 1. Cultures were grown in a glucose minimal medium (GMM) which contained per liter: 7 g K_2HPO_4, 2 g KH_2PO_4, 1 g $(NH_4)_2SO_4$, 200 mg $MgSO_4 \cdot 7H_20$, 24 mg $Ca(NO_3)_2 \cdot 4H_20$ and 10 g glucose as the sole carbon source. A 20 mM concentration of 4-(2-hydroxyethyl)-1-piperazineethanesulfonic acid) (HEPES) was added to buffer the pH at 7.2; subsequently the medium was sterilized by filtration though a 0.2 μm membrane. Water used for preparing GMM media, metal stocks and for acid-washing was purified by a Thermo Scientific Mega-Pure System. Bacteria were grown at 30º or 37ºC with rotary shaking at 150 rpm. As required kanamycin (50 μg/mL), ampicillin (100 μg/mL), chloramphenicol (25 μg/mL), tetracycline (10 μg/mL) and streptomycin (50 μg/mL) were added. Analytical grade $NiCl_2 \cdot 6H_20$ and $HgCl_2$ were obtained from Mallinckrodt. Stock solutions were 2% acidified with trace metal grade HNO_3.

Table 1. *E. coli* strains and plasmids used in this study

Strains	Relevant genotype	Source or reference
PHL628	MG1655 *malA-kan ompR234*; kan^R	34
PHL628 *csgA*$^-$	*csgA*$^-$; kan^R, cm^R	32, 13
S17-1	*λpir; hsdR pro recA; RP4 2-Tc::Mu-Km::Tn7, res-, mod+*; str^R, trm^R	Laboratory collection
Plasmids		
pBBR1MCS3	Broad-host-range cloning vector; tet^R	15
pBBR1MCS3:*csgA*	pBBR1MCS3 with *csgA* gene insert; tet^R	This study
pmerRFGP	Hg-uptake reporter vector; amp^R	9
pNLP55	curli-transcription reporter vector with P*csgBAC*::*luxCDABE*, kan^R	26
pNLP55<Tet-1>	curli-transcription reporter vector with P*csgBAC*::*luxCDABE*, tet^R	This study

Construction of pBBR1MCS3:*csgA*

A 528 bp PCR product containing the entire *csgA* gene was amplified using *E. coli* PHL628 as a template and primers csgAFKpnI and csgARApaI (see table 2). These primers contain KpnI and ApaI restriction sites respectively. The PCR product and the vector pBBR1MCS3 (15) were digested for 2 hours at 37ºC with KpnI and ApaI restriction enzymes. The ligation was performed for 12 hrs at 4ºC using T4 DNA ligase (Promega). The insertion was confirmed by PCR amplification with T7F and M13R and sequencing. All the transformations done for this work were conducted following the protocol described by Choi *et al.* (5).

Table 2. PCR primers used in this study

Primer name	Sequence (5'→ 3')	Source or reference
csgAFKpnI	GTTTCTGGTACCGCAAATGGCTATTCGCGTGACACA	This study
csgARApaI	GTTTCTGGGCCCATTAGTACTGATGAGCGGTCGCGT	This study
T7F	GTAATACGACTCACTATAGGGC	Stratagene
M13R	AACAGCTATGACCATG	Stratagene
merF	TTAAGGATCCCCTCATAGTTAATTTCT	9
merR	ATATCTCGAGCTAAGGCATAGCTGAC	9
pNLP10F	GCTTCCCAACCTTACCAGAG	26
pNLP10R	CACCAAAATTAATGGATTGCAC	26

Viability curves

Cultures of PHL628 pBBR1MCS3, PHL628 *csgA*$^{-}$ and PHL628 *csgA*$^{-}$ pBBR1MCS3*:csgA* grown for 24 hours in GMM were spiked with varying amounts of Hg(II) and incubated. After 3 hours of incubation, dilutions of the cell suspensions were plated in triplicate and allowed to grow for 24 hours. Colony forming units (CFU) were then counted.

Curli induction

The transcriptional activity of the *csgB* promoter was estimated from measurements of the luminescence of PHL628 pNLP55<TET-1> cells. The plasmid pNLP55, a kind gift of Prof. Raivio (University of Alberta, Canada) (26) contains the *PcsgBAC::luxCDABE* reporter, in which the entire intergenic region between the two curli operons was cloned in front of the luciferase genes, as well as a kanamycin resistance marker. However, because the PHL628 strain also contains a kanamycin resistance gene inserted in the *malA* locus of the chromosome, pNLP55 was mutagenized prior to the transformation of PHL628 in order to add a new selectable marker. Briefly, pNLP55 was mutagenized *in vitro* using the EZ-Tn5<TET-1> (Epicentre Biotechnologies, Madison WI) insertion kit. Following the mutagenesis, *E. coli* S17-1 cells were electroporated with the vector and transformants were selected on tetracycline and streptomycin and replica-plated on kanamycin plates. Colonies capable of growth on the tetracycline, streptomycin plates and unable to grow on the kanamycin plates were further screened by PCR using primers pNLP10F and pNLP10R. The fidelity of the promoter region was confirmed via sequencing. Finally, disruption of the kanamycin resistance gene was confirmed by sequencing with primers TET-1 FP-1 and TET-1 RP-1, provided with the kit. pNLP55<TET-1> was then used to transform PHL628 cells.

For analysis of *csgB* transcription the cells were grown at 30ºC in 0.25x Luria-Bertani broth supplemented with 0.1% mannitol containing a range of added Ni or Hg concentrations. The diluted LB medium was used instead of the defined GMM in order to be consistent with the work of Perrin *et al.* (25). OD_{600} and luminescence were measured at periodic intervals using a Bio-Tek μQuant spectrophotometer and a Packard LumiCount Luminescence Microplate Reader respectively. Triplicate samples

of each condition were prepared and the luminescence and OD_{600} values of the samples were averaged. Finally the upregulation of curli production was reported in the form of specific activity: (Luminescence – Initial Luminescence)/ OD_{600}.

Hg uptake

In order to test the hypothesis that curli act as a protective mechanism by preventing or retarding metal uptake cultures of PHL628 and PHL628 *csgA*$^-$ were transformed with pmerRGFP (Table 1) (9). Cultures of these strains were grown until early stationary phase at 30ºC in GMM and harvested. The bacteria were then exposed to varying Hg(II) concentrations after which the fluorescence and OD_{600} of the cultures was recorded at 15 minute intervals. Fluorescence and OD_{600} were measured with a Bio-Tek Synergy HT spectrophotometer with a 485/20 excitation filter and a 530/25 emission filter. For each condition, the fluorescence was divided by the OD_{600} in order to account for the variability in cell numbers. The results at 4 hours after the Hg addition were plotted versus Hg concentration.

Hg adsorption

Glassware used in this experiment was acid washed by soaking overnight in a 10% HNO_3 trace metal grade bath and rinsed with MilliQ deionized water. To minimize Hg(II) losses by adsorption to the walls, the Pyrex erlenmeyer flasks used for culturing were silanated using a 5% solution of dimethyldichlorosilane in carbon tetrachloride. Suspended cultures of *E. coli* PHL628 and *E. coli* PHL628 *csgA*$^-$ were grown in GMM at 30ºC to stationary phase. Aliquots of concentrated Hg solution were added to the cultures to yield total concentrations of 50 and 150 ppb Hg. The cultures were kept at constant temperature (30°C) and continuously mixed on a shaker at 150 rpm. At predetermined intervals (1, 2, 4, 8, and 24 h) aliquots were withdrawn and centrifuged

at 20,000 x g for 10 min. Soluble Hg concentrations were determined from the supernatants using a *Bacharach Coleman* model 50B *analyzer* system (Bacharach, Inc., Pittsburgh, PA) following a cold vapor atomic absorption method (12). The OD_{600} of the cultures was also recorded. The amount of sorbed Hg was calculated from the difference between the total added and measured dissolved Hg concentrations after correction for background values. The adsorbed Hg per cell data was used to fit a model using OriginPro8 (Northampton, MA). Quantification of the difference in adsorption kinetics relative to curli was done by modeling the adsorption process as the first order differential equation:

$$\frac{dC}{dt} = k(C^* - C) \qquad \text{Eq. 1}$$

with solution:

$$C(t) = C^*(1 - e^{-kt}) \qquad \text{Eq.2}$$

where,

C = Hg concentration adsorbed to cells (ppb/OD)

t = time (hrs)

k = rate constant (hr^{-1})

C* = Hg concentration adsorbed to cells at equilibrium (ppb/OD)

Results and Discussion

The research presented here was conducted with the purpose of evaluating the role curli play in binding Hg(II) and alleviating Hg(II) stress. We first evaluated the impact of Hg(II) on autoaggregation because cations can alter the total surface charge of

bacteria and thereby affect this property (7, 21, 30). Bacterial autoaggregation is a distinct phenotype that can be visualized macroscopically as flocculation and settling of cells in static liquid suspensions and is mediated by the expression of aggregation factors and surface structures like fimbriae, flagella, and curli (11, 33). As expected, the *csgA*$^{-}$ mutant stayed in suspension while the wild type settled; however, Hg(II) additions up to 300 ppb, which was the highest concentration that still permitted growth, did not alter settling (data not shown). This is likely because the concentration of mercury added was too low to significantly alter the surface charge.

Having confirmed the phenotype of our strains, we tested whether curli provided protection from Hg(II). Stationary phase cultures were exposed to varying Hg concentrations and incubated in the presence of the metal (Figure 1). The decrease in colony forming units with increasing mercury concentration was more pronounced in the curli-deficient strain and restored by complementation of the deletion. This result led us to conclude that curli provide moderate protection against mercury toxicity. We therefore performed a preliminary investigation into the mechanism for this increase in tolerance.

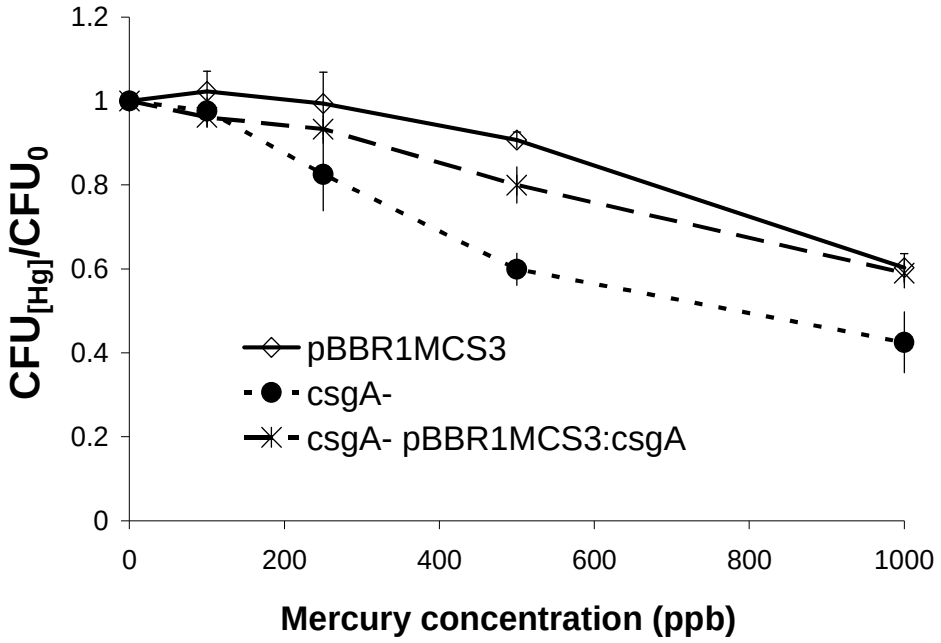

Figure 1. Viability curves. Colony forming units of PHL628 pBBR1MCS3 (solid), PHL628 *csgA*$^{-}$ (dashed, small) and PHL628 *csgA*$^{-}$ pBBR1MCS3:*csgA* (dashed, big) exposed to Hg(II) divided by the colony forming units of unexposed cultures plotted versus Hg concentration in ppb. Cultures were grown for 24 hours at 30°C in GMM, spiked with Hg(II) and incubated for 3 additional hours before the dilutions were prepared and plated. Error bars represent standard deviation of triplicate samples.

Recently, it was reported that *E. coli K12* strains exposed to subinhibitory concentrations of nickel upregulate curli production (25). This report led us to hypothesize that Hg might induce curli production and thereby protect the bacteria from the toxic effects of the metal. This hypothesis was tested using a *csgB-lux* bioreporter that was grown in the presence of nickel or mercury. After 14 hours of incubation, the upregulation of curli production, reported as luminescence specific activity, showed an increase of 95 fold and 60 fold in the presence of 50 μM (~2950 ppb) and 100 μM (~5900 ppb) nickel, respectively (Figure 2A) relative to basal levels. Nickel at 200 μM (~11700 ppb) was inhibitory of growth. In contrast to the results reported for nickel (25) and confirmed in Figure 2A, luminescence actually dropped in cultures exposed to Hg(II) when compared to the control (Figure 2B). Unfortunately, addition of Hg(II) at 400 ppb Hg(II) (2 μM) prohibited cell growth which precluded a direct comparison of the effect at equimolar concentrations. These results confirmed the prior report that sub-inhibitory concentrations of nickel result in an increase in the expression of the curli genes, but also demonstrated that mercury did not have such an effect. Hence, the possibility of a causal relationship between the transcriptional activation of curli genes and protection from exposure to heavy stress was discarded. Perrin *et al.* (25) also noted that magnesium additions also did not affect the expression of curli genes; therefore, it is possible that the effect of nickel on curli genes is specific to nickel.

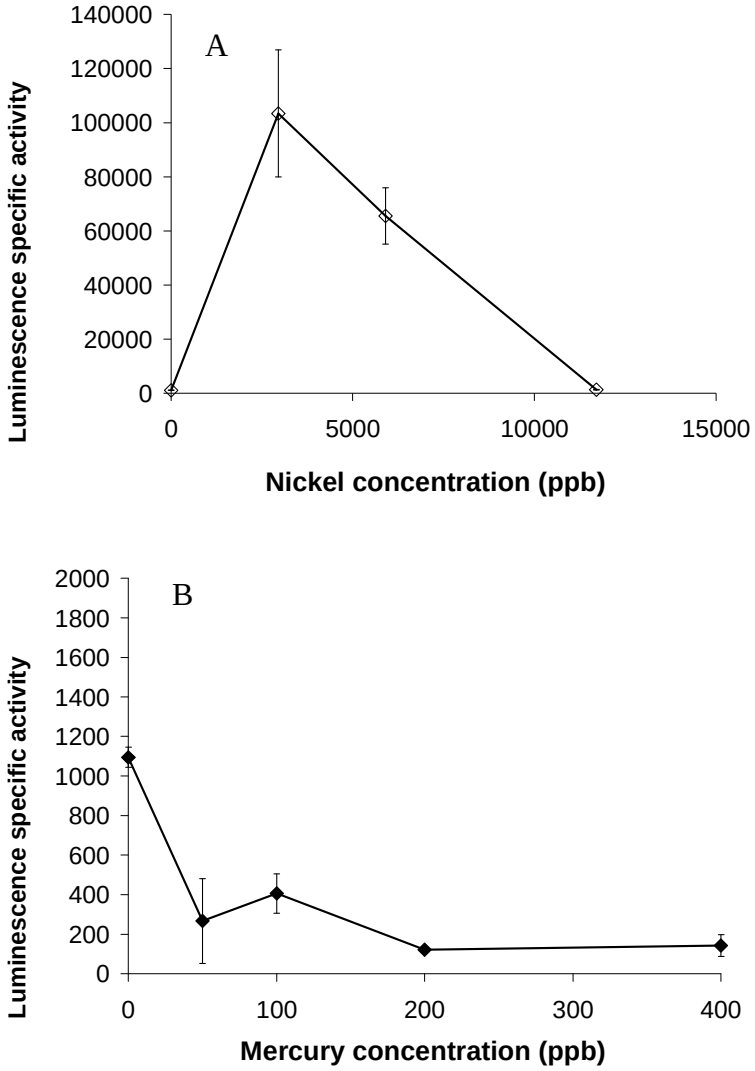

Figure 2. Induction of curli transcription by Ni and Hg. Luminescence specific activity (as defined by (Luminescence - Initial luminescence)/OD_{600}) of PHL628 pNLP55<TET-1> versus metal concentration (in ppb) of (A) Ni and (B) Hg at 14 hours after inoculation. Cultures were grown in 0.25x LB supplemented with 0.1% mannitol and varying metal concentrations at 30°C. Error bars represent standard deviation of triplicate samples.

Next, we assessed the potential for curli to alter the uptake of Hg(II). Fluorescence may be used as a surrogate measurement for mercury uptake in cells harboring pmerRGFP because fluorescence is produced only when Hg(II) enters the cytosol (8). We tested the response of PHL628 and PHL628 *csgA*$^{-}$ harboring pmerRGFP to mercury spikes ranging from 0 to 600 ppb and found that the curli-deficient strain had a higher normalized fluorescence (Fluorescence/OD_{600}) than the wild type strain over the range of concentrations tested (Figure 3). Several attempts at transforming cells harboring pBBR1MCS3:*csgA* with pmerRGFP proved unsuccessful, which was likely caused by plasmid incompatibility so unfortunately no uptake data could be obtained for the complement strain. The results with the other pmerRGFP reporters, however, support the idea that curli protect the bacteria from exposure to Hg(II) by reducing uptake. The simplest explanation for this result is that curli sequester the metal in the sheath they form on the outside of the cell, consequently preventing or delaying mercury from entering the cell.

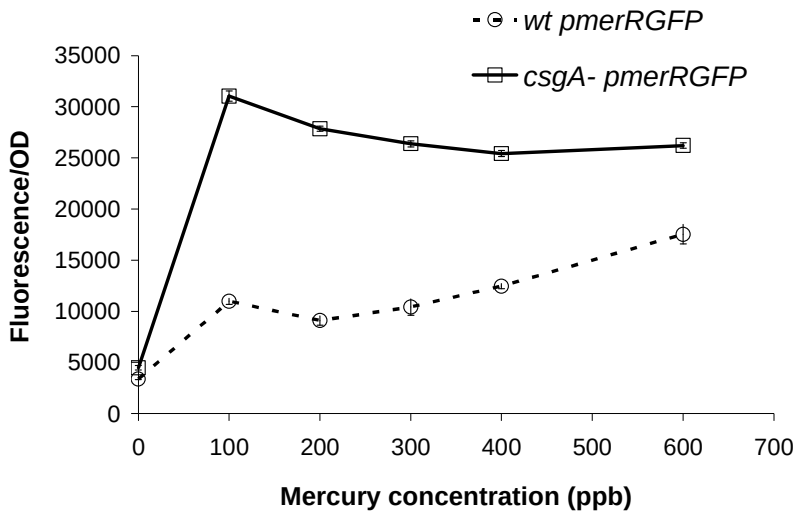

Figure 3. Hg uptake. PHL628 (dashed line) and PHL628 *csgA*$^-$ (solid line) cultures harboring pmerRGFP grown for 24 hours in GMM at 30°C were harvested and exposed to total Hg concentrations ranging from 0 to 600 ppb. Green fluorescence and OD_{600} of the cultures were recorded for the following 4 hours. For each condition, the fluorescence was divided by the OD_{600} and the resulting values from three independent experiments were averaged and plotted versus time. Error bars represent standard deviation of triplicate samples. Results at 4 hours after Hg introduction are shown.

To provide additional evidence in support of this hypothesis, and study the role of curli in Hg adsorption, we exposed stationary phase cells of PHL628 and PHL628 *csgA*$^-$ to a total Hg concentration of 50 or 150 ppb and measured the amount of Hg that sorbed to the cells at 1, 2, 4 8 and 24 hours (Figure 4). Quantitatively, these results indicate that curli speed up the kinetics of adsorption. More mercury adsorbed to cells with curli at equilibrium (see Table 3 and Figure 4) as would be expected if the curli provided additional surface area available for Hg(II) adsorption. The adsorption kinetics were modeled according to equation 2, and the rate constants and equilibrium concentrations obtained are shown in Table 3. At 150 ppb Hg(II) the magnitude of the fitted rate constant was approximately 40% lower for the curli-deficient strain. At 50 ppb Hg, the rate constant was approximately 80% lower. A more intuitive way of looking at this result is to calculate the time ($t_{1/2}$) required to reach half of the adsorbed Hg equilibrium value (C*/2) (Table 3). The presence of curli correlated with a $t_{1/2}$ approximately 5 and 2 fold lower at 50 ppb and 150 ppb Hg(II) respectively.

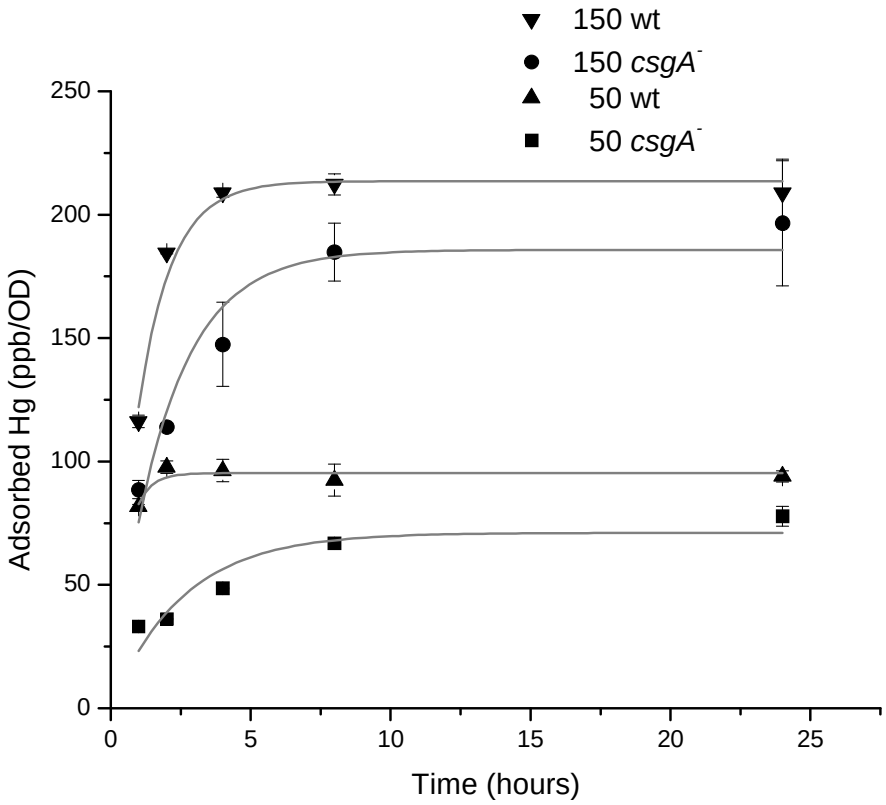

Figure 4. Hg adsorption kinetics to PHL628 strains at pH=7.2. Suspended cultures of *E. coli* PHL628 and *E. coli* PHL628 *csgA*$^-$ were grown in GMM at 30ºC to stationary phase. Aliquots of concentrated Hg solution were added to the cultures to yield total concentrations of 50 and 150 ppb Hg. Aliquots were withdrawn at predetermined intervals and soluble Hg concentrations were determined. Adsorbed Hg normalized by biomass was calculated as the difference between the total added and dissolved Hg concentrations and after correcting for background values it was divided by OD_{600} and plotted versus time. The points indicate the means ± the standard deviation of duplicate samples; the lines represent the calculated fit.

Table 3. Adsorption kinetics constants

Total Hg (ppb), strain	k (hr^{-1})	Standard deviation	C* (ppb/OD)	Standard deviation	$t_{1/2}$ (hr)
50, PHL628	2.00	0.30	95	2	0.35
50, PHL628 *csgA*$^-$	0.40	0.10	71	9	1.73
150, PHL628	0.85	0.07	214	5	0.82
150, PHL628 *csgA*$^-$	0.52	0.09	186	12	1.33

In this work we have shown that curli provide modest protection against mercury toxicity and appear to do so by sequestering the metal extracellularly, thereby reducing the amount that is bioavailable. This effect is likely a result of the increased curli-associated extracellular surface area available for metal adsorption. Curli have previously been shown to bind copper via a peptide repeat present in CsgA (QHGGGN) (4). Copper binding was assumed to be dependent on the imidazole moietie of the histidine residue in that motif. Given that Hg(II) is also known to form strong complexes with imidazole and histidine (3), it seems likely that the repeating QHGGGN motif also plays a role in the Hg-binding affinity we observed.

The prevalence of curli in biofilms from natural habitats has been demonstrated (17). Also, curli have been demonstrated to be involved in adhesion to surfaces, cell aggregation, environmental persistence, and biofilm formation, and are the main components of the extracellular matrix of many *Enterobacteriaceae* (2). Here we propose that curli can provide protection from toxic metals by sequestering them and hindering their transport into the cytoplasm. This conclusion is based on the following

observations: 1) the wild type was more resistant to toxic mercury concentrations than curli-deficient strains (Figure 1), 2) the uptake of Hg(II) increased in the absence of curli (Figure 3), and 3) bacteria without curli adsorb less Hg than curli-forming bacteria (Figure 4).

Taken together, our findings imply that Hg(II) is retained by sheath of curli fibers, reducing the concentration of mercury that reaches the cytoplasm and, as a result, provide protection to the cell from Hg(II) stress. This proposed mechanism will apply as long as there is an excess of curli adsorption sites to Hg. Once these sites are saturated, the protective effect of curli would disappear. To our knowledge, this is the first time that curli have been proven to protect bacteria from metal toxicity. Although more work is required in order to understand the exact mechanism of Hg(II) tolerance, the protective effect afforded by curli may be contribute to the widespread occurrence of these structures in enteric bacteria and environmental biofilms.

Acknowledgments

This research was supported, in part, by NSF grant EAR-0311767. Partial support for Gabriela Hidalgo was provided by the College of Engineering at Cornell University. We thank T. L. Raivio (University of Alberta, Canada) for providing plasmid pNLP55 and M. Virta (University of Turku, Finland) for plasmid pmerRGFP. We are grateful to J.M. Moran-Mirabal for help with the adsorption model.

REFERENCES

1. **Barkay, T., S. M. Miller, and A. O. Summers.** 2003. Bacterial mercury resistance from atoms to ecosystems. FEMS Microbiol Rev **27:**355-84.
2. **Barnhart, M. M., and M. R. Chapman.** 2006. Curli biogenesis and function. Annu Rev Microbiol **60:**131-47.
3. **Brooks, P., and N. Davidson.** 1960. Mercury(II) Complexes of Imidazole and Histidine. Journal of the American Chemical Society **82:**2118-2123.
4. **Cherny, I., L. Rockah, O. Levy-Nissenbaum, U. Gophna, E. Z. Ron, and E. Gazit.** 2005. The formation of Escherichia coli curli amyloid fibrils is mediated by prion-like peptide repeats. J Mol Biol **352:**245-52.
5. **Choi, K. H., A. Kumar, and H. P. Schweizer.** 2006. A 10-min method for preparation of highly electrocompetent Pseudomonas aeruginosa cells: application for DNA fragment transfer between chromosomes and plasmid transformation. J Microbiol Methods **64:**391-7.
6. **Fergusson, J. E.** 1990. The heavy elements: chemistry, environmental impact and health effects. Pergamon Press, New York, N.Y.
7. **Fletcher, M.** 1988. Attachment of Pseudomonas fluorescens to glass and influence of electrolytes on bacterium-substratum separation distance. J Bacteriol **170:**2027-30.
8. **Golding, G. R., C. A. Kelly, R. Sparling, P. C. Loewen, and T. Barkay.** 2007. Evaluation of mercury toxicity as a predictor of mercury bioavailability. Environmental Science & Technology **41:**5685-92.
9. **Hakkila, K., M. Maksimow, M. Karp, and M. Virta.** 2002. Reporter genes lucFF, luxCDABE, gfp, and dsred have different characteristics in whole-cell bacterial sensors. Anal Biochem **301:**235-42.

10. **Hammar, M., A. Arnqvist, Z. Bian, A. Olsen, and S. Normark.** 1995. Expression of two csg operons is required for production of fibronectin- and congo red-binding curli polymers in Escherichia coli K-12. Mol Microbiol **18:**661-70.

11. **Hammar, M., Z. Bian, and S. Normark.** 1996. Nucleator-dependent intercellular assembly of adhesive curli organelles in Escherichia coli. Proc Natl Acad Sci U S A **93:**6562-6.

12. **Hatch, W. R., and W. L. Ott.** 1968. Determination of submicrogram quantities of mercury by atomic absorption spectrophotometry. Analytical Chemistry **40:**2085-2087.

13. **Junker, L. M.** 2004. Examination of Biofilm Development Using Array Based and Molecular Approaches. Cornell University, Ithaca, NY.

14. **Keith, C. H., and W. A. Telliard.** 1979. Priority Pollutants I: a perspective view. Environ. Sci. Technol. Microbiol **13:**416-423.

15. **Kovach, M. E., P. H. Elzer, D. S. Hill, G. T. Robertson, M. A. Farris, R. M. Roop, 2nd, and K. M. Peterson.** 1995. Four new derivatives of the broad-host-range cloning vector pBBR1MCS, carrying different antibiotic-resistance cassettes. Gene **166:**175-6.

16. **Landini, P., G. Jubelin, and C. Dorel-Flamant.** 2006. The Molecular Genetics of Bioadhesion and Biofilm Formation, p. 21-40. *In* A. M. Smith and J. A. Callow (ed.), Biological Adhesives. Springer-Verlag, Heidelberg.

17. **Larsen, P., J. L. Nielsen, M. S. Dueholm, R. Wetzel, D. Otzen, and P. H. Nielsen.** 2007. Amyloid adhesins are abundant in natural biofilms. Environ Microbiol **9:**3077-90.

18. **Lederberg, J. (ed.).** 2000. Encyclopedia of Microbiology, vol. 3. Academic Press, San Diego.

19. **Leedjarv, A., A. Ivask, and M. Virta.** 2008. Interplay of different transporters in the mediation of divalent heavy metal resistance in Pseudomonas putida KT2440. J Bacteriol **190:**2680-9.

20. **Liss, S. N., I. G. Droppo, D. T. Flannigan, and G. G. Leppard.** 1996. Floc architecture in wastewater and natural riverine systems. Environmental Science & Technology **30:**680-686.

21. **McEldowney, S.** 1994. Effect of cadmium and zinc on attachment and detachment interactions of Pseudomonas fluorescens H2 with glass. Appl Environ Microbiol **60:**2759-65.

22. **Nies, D. H.** 2003. Efflux-mediated heavy metal resistance in prokaryotes. FEMS Microbiology Reviews **27:**313-339.

23. **Nies, D. H.** 2003. The Elements:Essential and Toxic Effects on Microorganisms. *In* K. Anke, M. Ihnat, and M. Stoeppler (ed.), Metals and their compounds in the environment. Wiley-VCH, Weinheim.

24. **Nies, D. H., and S. Silver (ed.).** 2007. Molecular Microbiology of Heavy Metals. Springer-Verlag, Berlin.

25. **Perrin, C., R. Briandet, G. Jubelin, P. Lejeune, M. A. Mandrand-Berthelot, A. Rodrigue, and C. Dorel.** 2009. Nickel promotes biofilm formation by Escherichia coli K-12 strains that produce curli. Appl Environ Microbiol **75:**1723-33.

26. **Price, N. L., and T. L. Raivio.** 2009. Characterization of the Cpx regulon in Escherichia coli strain MC4100. J Bacteriol **191:**1798-815.

27. **Prigent-Combaret, C., E. Brombacher, O. Vidal, A. Ambert, P. Lejeune, P. Landini, and C. Dorel.** 2001. Complex regulatory network controls initial adhesion and biofilm formation in Escherichia coli via regulation of the csgD gene. J Bacteriol **183:**7213-23.

28. **Romling, U., W. D. Sierralta, K. Eriksson, and S. Normark.** 1998. Multicellular and aggregative behaviour of Salmonella typhimurium strains is controlled by mutations in the agfD promoter. Mol Microbiol **28:**249-64.

29. **Silver, S.** 1996. Bacterial resistances to toxic metal ions--a review. Gene **179:**9-19.

30. **Song, B., and L. G. Leff.** 2006. Influence of magnesium ions on biofilm formation by Pseudomonas fluorescens. Microbiol Res **161:**355-61.

31. **Teitzel, G. M., A. Geddie, S. K. De Long, M. J. Kirisits, M. Whiteley, and M. R. Parsek.** 2006. Survival and growth in the presence of elevated copper: transcriptional profiling of copper-stressed Pseudomonas aeruginosa. J Bacteriol **188:**7242-56.

32. **Toba Francis, F. A.** 2008. Characterization of the Physiological Implications of Defective Lambdoid Phage DLP12 in *E. coli* Cornell University, Ithaca, NY.

33. **Ulett, G. C., R. I. Webb, and M. A. Schembri.** 2006. Antigen-43-mediated autoaggregation impairs motility in Escherichia coli. Microbiology **152:**2101-10.

34. **Vidal, O., R. Longin, C. Prigent-Combaret, C. Dorel, M. Hooreman, and P. Lejeune.** 1998. Isolation of an Escherichia coli K-12 mutant strain able to form biofilms on inert surfaces: involvement of a new ompR allele that increases curli expression. J Bacteriol **180:**2442-9.

CHAPTER 4

Hg(II) STRESS RESULTS IN UPREGULATION OF ARGININE BIOSYNTHESIS AND TRANSPORT IN *ESCHERICHIA COLI* MG1655

Abstract

A genome-wide transcriptional analysis was performed on *Escherichia coli* MG1655 cells grown in a subinhibitory concentration of Hg(II). Microarray analysis revealed upregulation of genes involved in metal homeostasis and heat-shock proteins, known bacterial responses to heavy metal stress. In addition, upregulation of genes for arginine biosynthesis and transport was observed. Growth of *E. coli* in Hg(II) did not reveal increased resistance to Hg(II) toxicity when the medium was supplemented with arginine. The upregulation of an arginine transport gene, *artJ*, by Hg(II) was confirmed with an *artJ-lux* reporter. Furthermore, exposure of the bioreporter to Zn(II) and Cd(II) revealed that these transition metals also induce transcription of *artJ*. A *merR-gfp* bioreporter for intracellular Hg(II) showed that arginine supplementation did not alter Hg uptake. Taken together our results indicate that group 12(IB) elements may act to induce the synthesis and transport of arginine, but that arginine production is not a strategy for alleviating their toxicity. To our knowledge, this is the first time a transcriptomic assay on Hg(II)-exposed cells has been conducted.

Introduction

Mercury and mercury derivatives are highly toxic to living organisms (44). Biotic and abiotic processes are involved in the cycling of Hg from soils and water to the atmosphere and back to the surface (3). One of the most important transformations of Hg(II) is its enzymatic methylation, which, in natural anaerobic environments, is mainly carried out by sulfate-reducing bacteria (10, 14, 15). In this reaction, soluble HgS is converted into methyl mercury (8), a potent neurotoxin that is bioaccumulated in the food web (3).

Another biotransformation of Hg(II) is its reduction by bacteria harboring the *mer* resistance operons. This reaction is part of a mercury detoxification strategy in which gene products encoded by the operon transport Hg^{2+} into the cytoplasm where mercuric reductases reduce it to Hg^0, a less soluble and therefore less bioavailable form (3, 44). The resulting Hg^0, can then leave the cell by passive diffusion and, because it is volatile, be removed from the growth environment (44). The *mer* operons are widespread and have been found in chromosomes, plasmids and transposons of Gram-negative and Gram-positive bacteria of both clinical and environmental origin (3). Broad-spectrum resistance operons are less common, but also confer the ability to resist toxic organic mercurial compounds such as methyl mercury and phenyl mercuric acetate by reduction to Hg^0 (9, 38, 41).

A more general strategy that bacteria utilize to cope with heavy metal stress is to actively export metal cations from the cytoplasm (45). P-type ATPases, CBA transporters and the cation diffusion facilitator (CDF) family of transporters are three types of export mechanisms (27, 33, 43). It is possible that other metal resistance

mechanisms also exist. For example, it has recently been reported that curli, amyloid extracellular fibers expressed by *Escherichia coli* and other enterobacteria, protect the cell from Hg(II) stress by acting as an extracellular adsorptive barrier that can inhibit transport of Hg(II) into the cytoplasm (22).

The purpose of this study was to utilize a genome-wide transcriptional analysis to determine how gene expression is affected by the presence of sublethal Hg(II) concentrations. *E. coli* MG1655 was used as a test organism and microarray technology was employed to evaluate changes in gene expression. Several prior studies have explored how *E. coli* responds to heavy metals such as cadmium (5, 21, 48, 50), zinc (5, 26) and copper (25, 52) and investigations have also considered the effect of heavy metals on the transcriptome of environmentally relevant bacterial species (36, 45). A review by Hobman *et al.* (23) summarizes the known biological effects of metal ion stress with data from genome-wide transcriptional profiling from different bacteria responding to these exposures. Although the transcriptional responses of bacterial cells to metals can be wide-ranging, in general metal ion stress causes bacteria to regulate genes responsible for metal ion homeostasis, oxidative stress responses, membrane stress responses, and the expression of metal ion efflux systems (23).

Amino acid synthesis pathways are also upregulated under many metal ion stress conditions. Hobman *et al.* (23) report that, in *E. coli* BW25113, Cu and Zn activate cysteine synthesis while Zn and Ni activate histidine synthesis (23). Wang and Crowley (48) observed the upregulation of *cys* genes responsible for cysteine biosynthesis in *E. coli* MG1655 after a Cd exposure. Lee *et al*. (26) report that in *E. coli* MG1655 cells exposed to Zn, *argA* and *argI*, genes that encode proteins in the

arginine biosynthesis pathway, as well as *astA*, a gene encoding a putative arginine transferase, were upregulated. Upregulation of arginine synthesis was also observed by Hobman *et al*. (23) after exposure to Ca(II) and to a lesser degree Fe(III).

Real-time gene-expression profiles for *E. coli* MG1655 after a mercury or a mitomycin spike have been described by Onnis-Hayden et al (34). For this study 93 different promoters of stress-response genes were fused to a fast folding *gfpmut2* to create a cell-array library. Exposure to Hg(II) revealed a number of genes encoding P-type ATPases and MerR family genes were upregulated and are hence presumed to be involved in mercury resistance. Particularly, the *zntA* gene which encodes a P-type ATPase known to transport the divalent soft-metals Pb^{+2}, Cd^{+2}, Zn^{+2} and Hg^{+2} (42) was upregulated in a concentration-sensitive manner. Relative to a traditional microarray, the approach presented by Onnis-Hayden *et al.* (34), has the advantage of allowing the recording of real-time change in gene-expression levels. On the other hand, this method can only analyze preselected genes. To the best of the authors' knowledge the investigation reported here is the first transcriptomic analysis of *E. coli* cells grown in Hg(II).

Materials and Methods

Bacterial strains and media

All experiments were carried out using *E. coli* strain MG1655 cells grown under aerobic conditions at 37°C. Liquid cultures were grown with rotary shaking at 150 rpm in a glucose minimal medium (GMMI) which contained per liter: 7 g K_2HPO_4, 2 g KH_2PO_4, 1 g $(NH_4)_2SO_4$, 200 mg $MgSO_4 \cdot 7H_20$, 24 mg $Ca(NO_3)_2 \cdot 4H_20$ and 10 g glucose as the sole carbon and energy source. A 20 mM concentration of 4-(2-

hydroxyethyl)-1-piperazineethanesulfonic acid) (HEPES) was added to buffer the pH at 7.2; subsequently the medium was sterilized by filtration though a 0.2 μm membrane. Glucose minimal medium II (GMMII) was prepared following the same procedure but 11.7 g/L (200 mM) NaCl was also added prior to sterilization. Water used for preparing GMM media and metal stocks was purified by a Thermo Scientific Mega-Pure System. As required, kanamycin (50 μg/mL) and ampicillin (100 μg/mL) were added. Analytical grade $HgCl_2$ was obtained from Mallinckrodt and used to prepare stock solutions which were acidified with a 70% concentration of trace metal grade HNO_3 to obtain a final 2% concentration of HNO_3.

Transcriptional profiling experiments

The culture conditions used in this study were as follows: a single colony was isolated from overnight culture on Luria-Bertani (LB) agar plates and inoculated into 5 mL of fresh GMMI. The overnight liquid culture was used as inoculum for fresh media (GMMI or II as indicated) and placed in 125 ml flasks. Aliquots of the $HgCl_2$ stock solution were added to achieve final concentrations of 0.00, 0.12, or 0.14 μM. All the liquid cultures used for this research were incubated at 37°C with rotary shaking at 150 rpm. Cell growth was monitored by harvesting 1 mL samples and placing them in 1 mm gap cuvettes. The optical density (OD_{600}) of the samples was measured at 600 nm using an Eppendorf Biophotometer spectrophotometer. 10 hours after incubation, 3 mL of culture were harvested in RNA Protect (QIAGEN) to stabilize the RNA. Total RNA was purified by using a QIAGEN RNeasy Mini kit as recommended by the supplier and RNA quality was assessed using an Agilent RNA 6000 Nano Kit with the Agilent 2100 Bioanalyzer. For each condition, samples were grown in triplicate and RNA from the different flasks individually analyzed. Synthesis of cDNA and application to the microarray were performed following the standard Affimetrix

protocol (Affimetrix Inc., Santa Clara, CA) for prokaryotic RNA. In this method, ds-cDNA is generated from 10 μg total RNA and labeled terminally with biotin. The arrays were scanned by GeneChip Scanner 3000.

The raw array data was processed by Affymetrix GCOS software to obtain detection calls and signal values. Further data analysis was performed using R statistical package (http://www.r-project.org/). The signals were $\log_2$-transformed after offset by 8. Gene filtering was applied to include only 6835 probe sets having at least 2 present call in the data set for further analysis. Two sample t tests were applied on the normalized log ratio of each probe set to evaluate differential gene expression between Hg(II)-treated versus untreated samples. Genes were considered to be differentially regulated if the P value was <0.05 and the absolute change (n-fold) was >1.5. cDNA synthesis, hybridization, scanning and data analysis were performed by the DNA Microarray Facility in the Life Sciences Core Laboratories Center at Cornell University.

Thermodynamic speciation

Mercury speciation in GMMI and II was calculated using the chemical equilibrium software MINEQL+ Version 4.5 (Environmental Research Software, Hallowell, ME) (40). The system was modeled as strictly aerobic (pe=10), open to the atmosphere (log P_{CO2}= -3.50) and with an ionic strength of 0.12 M and 0.32 M for GMMI and GMMII respectively. The pH was fixed at 7.2. Hg(II) speciation was calculated for two levels of chloride (0 and 200 mM) and is summarized in Table 1. Stability constants missing from the MINEQL+ database were obtained from Martell and Smith's Critical Stability Constants (31).

Table 1. Calculated speciation of main dissolved Hg(II) species in glucose minimal medium using MINEQL+. Calculations were carried out at 1.5 μM Hg(II).

Medium	$[Cl^-]$ (M)	Mercury species (as a percent of total Hg)	
GMMI	0	$Hg(NH_3)_2^{+2}$	99.3%
		$Hg(OH)_2$	0.7%
GMMII	200	$HgCl_2$	16.3%
		$HgCl_3^-$	33%
		$HgCl_4^-$	50.7%

Genetic methods

The ΔartJ::Kan^R mutation was transferred from *E. coli* strain BW25113 (1) to MG1655 by phage P1 *vir* transduction as described by Miller (32). Colonies resistant to kanamycin were selected and the mutation was confirmed by PCR amplification with primers internal and external to *artJ* (Table 2). Complementation of the mutant was achieved by transformation with the plasmid pNT3:*artJ* (39) followed by selection on kanamycin and ampicillin plates. Induction was achieved by adding isopropyl β-D-1-thiogalactopyranoside (IPTG) at 1 mM. Plasmid pmerRGFP (19) was used to transform MG1655 cells. All the transformations performed for this work were conducted as described by Choi *et al*. (7).

Table 2. PCR primers used in this study

Primer name	Sequence (5'→ 3')	Source or reference
artJF int	TTTCAGCCATTCGTTTACCACCGC	This study
artJR int	TTCAGCCACCTATCCACCCTTTGA	This study
artJF ext	GCGGCTTCAGATTGCTGACAAAGT	This study
artJR ext	CGGCGAAATTAATGTGGCTGCGTA	This study
pNLP10-F	GCTTCCCAACCTTACCAGAG	This study
pNLP10-R	CACCAAAATTAATGGATTGCAC	This study
DC393f	GGAATTCCGGACAACCCACTAAGTTG	Caldara, 2007
DC394r	CGGGATCCTTATGATTTTTGGCCGTG	Caldara, 2007

A P*artJ-lux* transcriptional *lux* reporter fusion was constructed by inserting the promoter-operator region P*artJ* in vector pNLP10 (37). P*artJ* was obtained as an EcoRI-BamHI, 124 bp long fragment by PCR amplification using *E. coli* MG1655 as a template and the primer pairs DC393f and DC394r designed by Caldara *et al.* (6). The PCR product and the vector were digested for 2 hours at 37°C with the restriction enzymes and ligated for 12 hours at 4°C. The insertion was confirmed by PCR amplification with primers pNLP10-F and pNLP10-R, which amplify the MCS region of pNLP10 (37). Subsequently the PCR product was purified and sequenced. All the primers used in this research are listed in table 2 and the strains and plasmids are in listed in table 3.

Table 3. *E. coli* strains and plasmids used in this study

Strains	Description	Source or reference
MG1655	F-, λ^-, *rph-1*	Laboratory collection
BW25113	Δ*artJ*::Kan^R	Baba, 2006
MG1655 *artJ*-	F-, λ^-, *rph-1*, Δ*artJ*::Kan^R	This study
JA200	F$^+$ *thr-1*, *leu-6*, DE*(trpE)5*, *recA*, *lacY*, *thi*, *gal*, *xyl*, *ara*, *mtl*	Saka, 2005
Plasmids		
pmerRFGP	Hg-uptake reporter vector; Amp^R	Hakkila, 2002
pNLP10	Low copy-number vector with promoterless luxCDABE operon, Kan^R	Price, 2009
pNLP10:*PartJ::luxCDABE*	pNLP10 with *PartJ::luxCDABE*, Kan^R	This study
pNT3:*artJ*	Low copy-number, IPTG inducible vector containing the entire *artJ* ORF plus 20 bp of the upstream region, Amp^R	Saka, 2005

Induction of arginine uptake by Hg(II), Zn(II) and Cd(II)

MG1655 pNLP10:*PartJ-lux* was grown in GMMI with arginine added at concentrations ranging from 0 to 10^{-2} M. Aliquots of Hg(II) were also added at subinhibitory concentrations ranging from 0 to $1.5x10^{-6}$ M. OD_{600} and luminescence of the cultures were measured over time using a Bio-Tek μQuant spectrophotometer and

a Packard LumiCount Luminescence Microplate Reader respectively. Triplicate samples of each condition were prepared and the luminescence and OD_{600} values of the replicate samples were averaged. Finally the transcriptional activity of the *artJ* promoter was quantified as relative luminescence units (RLU)/OD_{600}. The experiment was repeated adding Zn(II) at 10^{-4} M and $3x10^{-4}$ M or Cd(II) at $3x10^{-4}$ M instead of Hg(II) and arginine at 0, 10^{-6} and 10^{-3} M.

Growth curves in the presence of arginine and Hg(II)

An overnight GMMI culture of MG1655 was diluted 1:100 into fresh media. Aliquots of this suspension were placed in 50 mL sterile tubes and supplemented with arginine concentrations ranging from 10^{-7}M to 10^{-3} M. The cultures were also grown in the presence of Hg(II) at $1.5x10^{-6}$ M . A control culture with no added Hg(II) or arginine was also examined. OD_{600} was measured at periodic intervals by retrieving 200 μL aliquots and placing them in a 96-well microtiter plate; readings were made with a Bio-Tek μQuant spectrophotometer. MG1655 *artJ*- and MG1655 *artJ*- pNT3:*artJ* were also grown as described above and their OD_{600} recorded.

Hg uptake

A culture of MG1655 pmerRGFP was grown in GMMI. 10 hours after inoculation arginine was added to achieve final concentrations of 0, 10^{-7}, 10^{-5}, 10^{-4} and 10^{-2} M to aliquots of the culture. Hg(II) was also added at 0, $0.25x10^{-6}$, $0.5x10^{-6}$ and 10^{-6} M. OD_{600} and green fluorescence were recorded using a Bio-Tek Synergy HT spectrophotometer, with a 485/20 excitation filter and a 530/25 emission filter for fluorescence measurements. Each condition was performed in triplicate. Fluorescence was normalized diving by the corresponding OD_{600} of each culture.

Results and Discussion

In this study *E. coli* MG1655 was grown in a defined glucose minimal medium (GMM) at two different Cl^- concentrations: 0 (GMMI) and 200 mM (GMMII). Mercury was added at 0, 0.12 and $0.14x10^{-6}$ M Hg(II) (Figure 1). The speciation of mercury in the different media was calculated and is shown in Table 1. In the absence of chloride the speciation is dominated by the positively charged $Hg(NH_3)_2^{+2}$. At 200 mM Cl^-, the speciation becomes dominated by the negatively charged complexes $HgCl_4^-$ and $HgCl_3^-$ which account for approximately 51 and 33% of the total mercury added respectively. The neutral complex $HgCl_2$ accounts for the remaining 16%.

The transcriptomic response of *E. coli* in these different media was examined because a consensus within the scientific community has not been reached on the cellular mechanisms responsible for Hg uptake. One suggested mechanism for Hg uptake is via passive diffusion of nonionic Hg complexes such as $HgCl_2^0$ and $Hg(OH)_2^0$ (2, 4, 13, 18, 29). A second hypothesis is that import of Hg(II) occurs by facilitated uptake and is therefore mediated by a cellular protein and independent of Hg speciation (16, 17, 24). In this study a Hg(II) concentration of $0.14x10^{-6}$ M inhibited cell growth in GMMII (200 mM Cl^-); however, the same Hg concentration was only mildly toxic in GMMI (0 Cl^-). Hence, our cell growth data shows that Hg toxicity is dependent on metal speciation and is consistent with prior reports of diffusive uptake of neutral Hg(II) species such as $HgCl_2$.

RNA for transcriptional analysis was extracted from cultures grown at 0 and $0.12x10^{-6}$ M Hg(II) in GMMI and II at 10 hours after inoculation, during mid-log phase. Table 4 lists the top 15 genes with mRNA levels increased by a factor of more than 1.5 in the Hg treated culture relative to the control in either medium.

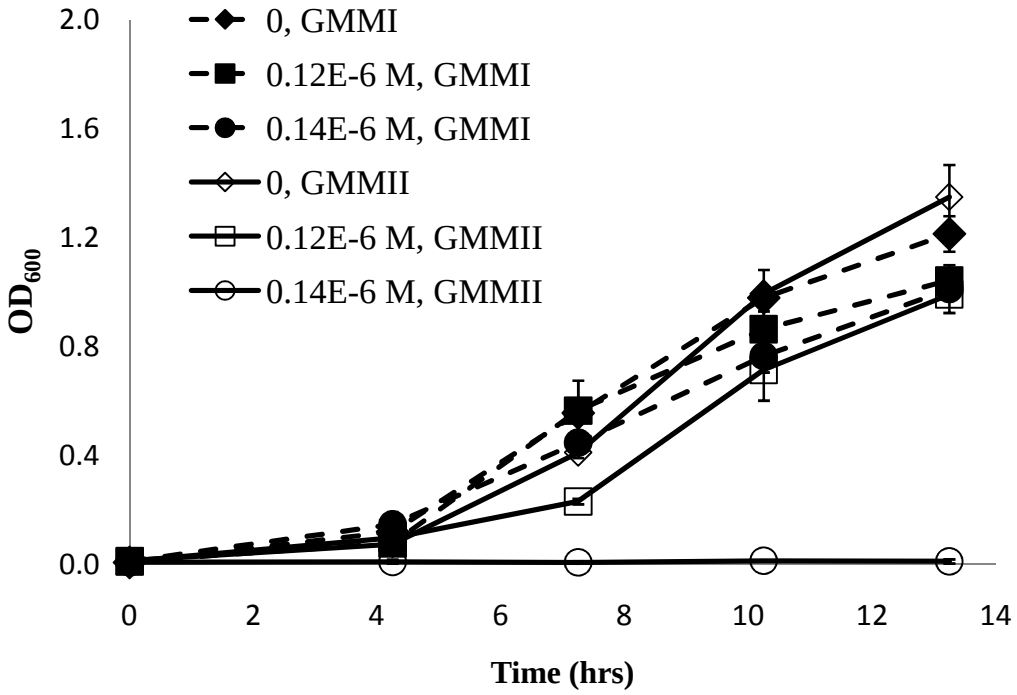

Figure 1. Growth curves of cultures used for transcriptional profiling. *E. coli* MG1655 cells were grown in GMMI (dashed lines) or GMMII (solid lines) at 0, 0.12 or 0.14 μM Hg(II). RNA was extracted at the 10-hour point for the cultures grown in GMMI at 0 (♦) and 0.12 μM Hg(II) (■) and in GMMII at 0 (◊) and 0.12 μM Hg(II) (□). Error bars represent standard deviation of triplicate samples.

Among the upregulated genes is *zraP*, which has also been shown to be induced by Zn(II) and by Pb(II) (28). The gene product of *zraP* is a periplasmic protein involved in zinc homeostasis (28). This is an expected result given that metal ion stress is known to induce the expression of metal homeostasis systems (23). More specifically, the detoxification of Hg by a Zn efflux pump has been reported by other laboratories (35) and is reasonable given that both Zn and Hg are group 12(IB) elements.

The gene encoding for the heat shock protein IbpB was also found to be upregulated when the bacteria were grown in Hg(II). Induction of heat shock proteins upon Hg exposure has been previously observed (35). Hg is a thiophilic metal and once it enters the cells it will coordinate to the sulfur-containing side chains of cysteine and methionine and cross-link thiol groups (23). This reaction results in the distortion of protein structure; therefore, the upregulation of chaperones that assist in the assembly and folding of proteins is expected (23). It is noteworthy that in the research reported by Onnis-Hayden *et al. (35)*, neither *zraP* nor *ibpB* were preselected for assessment of their response to Hg. Other genes upregulated in the presence of Hg are shown in Table 4.

Table 4. Top 15 genes whose mRNA levels displayed >1.5 fold increase for at least one of the two media after the addition of 0.12×10^{-6} M Hg(II) ($P<0.05$)

Gene	Gene product and/or function	Fold change in GMMI[a]	Fold change in GMMII[b]
ibpB	Heat shock protein	2.02	2.16
ygaW	Putative inner membrane protein	1.77	0.70
rpmE	L31 protein subunit of the ribosome	1.71	1.34
slp	Slp (starvation lipoprotein) is believed to take part in acid resistance.	1.53	0.96
yjbE	YjbE may be involved in biofilm formation.	1.53	1.21
zraP	Periplasmic protein involved in zinc homeostasis. ZraP binds zinc and, to a lesser extent, cobalt and cadmium.	1.31	3.62
fecD	Integral membrane protein part of the iron dicitrate ABC transporter.	1.02	1.52
fldA	FldA is a flavodoxin, a small, acidic electron transfer protein.	1.01	1.56
argD	ArgD catalyzes the amination step in lysine, ornithine, and arginine biosynthesis.	1.0	3.01
artJ	Component of the arginine ABC transporter. L-arginine is the natural substrate for ArtJ.	0.92	4.13
argB	Catalyzes the second step in ornithine and arginine biosynthesis.	0.88	2.39
argC	Catalyzes the third step in ornithine and arginine biosynthesis.	0.86	3.91

Table 4. (continued)

Gene	Gene product and/or function	Fold change in GMMI[a]	Fold change in GMMII[b]
argF	Subunit of ornithine carbamoyltransferase that catalyzes the sixth step in arginine biosynthesis.	0.69	3.76
carB	Subunit of carbamoyl phosphate synthetase which catalyzes reactions in the biosynthesis of pyrimidine nucleotides and arginine.	0.63	2.01
cvpA	Membrane protein required for colicin V production.	0.57	2.00

[a] Fold change refers to growth in GMMI relative to growth in GMMI + $0.12x10^{-6}$ M Hg(II)

[b] Fold change refers to growth in GMMII relative to growth in GMMII + $0.12x10^{-6}$ M Hg(II)

Upregulation of several arginine biosynthesis genes was also observed in the presence of Hg(II) (Table 4). Closer inspection reveals that these enzymes are active in the arginine biosynthesis pathway I, a linear pathway that has been identified in the *Enterobacteriaceae* (12) and other bacterial families (20, 46, 47, 51). The biosynthesis of arginine in this pathway begins with glutamate, which is acetylated to *N*-acetyl-glutamate (NAG) by the enzyme NAG synthase, encoded by the *argA* gene. In the following three steps NAG is converted to *N*-acetyl-ornithine. Removal of the acetyl group by the enzyme acetylornithine deacetylase, encoded by *argE*, results in L-ornithine. This intermediary is then combined with carbamoyl phosphate to form citrulline, which is converted by a two step process into L-arginine (12). Additionally,

arginine may be acquired via the ArtPMQJI arginine transporter, a member of the ATP-binding cassette (ABC) transporter superfamily (30). Arginine transport and biosynthesis pathway I are depicted in figure 2; the enzymes whose genes were upregulated in the Hg(II)-treated cultures are shown in bold.

One of the arginine metabolism genes that was upregulated in the Hg(II)-exposed cultures was *artJ*. In *E. coli*, ArtJ is located in the periplasm and hybridization studies indicated that L-arginine is the natural substrate for ArtJ (49). Overexpression of ArtJ resulted in stimulation of arginine uptake (49). Moreover, the amount of ArtJ found in the periplasmic extracts of *E. coli* was strongly reduced in bacteria grown with excess arginine (49). For the research presented here, we obtained *E. coli argB, carB* and *artJ* knockout mutants. Unfortunately, the *argB* and *carB* knockout mutants were not viable in the GMM media (data not included) so our further work focused on the *artJ* gene.

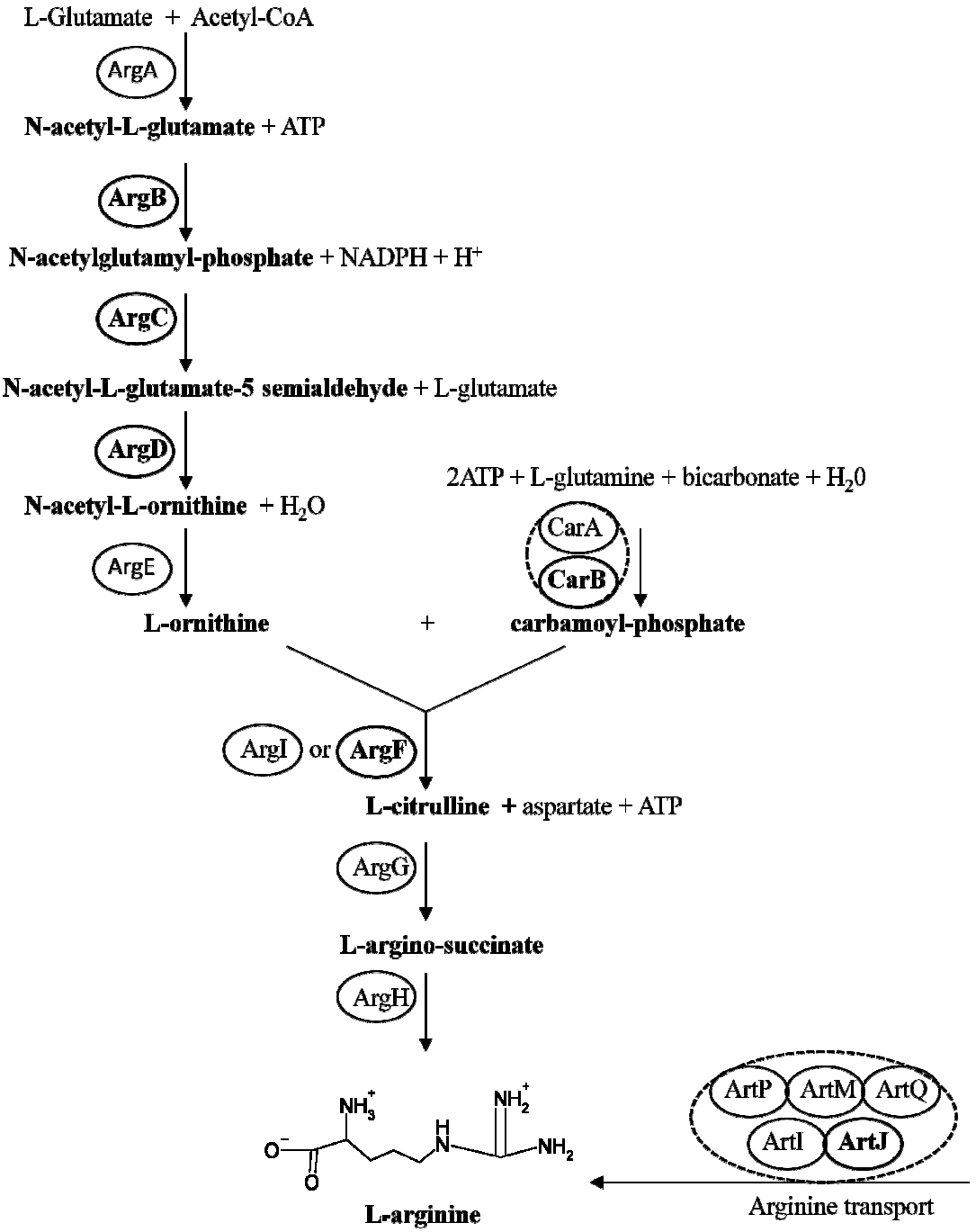

Figure 2. Arginine biosynthesis pathway I (based on http://biocyc.org/ECOLI/NEW-IMAGE?type=PATHWAY&object=ARGSYN-PWY) and transport. Enzymes are encased in an oval. Enzymatic complexes are further enclosed in a dashed-line oval. Enzymes of genes upregulated during growth on Hg(II) are shown in bold.

To our knowledge, there are no previous reports on the upregulation of arginine metabolism as a result of the exposure to Hg(II). We initially hypothesized that *E. coli* induces arginine acquisition and biosynthesis genes because complexation of the Hg(II) by arginine reduces the concentration of bioavailable Hg and thus results in a reduction of the toxic effects of Hg. Growth curves in GMMI supplemented with arginine concentrations ranging from 0 to 10^{-3} M and Hg(II) at a concentration of $1.5x10^{-6}$ M revealed that the presence of arginine did not result in increased Hg(II) tolerance (Figure 3A). Growth curves for the *artJ* knockout and the complement strain (Figures 3B and 3C respectively) confirmed that presence of arginine in the medium did not alleviate the toxic effects of Hg(II). The absence of the arginine transporter ArtJ did not alter the sensitivity to Hg(II). These results indicate that the upregulation of arginine biosynthesis and transport is not a means to reduce Hg(II) toxicity.

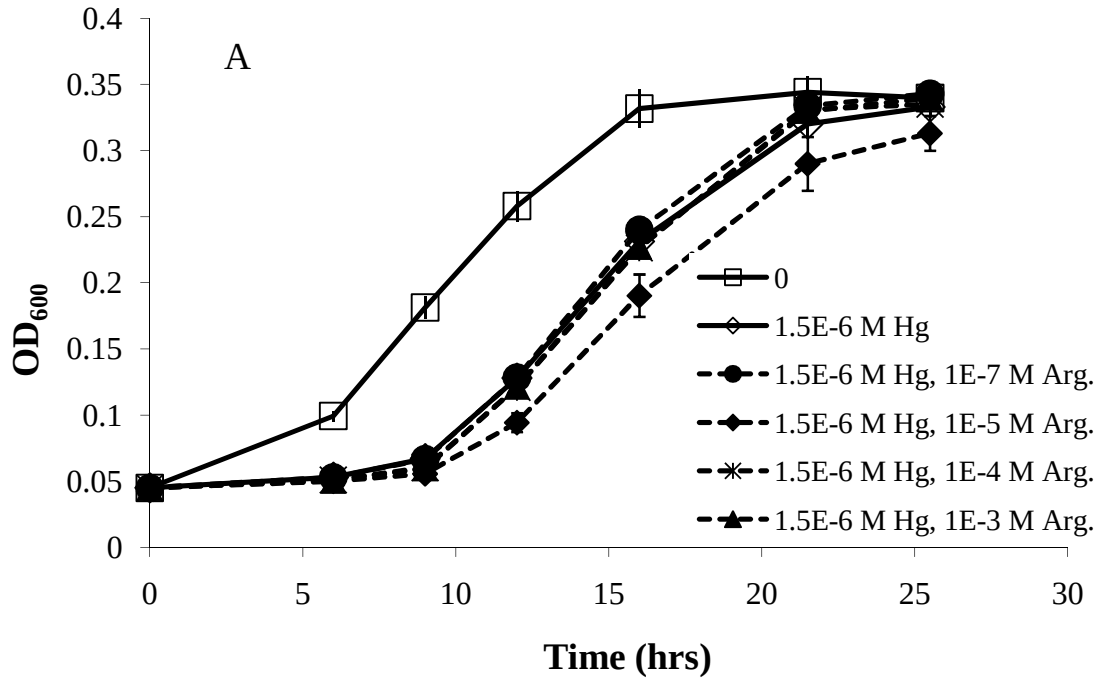

Figure 3. Growth curves for *E. coli* MG16155 strains in Hg(II) and arginine. (A) MG1655, (B) MG1655 *artJ*- and (C) MG1655 *artJ*- pNT3:*artJ* in GMMI at 0 and 1.5 μM Hg(II). Solid lines indicate the cells were grown in the basic medium, dashed lines indicate the bacteria were grown with an arginine supplement as indicated (where, for example, 1E-7 represents 1 x 10^{-7}, and Arg. stands for arginine). Error bars represent the standard deviation of triplicate samples. Figures 3B and 3C are shown on the following page.

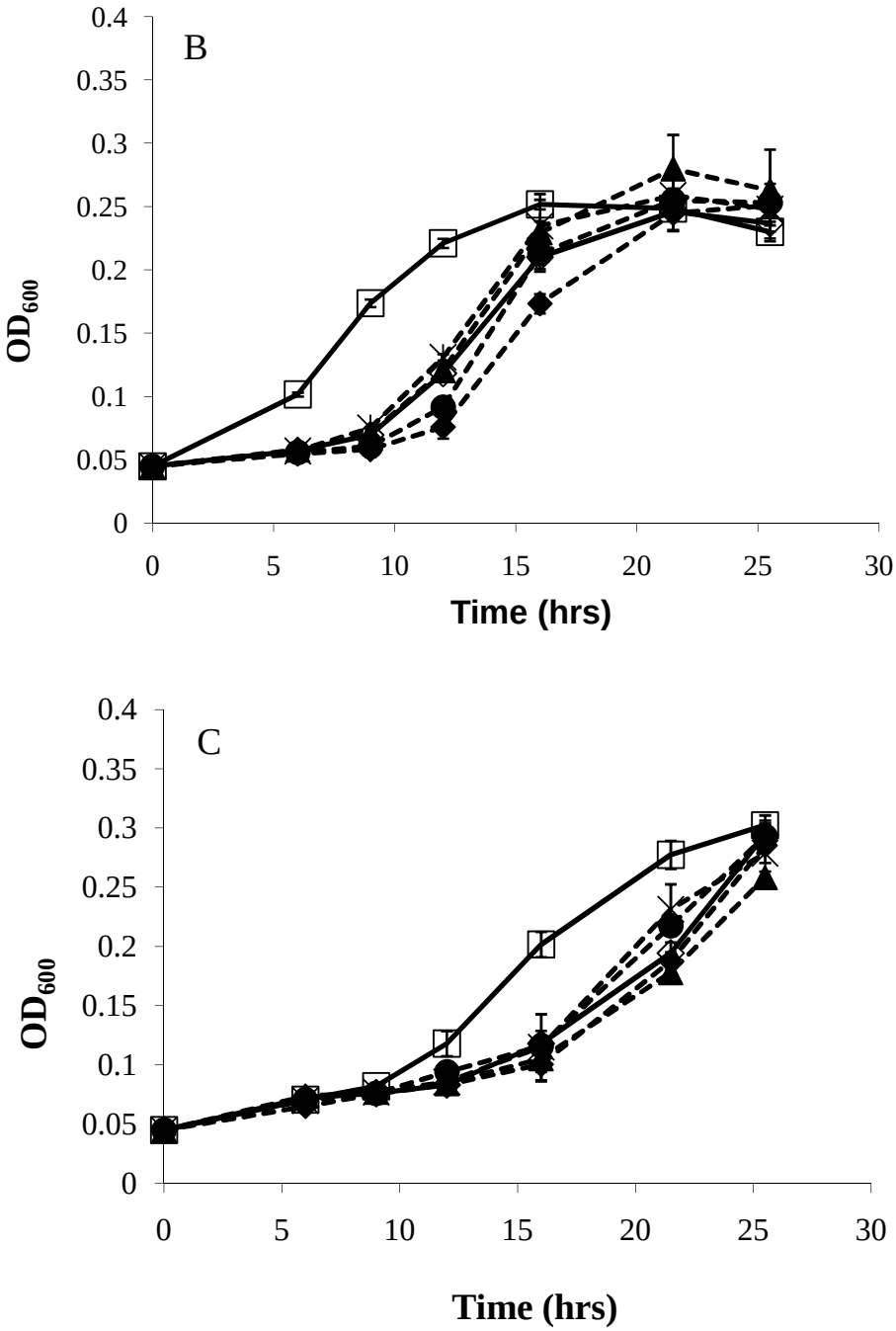

Figure 3. (continued) Growth curve for (B) MG1655 *artJ*- and (C) MG1655 *artJ*-pNT3:*artJ* in GMMI at 0 and 1.5 μM Hg(II).

The *artJ-lux* reporter results confirmed that arginine transport is upregulated in the presence of mercury in GMMI. As shown in figure 4A, increasing concentrations of mercury result in an increase in the specific luminescence (RLU/OD_{600}). Also, as expected, the specific luminescence decreases with increasing arginine concentration. Since *artJ* was upregulated in the presence of Hg(II) but arginine did not seem to protect the cells from Hg toxicity, we considered the possibility that arginine is complexed by Hg(II), rendering it unavailable and that *E. coli* then upregulates arginine biosynthesis and transport to supply needed arginine residues. Under this scenario exposure of the cells to the other group 12(IB) metals (Zn and Cd) should also result in upregulation of *artJ* because these metals should have a similar affinity for the amino acid as Hg. This hypothesis was tested by growing the *artJ-lux* reporter in the presence of Zn(II) and Cd(II) at subinhibitory concentrations (Figure 4B and 4C respectively). An increase in the luminescence/cell correlated with an increase in the metal concentration. This observation is consistent with the proposed model, *i.e.* that the increment in the level of expression of *artJ* with increasing group 12(IB) transition metal concentration is a result of the decrease of bioavailable, un-complexed arginine necessary for cellular metabolic needs.

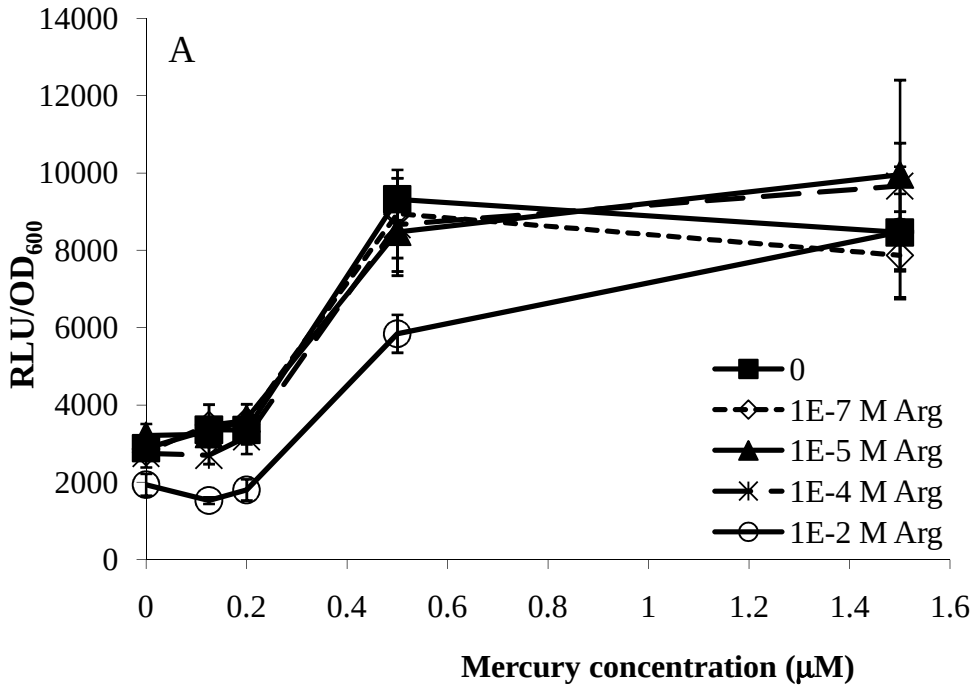

Figure 4. Luminescence/OD_{600} of the *artJ-lux* reporter versus metal concentration. Bacteria were grown in the presence of (A) Hg(II), (B) Zn(II) and (C) Cd(II) and varying concentrations of arginine. The results show how the specific luminescence increases with increasing metal concentration and decreases with increasing arginine concentration. Error bars represent standard deviation of triplicate samples. Figures 4B and 4C are shown on the following page.

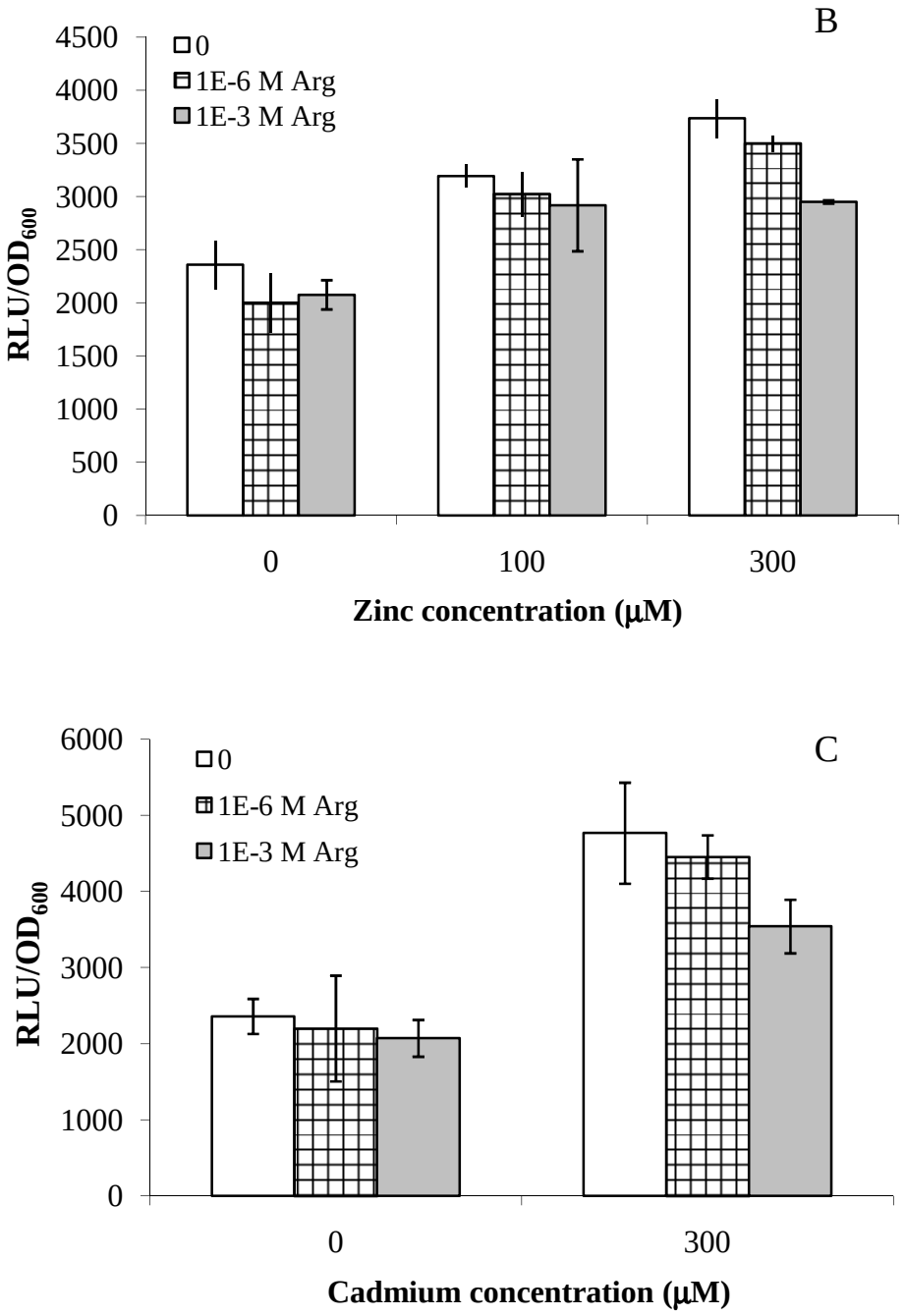

Figure 4. (continued) Luminescence/OD_{600} of the *artJ-lux* reporter versus metal concentration. Bacteria were grown in the presence of (A) Hg(II), (B) Zn(II) and (C) Cd(II) and varying concentrations of arginine.

A complementary approach used to test our hypothesis was to measure the uptake of Hg(II) in the presence of arginine. For this, *E. coli* K-12 MG1655 bacteria were transformed with pmerRGFP (Table 3) (19), a plasmid in which the reporter gene (*gfp*) is controlled by a mercury (*mer*) responsive regulatory unit. Fluorescence in transformed cells may be used as a surrogate measurement for mercury uptake because fluorescence is generated only when Hg(II) enters the cytoplasm (16). The *mer-gfp* reporter bacteria were grown and shocked with Hg(II) in media containing varying concentrations of arginine and the fluorescence and OD_{600} were measured. Figure 5 shows that the specific fluorescence (Fluorescence/OD_{600}) increased with increasing mercury concentration. However, for any given mercury concentration, the presence or absence of arginine did not alter the specific fluorescence.

The specific fluorescence data is consistent with our observation, based on cell growth curves, that arginine did not influence mercury toxicity. However, the result would only be consistent with the proposed effect of Hg on arginine uptake via arginine complexation if arginine speciation was primarily in the form of Hg complexes. Speciation calculations performed using the stability constants reported by Martell and Smith (31) indicate that mercury concentration was not dominated by complexation with arginine, even at a high molar ratio of Hg to arginine. Furthermore, the speciation of arginine in the medium showed that in an aquatic, aerobic and pH-neutral environment, arginine speciation is dominated by protonated arginine species. Specifically, in GMMI the $(H_2Arg)^+$ and HArg complexes account for approximately 99% and 1 % of the total arginine respectively. This result is independent of arginine, mercury or chloride concentration and is explained by the fact that guanidium, the arginine side chain, has a relatively high pKa (approximately 12.5) (11). The net free energy cost associated with proton dissociation from the guanidium group is very

high; therefore, this amino acid is not ordinarily considered an effective metal ligand (11, 53). Based on this data it would appear that the mechanism of the effect of Hg on upregulation of genes for arginine transport does not involve Hg complexation of arginine.

Since Hg does not interfere with the extracellular speciation of arginine, the remaining role it may play is through interfering with the proteins involved in making arginine available to the cell. For example it is possible that Hg(II) binds with the ArtJ transport protein and directly acts to interfere with the cellular supply of arginine. Hg interference with ArtJ would likely result in the observed upregulation of genes for arginine transport and synthesis.

In conclusion, our transcriptome assay of *E. coli* MG1655 cells exposed to a subinhibitory Hg(II) concentration showed a strong upregulation of arginine biosynthesis and uptake genes. Additional research showed that arginine does not reduce Hg toxicity or uptake and that other group 12(IB) transition metals also induce *artJ* transcription. Based on our results, we speculate that the mode of Hg(II) interaction with *E. coli* that elicits upregulation of the gene that codes for the ArtJ arginine transport protein, may be through Hg binding with the ArtJ transport protein. This proposed mechanism awaits experimental confirmation.

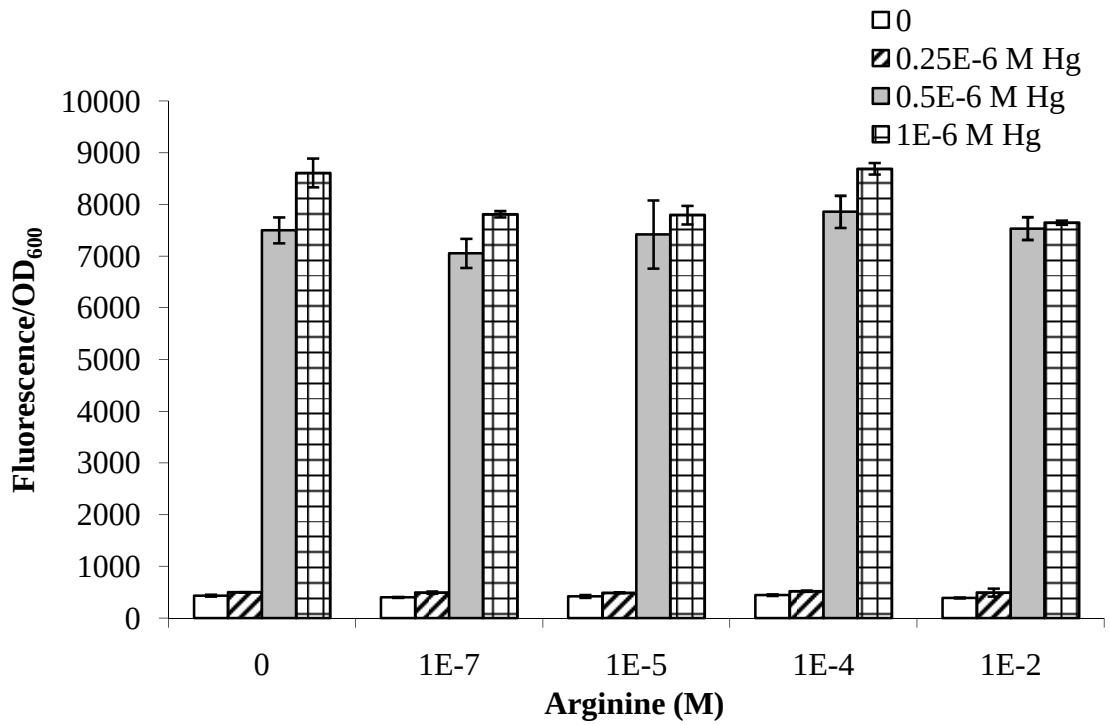

Figure 5. Hg uptake in the presence of arginine. MG1655 pmerRGFP cells were grown in GMMI and shocked with Hg(II) at 0, 0.25, 0.5 or 1E-6 M Hg(II). They were also supplemented with arginine at concentrations ranging from 0 to 10^{-2} M arginine. The results show how the presence of arginine did not alter Hg uptake. Data 4 hours after Hg(II) addition is shown. Error bars represent standard deviation of triplicate samples.

Acknowledgements

We thank T. L. Raivio (University of Alberta, Canada) for providing plasmid pNLP10 and M. Virta (University of Turku, Finland) for plasmid pmerRGFP. We also thank H. Niki and the National BioResource Project (NIG, Japan) for plasmid pNT3*:artJ*. Special thanks to W. Wang at the DNA Microarray Facility, Life Sciences Core Laboratories Center at Cornell University. Partial support for Gabriela Hidalgo was provided by the College of Engineering at Cornell University and NSF grant EAR-0311767.

REFERENCES

1. **Baba, T., T. Ara, M. Hasegawa, Y. Takai, Y. Okumura, M. Baba, K. A. Datsenko, M. Tomita, B. L. Wanner, and H. Mori.** 2006. Construction of Escherichia coli K-12 in-frame, single-gene knockout mutants: the Keio collection. Mol Syst Biol **2:**2006 0008.
2. **Barkay, T., M. Gillman, and R. R. Turner.** 1997. Effects of dissolved organic carbon and salinity on bioavailability of mercury. Appl Environ Microbiol **63:**4267-71.
3. **Barkay, T., S. M. Miller, and A. O. Summers.** 2003. Bacterial mercury resistance from atoms to ecosystems. FEMS Microbiol Rev **27:**355-84.
4. **Benoit, J. M., R. P. Mason, and C. C. Gilmour.** 1999. Estimation of mercury-sulfide speciation in sediment pore waters using octanol-water partitioning and implications for availability to methylating bacteria. Environmental Toxicology and Chemistry **18:**2138-2141.
5. **Brocklehurst, K. R., and A. P. Morby.** 2000. Metal-ion tolerance in Escherichia coli: analysis of transcriptional profiles by gene-array technology. Microbiology **146 (Pt 9):**2277-82.
6. **Caldara, M., P. N. Minh, S. Bostoen, J. Massant, and D. Charlier.** 2007. ArgR-dependent repression of arginine and histidine transport genes in Escherichia coli K-12. J Mol Biol **373:**251-67.
7. **Choi, K. H., A. Kumar, and H. P. Schweizer.** 2006. A 10-min method for preparation of highly electrocompetent Pseudomonas aeruginosa cells: application for DNA fragment transfer between chromosomes and plasmid transformation. J Microbiol Methods **64:**391-7.

8. **Choi, S. C., T. Chase, and R. Bartha.** 1994. Metabolic Pathways Leading to Mercury Methylation in Desulfovibrio-Desulfuricans Ls. Applied and Environmental Microbiology **60:**4072-4077.

9. **Clark, D. L., A. A. Weiss, and S. Silver.** 1977. Mercury and organomercurial resistances determined by plasmids in Pseudomonas. J Bacteriol **132:**186-96.

10. **Compeau, G. C., and R. Bartha.** 1985. Sulfate-Reducing Bacteria: Principal Methylators of Mercury in Anoxic Estuarine Sediment. Appl Environ Microbiol **50:**498-502.

11. **Creighton, T. E.** 1992. Proteins: structures and molecular properties, 2 ed. W.H. Freeman, New York.

12. **Cunin, R., N. Glansdorff, A. Pierard, and V. Stalon.** 1986. Biosynthesis and metabolism of arginine in bacteria. Microbiol Rev **50:**314-52.

13. **Farrell, R. E., J. J. Germida, and P. M. Huang.** 1993. Effects of chemical speciation in growth media on the toxicity of mercury(II). Appl Environ Microbiol **59:**1507-14.

14. **Gilmour, C. C., and E. A. Henry.** 1991. Mercury methylation in aquatic systems affected by acid deposition. Environ Pollut **71:**131-69.

15. **Gilmour, C. C., E. A. Henry, and R. Mitchell.** 1992. Sulfate Stimulation of Mercury Methylation in Fresh-Water Sediments. Environmental Science & Technology **26:**2281-2287.

16. **Golding, G. R., C. A. Kelly, R. Sparling, P. C. Loewen, and T. Barkay.** 2007. Evaluation of mercury toxicity as a predictor of mercury Bioavailability. Environmental Science & Technology **41:**5685-5692.

17. **Golding, G. R., C. A. Kelly, R. Sparling, P. C. Loewen, J. W. M. Rudd, and T. Barkay.** 2002. Evidence for facilitated uptake of Hg(II) by Vibrio anguillarum and Escherichia coli under anaerobic and aerobic conditions. Limnology and Oceanography **47:**967-975.

18. **Gutknecht, J.** 1981. Inorganic Mercury (Hg2+) Transport through Lipid Bilayer-Membranes. Journal of Membrane Biology **61:**61-66.

19. **Hakkila, K., M. Maksimow, M. Karp, and M. Virta.** 2002. Reporter genes lucFF, luxCDABE, gfp, and dsred have different characteristics in whole-cell bacterial sensors. Anal Biochem **301:**235-42.

20. **Harris, B. Z., and M. Singer.** 1998. Identification and characterization of the Myxococcus xanthus argE gene. J Bacteriol **180:**6412-4.

21. **Helbig, K., C. Grosse, and D. H. Nies.** 2008. Cadmium toxicity in glutathione mutants of Escherichia coli. J Bacteriol **190:**5439-54.

22. **Hidalgo, G., X. Chen, A. G. Hay, and L. W. Lion.** 2010. Curli Produced by Escherichia coli PHL628 Provide Protection from Hg(II) Submitted to Appl Environ Microbiol.

23. **Hobman, J. L., K. Yamamoto, and T. Oshima.** 2007. Transcriptomic Responses of Bacterial Cells to Sublethal Metal Ion Stress. *In* D. H. Nies (ed.), Molecular Microbiology of Heavy Metals. Springer-Verlag, Berlin.

24. **Kelly, C. A., J. W. M. Rudd, and M. H. Holoka.** 2003. Effect of pH on mercury uptake by an aquatic bacterium: Implications for Hg cycling. Environmental Science & Technology **37:**2941-2946.

25. **Kershaw, C. J., N. L. Brown, C. Constantinidou, M. D. Patel, and J. L. Hobman.** 2005. The expression profile of Escherichia coli K-12 in response to minimal, optimal and excess copper concentrations. Microbiology **151:**1187-98.

26. **Lee, L. J., J. A. Barrett, and R. K. Poole.** 2005. Genome-wide transcriptional response of chemostat-cultured Escherichia coli to zinc. J Bacteriol **187:**1124-34.

27. **Leedjarv, A., A. Ivask, and M. Virta.** 2008. Interplay of different transporters in the mediation of divalent heavy metal resistance in Pseudomonas putida KT2440. J Bacteriol **190:**2680-9.

28. **Leonhartsberger, S., A. Huber, F. Lottspeich, and A. Bock.** 2001. The hydH/G Genes from Escherichia coli code for a zinc and lead responsive two-component regulatory system. J Mol Biol **307:**93-105.

29. **Lin, C. C., and J. A. Jay.** 2007. Mercury methylation by planktonic and biofilm cultures of Desulfovibrio desulfuricans. Environmental Science & Technology **41:**6691-6697.

30. **Linton, K. J., and C. F. Higgins.** 1998. The Escherichia coli ATP-binding cassette (ABC) proteins. Mol Microbiol **28:**5-13.

31. **Martell, A. E., and R. M. Smith.** 1977. Critical stability constants. Plenum Press, New York.

32. **Miller, J. E.** 1972. Experiments in molecular genetics. Cold Spring Harbor Laboratory, Cold Spring Harbor, NY.

33. **Nies, D. H.** 2003. Efflux-mediated heavy metal resistance in prokaryotes. FEMS Microbiol Rev **27:**313-39.

34. **Onnis-Hayden, A., H. Weng, M. He, S. Hansen, V. Ilyin, K. Lewis, and A. Z. Guc.** 2009. Prokaryotic real-time gene expression profiling for toxicity assessment. Environ Sci Technol **43:**4574-81.

35. **Onnis-Hayden, A., H. F. Weng, M. He, S. Hansen, V. Ilyin, K. Lewis, and A. Z. Gu.** 2009. Prokaryotic Real-Time Gene Expression Profiling for Toxicity Assessment. Environmental Science & Technology **43:**4574-4581.

36. **Park, S., and R. L. Ely.** 2008. Genome-wide transcriptional responses of Nitrosomonas europaea to zinc. Arch Microbiol **189:**541-8.

37. **Price, N. L., and T. L. Raivio.** 2009. Characterization of the Cpx regulon in Escherichia coli strain MC4100. J Bacteriol **191:**1798-815.

38. **Rochelle, P. A., M. K. Wetherbee, and B. H. Olson.** 1991. Distribution of DNA Sequences Encoding Narrow- and Broad-Spectrum Mercury Resistance. Appl Environ Microbiol **57:**1581-1589.

39. **Saka, K., M. Tadenuma, S. Nakade, N. Tanaka, H. Sugawara, K. Nishikawa, N. Ichiyoshi, M. Kitagawa, H. Mori, N. Ogasawara, and A. Nishimura.** 2005. A complete set of Escherichia coli open reading frames in mobile plasmids facilitating genetic studies. DNA Res **12:**63-8.

40. **Scherer, W. D., and D. C. McAvoy.** 1994. MINEQL+: a chemical equilibrium program for personal computers., Environmental Research Software, Hallowell, Maine.

41. **Schottel, J., A. Mandal, D. Clark, S. Silver, and R. W. Hedges.** 1974. Volatilisation of mercury and organomercurials determined by inducible R-factor systems in enteric bacteria. Nature **251:**335-7.

42. **Sharma, R., C. Rensing, B. P. Rosen, and B. Mitra.** 2000. The ATP hydrolytic activity of purified ZntA, a Pb(II)/Cd(II)/Zn(II)-translocating ATPase from Escherichia coli. J Biol Chem **275:**3873-8.

43. **Silver, S.** 1996. Bacterial resistances to toxic metal ions - A review. Gene **179:**9-19.

44. **Silver, S., and J. L. Hobman.** 2007. Mercury Microbiology: Resistance Systems, Environmental Aspects, Methylation and Human Health. *In* D. H. Nies and S. Silver (ed.), Molecular Microbilogy of Heavy Metals. Springer-Verlag, Berlin.

45. **Teitzel, G. M., A. Geddie, S. K. De Long, M. J. Kirisits, M. Whiteley, and M. R. Parsek.** 2006. Survival and growth in the presence of elevated copper: transcriptional profiling of copper-stressed Pseudomonas aeruginosa. J Bacteriol **188:**7242-56.

46. **Vahedi-Faridi, A., V. Eckey, F. Scheffel, C. Alings, H. Landmesser, E. Schneider, and W. Saenger.** 2008. Crystal structures and mutational analysis of the arginine-, lysine-, histidine-binding protein ArtJ from Geobacillus stearothermophilus. Implications for interactions of ArtJ with its cognate ATP-binding cassette transporter, Art(MP)2. J Mol Biol **375:**448-59.

47. **Vandecasteele, M., M. Demarez, C. Legrain, N. Glansdorff, and A. Pierard.** 1990. Pathways of Arginine-Biosynthesis in Extreme Thermophilic Archaebacteria and Eubacteria. Journal of General Microbiology **136:**1177-1183.

48. **Wang, A., and D. E. Crowley.** 2005. Global gene expression responses to cadmium toxicity in Escherichia coli. J Bacteriol **187:**3259-66.

49. **Wissenbach, U., S. Six, J. Bongaerts, D. Ternes, S. Steinwachs, and G. Unden.** 1995. A third periplasmic transport system for L-arginine in Escherichia coli: molecular characterization of the artPIQMJ genes, arginine binding and transport. Mol Microbiol **17:**675-86.

50. **Worden, C. R., W. K. Kovac, L. A. Dorn, and T. R. Sandrin.** 2009. Environmental pH affects transcriptional responses to cadmium toxicity in Escherichia coli K-12 (MG1655). FEMS Microbiol Lett **293:**58-64.

51. **Xu, Y., Z. Liang, C. Legrain, H. J. Ruger, and N. Glansdorff.** 2000. Evolution of arginine biosynthesis in the bacterial domain: novel gene-enzyme relationships from psychrophilic Moritella strains (Vibrionaceae) and evolutionary significance of N-alpha-acetyl ornithinase. J Bacteriol **182:**1609-

15.

52. **Yamamoto, K., and A. Ishihama.** 2005. Transcriptional response of Escherichia coli to external copper. Mol Microbiol **56:**215-27.

53. **Yamauchi, O., and A. Odani.** 1996. Stability Constants of Metal Complexes of Amino Acids with Charged Side Chains - Part I: Positively Charged Side Chains Pure and Applied Chemistry **68:**469-496.

CHAPTER 5

CONCLUSIONS AND FUTURE WORK

Conclusions

The main conclusions stemming from the research reported in this thesis are:

- Ratiometric fluorescent silica nanoparticle sensors may be used for high resolution three-dimensional and time-domain functional fluorescence imaging of pH gradients in microbial biofilms. Particle size is a critical design criterion for nanoparticle probes for biofilm interrogation. 10 nm particles were successfully incorporated into biofilm matrices. Within a biofilm, pH microenvironments develop after the addition of a carbon source.

- Cells capable of synthesizing curli fibers are more resistant to toxic Hg(II) concentrations than curli-deficient strains. Curli interfere with Hg(II) uptake by slowing its internalization. Curli-forming bacteria adsorb more Hg(II) and at a faster rate than bacteria without curli. Hg(II) does not induce the transcription of curli genes.

- Exposure to subinhibitory concentrations of Hg(II) results in the upregulation of arginine biosynthesis and transport genes. Arginine uptake does not reduce Hg(II) toxicity or uptake. Zn(II) and Cd(II) also induce transcription of *artJ*, a gene that codes for an arginine uptake protein.

Future work

In the second chapter of this dissertation the research conducted on the morphology and temporal evolution of pH microenvironments in *E. coli* PHL628 and mixed-culture wastewater biofilms using C dot sensors is described. This novel technique allowed the observation, in real time, of the development of pH gradients within the bacterial biofilms after a glucose overlay.

This investigation may be taken one step further with the development of C dots that allow the simultaneous detection of metal ionss and pH in a minimally intrusive manner in live, hydrated biofilms. These sensors would be a valuable tool because pH is one of the main variables that determine metal speciation. Furthermore, metal toxicity usually correlates with the concentration of free metal cations so the proposed sensors would permit the investigator to determine the relationship between pH, metal speciation and biomass activity within a biofilm.

During the course of this research I observed that in the mixed-culture biofilm, different topographic morphologies were associated with areas of high or low pH. Therefore, another interesting approach in which this project could be pursued would be to use combined imaging techniques to simultaneously identify bacterial groups and pH within defined consortia biofilms. This type of research might be carried out by imaging C dot sensors concurrently with fluorescence *in situ* hybridization (FISH) probes or fluorescently labeled lectins. This protocol could aid in the identification of bacterial species or bacterial groups responsible for lowering or increasing the pH in environmentally or clinically relevant biofilm communities.

The third thesis chapter describes the research that was done to assess the effect that curli have on Hg toxicity, uptake and adsorption. This work showed that curli provide modest protection against mercury toxicity, probably by sequestering the metal extracellularly and therefore reducing the amount that is bioavailable. It is likely that the shielding effect of curli is a result of the increased curli-associated extracellular surface area available for metal adsorption. Furthermore, the protection afforded by curli may result from Hg(II) binding to the histidine residue present in the peptide repeat (QHGGGN) encoded by *csgA*.

To fully understand the mechanism of Hg(II) tolerance it would be necessary to demonstrate the direct binding of Hg(II) by the peptide repeat of the CsgA protein. This may be achieved using circular dichroism (CD) spectroscopy because Hg(II) binding by the peptide should alter the visible and UV regions of the CD spectra. Moreover, analysis of the CD spectra could yield information about the stoichiometry of the binding reaction. Ultimately, this would allow the estimation of the total Hg(II) binding capacity of curli.

The effect of Hg on the transcription of curli encoding genes was also evaluated as a part of this research. Using a *csgB-lux* reporter, it was demonstrated that exposure to Hg(II), as opposed to Ni(II), does not result in the upregulation of curli synthesis genes. However, it is reasonable to presume that nickel, like mercury, is sequestered extracellularly by the curli. Under that assumption, a curli-deficient (*csgA*-) strain would be expected have a higher intracellular concentration of nickel than the wild type, under equal total nickel concentrations. This hypothesis could be tested by evaluating the responsiveness of the *csgB-lux* reporter to nickel in a *csgA*- strain and

comparing it to the wild type. If in the *csgA*- strain lower concentrations of nickel are required to produce a similar specific luminescence signal than in the wild type strain, it might be concluded that some of the nickel is bound by the curli. With this experiment, the observation that curli adsorb Hg(II) could be generalized to Ni(II). Alternatively the adsorption of Ni(II) by curli could be directly measured by atomic absorption spectrometry.

The fourth chapter of the dissertation describes a genome-wide transcriptional analysis of *E. coli* MG1655 cells exposed to Hg(II). The results revealed the upregulation of arginine biosynthesis and transport genes upon Hg(II) exposure. Additional work led me to conclude that Hg(II) does not interfere with the extracellular speciation of arginine and that arginine does not protect the bacteria from the toxic effects of Hg(II). A possible explanation for the upregulation of arginine biosynthesis and transport genes is that Hg interferes with one of the enzymes in the arginine biosynthetic pathway. An initial experiment that may be conducted to test this hypothesis would be to grow the bacteria in a minimal medium supplemented with ^{14}C-glutamate (the arginine precursor) and all the amino acids save for arginine. The cells could be harvested after 10 or 12 hours of growth and lysed. Thin layer chromatography (TLC) followed by autoradiography of the lysates should reveal arginine and its metabolic intermediates on the gel. By comparing the lysates of cells exposed to Hg(II) to unexposed ones it should be possible to identify whether there accumulation of a particular intermediate. This would be an indication that Hg(II) is interfering with the enzyme active in the step following where the accumulation was observed.

The microarray analysis also revealed that *zraP*, a gene that encodes a periplasmic protein involved in zinc homeostasis is upregulated after a Hg(II) exposure. It has been reported that transcription of *zraP* is induced by Pb(II) and Zn(II) so it is reasonable to presume that Hg(II) also induces the transcription of *zraP*. This hypothesis may be tested by constructing a *zraP* reporter where induction of zraP would result in the production of some measurable signal, such as fluorescence or luminescence. *zraP* induction by Hg(II) could be confirmed if exposure of the bioreporter to Hg(II) results in an increase of the signal. Establishing correlations between Hg and Zn homeostasis might also be possible, for example, by testing if bacteria overexpressing *zraP* or if a *zraP* knockout are, respectively, more or less resistant to Hg(II) than the wild type. Furthermore, exposure to concentrations of Zn(II) or Pb(II) that induce *zraP* and that are subinhibitory should also result in increased tolerance to Hg(II).

APPENDIX 1

CYSTEINE INDUCES Hg(II) UPTAKE BUT REDUCES ITS TOXICITY TO *ESCHERICHIA COLI* MG1655

Abstract

The effect of cysteine on Hg(II) toxicity and bioavailability was tested. My results indicate that cysteine increases the uptake of Hg and that it also reduces Hg(II) toxicity. These results are consistent with a model in which a Hg-cysteine complex is more readily imported into the cell than the $Hg(NH_3)_2^{+2}$ complex which dominates Hg speciation in the absence of cysteine. Furthemore, an Hg-cysteine complex would have decreased affinity to bind other thiols within the cytoplasm, thus decreasing its toxicity to the cell. A *fliY*$^-$ mutant, deficient in the cystine uptake protein FliY, proved to be more sensitive to Hg(II) than the wild type strain.

Main Text

Mercury is a highly toxic metal that is found both naturally and as an introduced contaminant in the environment (7). The strong thiophilicity of mercury results in its coordination to the sulfur-containing side chains of cysteine and methionine and in the cross-linking of thiol groups, thereby disrupting protein structure and function (21). Nonetheless, the toxicity of mercury is determined, in great part, by the form in which it is present (26). For example, the organometallic compound methylmercury, CH_3Hg^+, is a potent neurotoxin that may be accumulated in the food web leading to adverse health effects on wild life and humans (17, 19). Biotic methylation of mercury in the environment is carried out by sulphate-reducing bacteria (6, 9) and other

anaerobes, such as iron-reducers (8, 13). On the other hand, Hg(II) may be reduced by bacteria harboring the *mer* resistance operons as a part of a detoxification strategy. In this reaction the gene products encoded by the *mer* operon transport ionic Hg^{2+} into the cytoplasm where mercuric reductases will reduce it to Hg^0, a volatile, less bioavailable form (2, 26). Given that bacteria may transform this hazardous pollutant into more or less toxic forms, a thorough understanding of the interactions between bacteria and mercury is of fundamental importance.

It has recently been reported that mercury methylation by the anaerobic bacterium *Geobacter sulfurreducens* is greatly enhanced in the presence of the amino acid cysteine (24). The goal of the work presented here was to assess the effect that cysteine would have on Hg(II) toxicity and uptake in an aerobic medium using the model bacterium *Escherichia coli* MG1655.

E. coli MG1655 harboring the pmerRGFP vector (11), a Hg(II) uptake reporter, was grown under aerobic conditions at 37°C in a glucose minimal medium (GMM) containing 7 g K_2HPO_4, 2 g KH_2PO_4, 1 g $(NH_4)_2SO_4$, 200 mg $MgSO_4 \cdot 7H_20$, 24 mg $Ca(NO_3)_2 \cdot 4H_20$, and 10 g glucose per liter. This solution was buffered with 4-(2-hydroxyethyl)-1-piperazineethanesulfonic acid) (HEPES) at pH = 7.2. After 12 hours of growth, the bacteria were centrifuged and resuspended in fresh media that was supplemented with enough cysteine to achieve concentrations ranging between 10^{-6} and 10^{-3} M. Hg(II) was added to a final concentration of 0 or $1.5x10^{-7}$ M. Fluorescence and optical density at 600 nm (OD_{600}) were recorded using a Bio-Tek Synergy HT spectrophotometer. Figure 1A shows the results 4 hours after the Hg(II) and cysteine addition and indicates how incubation in the presence of cysteine enhances the Fluorescence/OD_{600} signal. In these cells fluorescence may be used as an indicator of

mercury uptake because the fluorescent signal is only generated when Hg(II) enters into the cytoplasm (10); therefore, it may be concluded that the presence of cysteine results in an increase of Hg(II) uptake. Other amino acids (arginine, leucine, histidine) and carbon sources (acetate) were tested for fluorescence induction, but only cysteine showed the inductive effect (Figure 1B).

The behavior observed in figure 1A is similar to the one reported by Shaefer *et al.* (24) for the measurement of mercury methylation rate versus cysteine concentration. The authors proposed that cysteine is complexed by Hg(II). When the experiment was repeated in the presence of Cl^-, a competing ligand, they observed that Cl^- additions reduce Hg methylation rates. This was attributed to Cl^- outcompeting cysteine for the Hg, thereby preventing the formation of Hg-cysteine complexes. The sudden drop in Fluorescence/OD_{600} that occurs at 1 mM cysteine (Figure 1A) was also observed by Schaefer and Morel as a decrease in the methylation rate (19) and likely results of the formation of a tris complex ($Hg(cys)_3^{-4}$) (14).

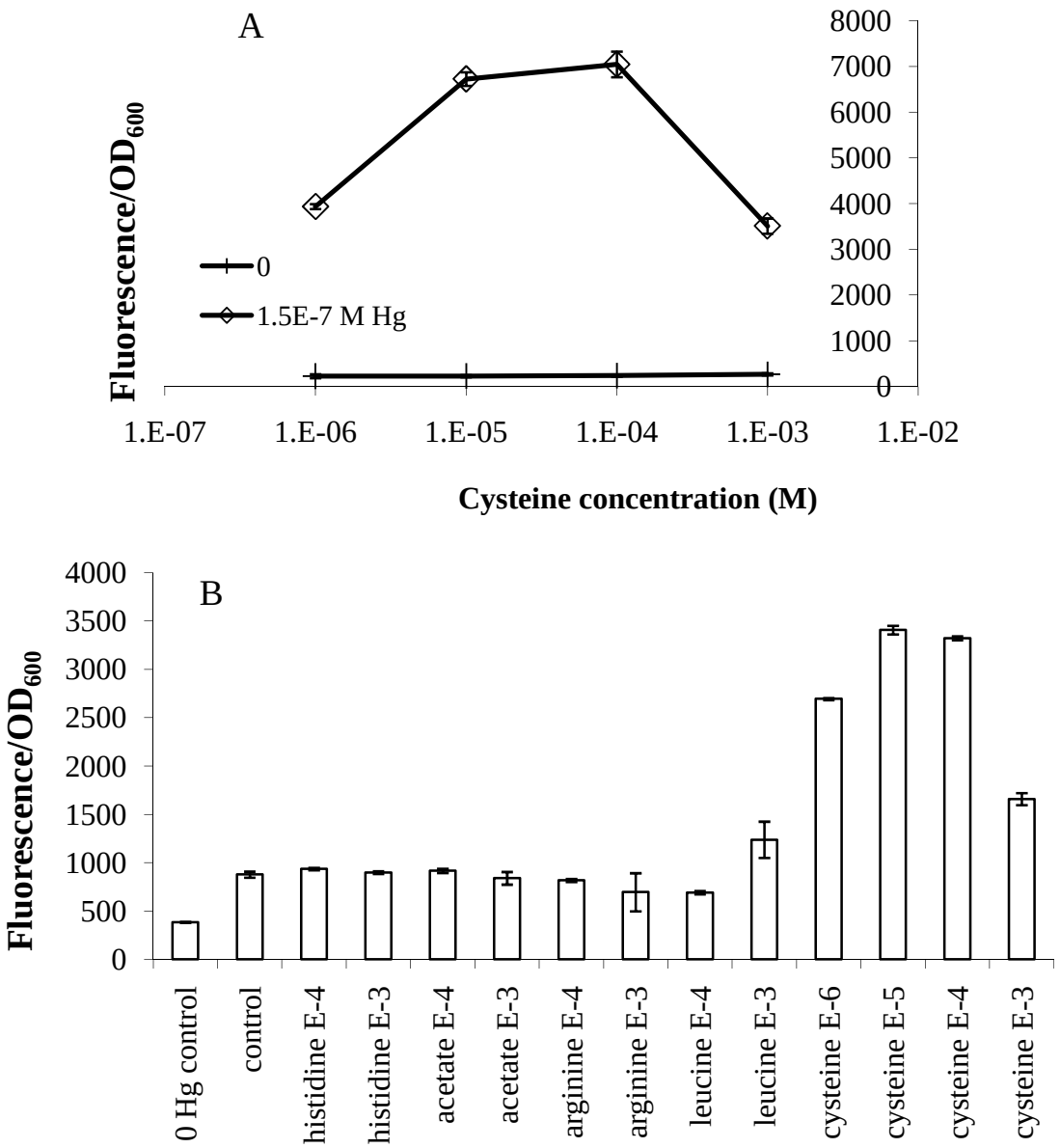

Figure 1. Cysteine induction of Hg(II) uptake. (A) Fluorescence/OD_{600} of *E. coli* MG1655 pmerRGFP cells induced with 0 (+) or $1.5x10^{-7}$ M Hg(II) (◊) in the presence of varying concentrations of cysteine. (B) Fluorescence/OD_{600} after a $1.5x10^{-7}$ M Hg(II) spike in media supplemented with the compounds indicated. The data shows points 4 hours after Hg(II) addition. Error bars represent the standard error of triplicate samples.

We assessed the formation of a Hg(II)-cysteine complex by calculating the thermodynamic speciation of mercury in GMM using the chemical equilibrium software MINEQL+ Version 4.5 (25). Missing stability constants from the MINEQL+ database were added as required (4, 16). The calculation showed that in GMM, Hg speciation is dominated by the $Hg(NH_3)_2^{+2}$ complex which accounts for 99% of the total Hg added. However, any cysteine added will complex the Hg and form $Hg(Cys)_2^{-2}$. Ultimately, if enough cysteine is available, 100% of the Hg added will be present in the $Hg(Cys)_2^{-2}$ form.

MerR is a dimeric, DNA-binding protein that regulates expression of the *mer* operon genes (2). The apo-MerR sits on the promoter/operator region of the operon and blocks access to the RNA polymerase, thereby repressing transcription (23). Addition of Hg(II) results in a conformational change of MerR that allows the polymerase to initiate transcription (23). MerR is a highly sensitive receptor that responds to nanomolar intracellular concentrations of Hg(II) (22). Each monomer of MerR has three of its four cysteine residues available for Hg(II) binding at the high-affinity binding site (12). In the plasmid pmerRGFP transcription of the reporter gene, *gfp* is regulated by MerR (11). Because of its higher affinity for Hg(II), MerR should be capable of pulling the Hg(II) from the $Hg(Cys)_2^{-2}$ complex. In this manner, induction of fluorescence can be achieved by the $Hg(Cys)_2^{-2}$ complex.

To test the effect of cysteine on Hg(II) toxicity, the bacteria were grown in GMM supplemented with cysteine at 0, 10^{-6}, 10^{-5} and 10^{-4} M and exposed to a suite of Hg(II) concentrations that ranged from 0 to $5x10^{-6}$ M. A time point at stationary phase for the growth curve is shown in Figure 2. This graph demonstrates how supplementation with cysteine reduced Hg(II) toxicity.

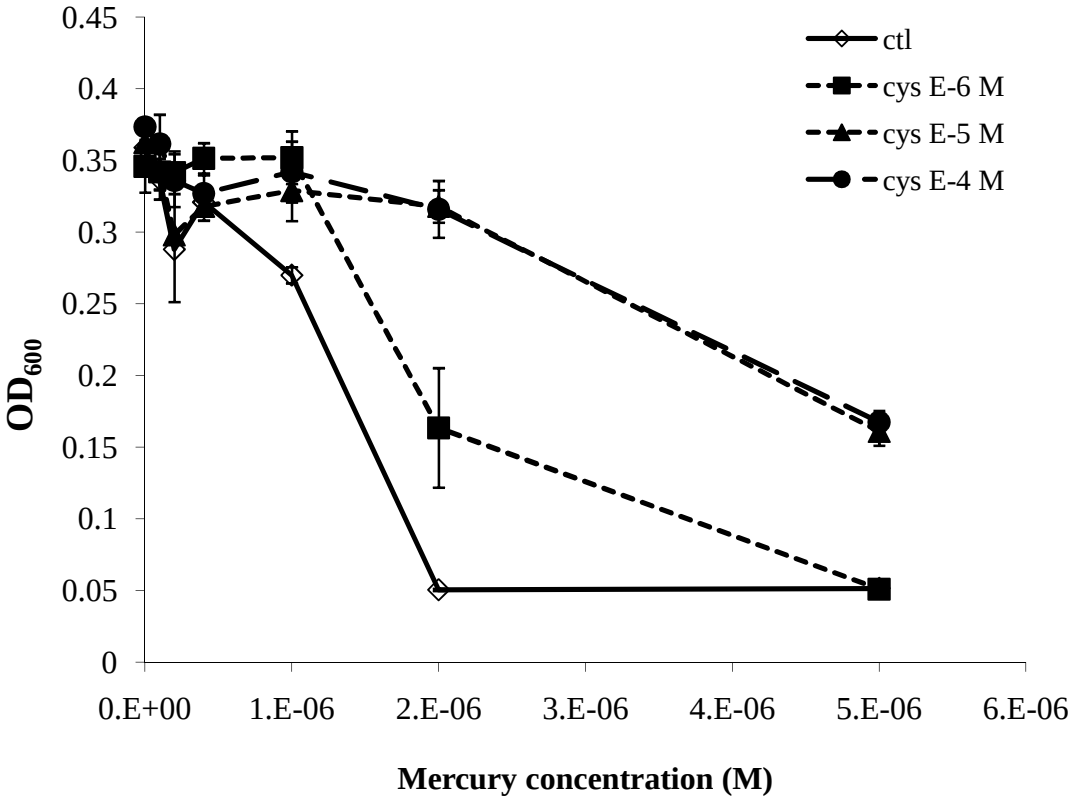

Figure 2. Growth curves for *E. coli* MG1655 in Hg(II) and cysteine. OD_{600} versus Hg(II) concentration for a culture of *E. coli* MG1655 grown in GMM and supplemented with cysteine at 0 (◊), 10^{-6} (■), 10^{-5}(▲) or 10^{-4} M (●) cysteine. The data shows a point in the stationary phase of the growth, 20 hours after inoculation. Error bars represent the standard deviation of triplicate samples.

Kinetic studies have shown that *E. coli* may actively transport L-cystine by either a high or a low affinity uptake system (3, 15) that are distinguishable on the basis of specificity and affinity for substrate. FliY is a periplasmic (20), cystine-binding protein (5) that comprises the high affinity cystine uptake system (20). The gene *fliY*, which encodes for this protein, is located within *fliAZY*, an operon related to flagella synthesis, but has been shown to have its own internal promoter (27) and its overexpression does not affect motility (20). To date, the low-affinity cystine uptake system has not been identified in the genome.

To gain further insight into the relationship between Hg(II) and cysteine we obtained a *fliY* mutant. The Δ*fliY*::Kan^R mutation was transferred from *E. coli* strain BW25113 (1) to MG1655 by phage P1 *vir* transduction as described by Miller (18). After selection on kanamycin, the mutation was confirmed by PCR amplification with internal primers FliYF (5'-TCACTGCTTTCAGCAGGTCCTCAT-3') and FliYR (5'-ACATCTGGGACGTCAGGCATTGAT-3'), and external primers Ext-FliYF (5'-TCTGCCGCGAGAAATTCCAGCTTA-3') and Ext-FliYR (5'-TTACCGCATCGCGTTACGGAAGTA-3'). The wild type strain and the *fliY*$^-$ mutant were grown in GMM with Hg(II) at 0, $5x10^{-7}$ and $1.5x10^{-6}$ M. Figure 3 shows that *fliY*$^-$ is more sensitive to Hg(II) than the wild type, as a concentration of $1.5x10^{-6}$ M Hg(II) inhibits growth of the mutant but not of the wild type strain.

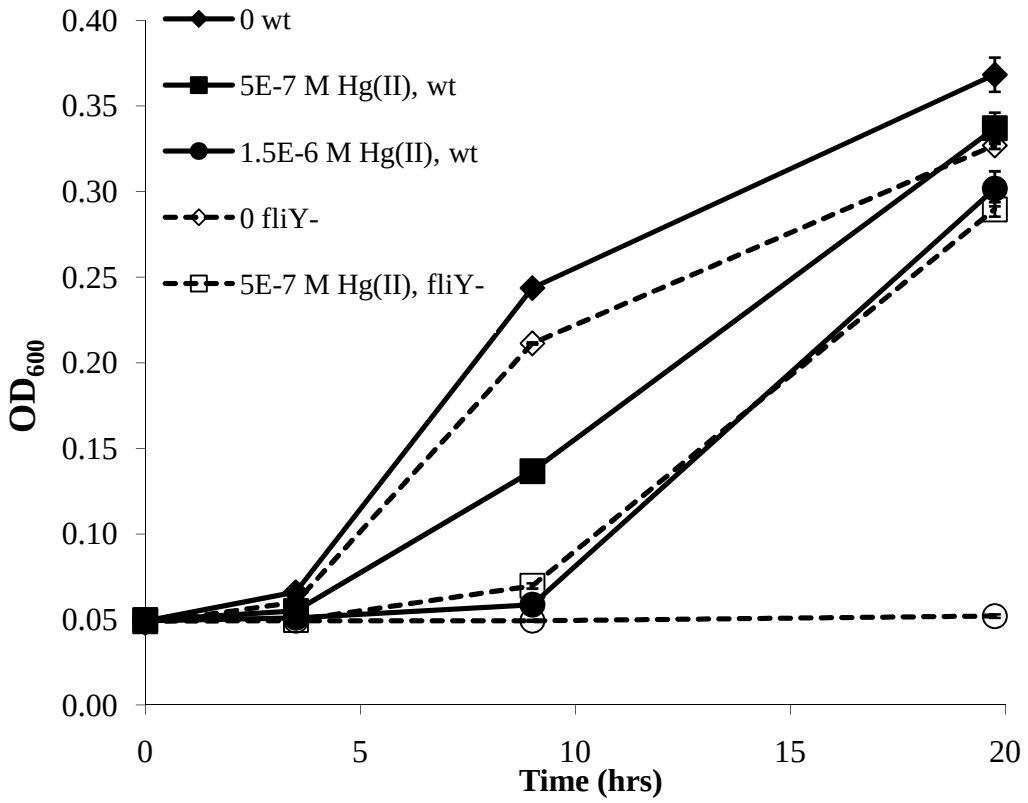

Figure 3. Growth curves of *E. coli* MG1655 and MG1655 *fliY*- in Hg(II) and cysteine. OD_{600} versus time for a culture of *E. coli* MG1655 (wild type, wt) (solid figures and lines) or MG1655 Δ*fliY*::Kan^R (*fliY*-) (dashed lines, empty figures) grown in GMM and Hg(II) at 0 (rhombus), $5x10^{-7}$ (square) or $1.5x10^{-6}$ M (circle). Error bars represent the standard deviation of triplicate samples.

In summary the results obtained are: 1) cysteine increases Hg(II) uptake, 2) cysteine reduces Hg(II) toxicity, 3) a reduced capacity for cysteine uptake results in increased Hg(II) sensitivity. Together, the data indicates that the $Hg(Cys)_2$ complex is more readily taken up by the cell, resulting in an increase in the specific fluorescence of a *mer-gfp* reporter. However, this complex appears to be less toxic than Hg(II) in other forms perhaps because it is less available for attack on other intracellular thiols. Absence of the FliY protein results in increased Hg(II) sensitivity. More experiments should be conducted to determine if the FliY protein is responsible for transporting the $Hg(Cys)_2$ complex.

Future Work

In order to obtain a more thorough understanding of the relationship between Hg, cysteine and their interactions with *E. coli* the following experiments are proposed:

- To create a *fliY* complement strain as well as a *fliY* overexpressing strain. Complementation of the *fliY* gene in the *fliY*$^-$ mutant should restore resistance to Hg(II) to wild type levels. Moreover, a strain that overexpresses *fliY* should be more resistant to Hg(II) than the wild type since higher intracellular concentrations of cysteine would be available to prevent Hg(II) caused toxicity.

- To create a *fliY*$^-$ pmerRGFP strain and repeat the induction experiment. If FliY transports cysteine exclusively and not the Hg-cysteine complex, the specific fluorescence of *fliY*- should be similar to that of the wild type. However if FliY does transport the Hg-cysteine complex, then the *fliY* mutant will show a reduction in fluorescence.

These recommended experiments would confirm that FliY provides the cell with cysteine, which reduces Hg(II) toxicity but that it is not responsible for transporting Hg into the cytoplasm.

REFERENCES

1. **Baba, T., T. Ara, M. Hasegawa, Y. Takai, Y. Okumura, M. Baba, K. A. Datsenko, M. Tomita, B. L. Wanner, and H. Mori.** 2006. Construction of Escherichia coli K-12 in-frame, single-gene knockout mutants: the Keio collection. Mol Syst Biol **2:**2006 0008.
2. **Barkay, T., S. M. Miller, and A. O. Summers.** 2003. Bacterial mercury resistance from atoms to ecosystems. FEMS Microbiol Rev **27:**355-84.
3. **Berger, E. A., and L. A. Heppel.** 1972. A binding protein involved in the transport of cystine and diaminopimelic acid in Escherichia coli. J Biol Chem **247:**7684-94.
4. **Berthon, G.** 1995. Critical Evalution of the Stability-Constants of Metal-Complexes of Amino-Acids with Polar Side-Chains. Pure and Applied Chemistry **67:**1117-1240.
5. **Butler, J. D., S. W. Levin, A. Facchiano, L. Miele, and A. B. Mukherjee.** 1993. Amino acid composition and N-terminal sequence of purified cystine binding protein of Escherichia coli. Life Sci **52:**1209-15.
6. **Compeau, G. C., and R. Bartha.** 1985. Sulfate-Reducing Bacteria: Principal Methylators of Mercury in Anoxic Estuarine Sediment. Appl Environ Microbiol **50:**498-502.
7. **Fergusson, J. E.** 1990. The Heavy Elements: Chemistry, Environmental Impact, and Health Effects. Pergamon Press, Oxford.
8. **Fleming, E. J., E. E. Mack, P. G. Green, and D. C. Nelson.** 2006. Mercury methylation from unexpected sources: molybdate-inhibited freshwater sediments and an iron-reducing bacterium. Appl Environ Microbiol **72:**457-64.
9. **Gilmour, C. C., E. A. Henry, and R. Mitchell.** 1992. Sulfate Stimulation of

Mercury Methylation in Fresh-Water Sediments. Environmental Science & Technology **26:**2281-2287.

10. **Golding, G. R., C. A. Kelly, R. Sparling, P. C. Loewen, and T. Barkay.** 2007. Evaluation of mercury toxicity as a predictor of mercury Bioavailability. Environmental Science & Technology **41:**5685-5692.
11. **Hakkila, K., M. Maksimow, M. Karp, and M. Virta.** 2002. Reporter genes lucFF, luxCDABE, gfp, and dsred have different characteristics in whole-cell bacterial sensors. Anal Biochem **301:**235-42.
12. **Helmann, J. D., B. T. Ballard, and C. T. Walsh.** 1990. The Merr Metalloregulatory Protein Binds Mercuric Ion as a Tricoordinate, Metal-Bridged Dimer. Science **247:**946-948.
13. **Kerin, E. J., C. C. Gilmour, E. Roden, M. T. Suzuki, J. D. Coates, and R. P. Mason.** 2006. Mercury methylation by dissimilatory iron-reducing bacteria. Appl Environ Microbiol **72:**7919-21.
14. **Kõszegi-Szalai, H., and T. L. Paál.** 1999. Equilibrium studies of mercury(II) complexes with penicillamine. Talanta **48**.
15. **Kull, F. J., C. Lindblow-Kull, and A. Shrift.** 1987. The transport systems for selenomethionine/methionine and selenocystine/cystine in Escherichia coli K-12 appear to be cooperative. Membr Biochem **7:**207-17.
16. **Martell, A. E., and R. M. Smith.** 1977. Critical stability constants. Plenum Press, New York.
17. **Mason, R. P., J. Reinfelder, and F. M. M. Morel.** 1995. Bioaccumulation of mercury and methylmercury. Water, Air, Soil Pollut. **80:**915-921.
18. **Miller, J. E.** 1972. Experiments in molecular genetics. Cold Spring Harbor Laboratory, Cold Spring Harbor, NY.
19. **Morel, F. M. M. K., A. M. L.; Amyot, M.** 1998. The chemical cycle and

bioaccumulation of mercury. Annu. Rev. Ecol. Syst. **29:**543-566.

20. **Mytelka, D. S., and M. J. Chamberlin.** 1996. Escherichia coli fliAZY operon. J Bacteriol **178:**24-34.

21. **Nies, D. H.** 2003. The Elements: Essential and Toxic Effects on Microorganisms. *In* A. Anke, M. Ihnat, and M. Stoeppler (ed.), Metals and their compounds in the environment. Wiley-VCH, Weinheim.

22. **O'Halloran, T. V.** 1993. Transition metals in control of gene expression. Science **261:**715-25.

23. **Outten, C. E., F. W. Outten, and T. V. O'Halloran.** 1999. DNA distortion mechanism for transcriptional activation by ZntR, a Zn(II)-responsive MerR homologue in Escherichia coli. J Biol Chem **274:**37517-24.

24. **Schaefer, J. K., and F. M. M. Morel.** 2009. High methylation rates of mercury bound to cysteine by *Geobacter sulfurreducens*. Nature Geoscience **2:**123-126.

25. **Scherer, W. D., and D. C. McAvoy. 1994. MINEQL+: a chemical equilibrium program for personal computers.** 1994. MINEQL+: a chemical equilibrium program for personal computers, 4.5 ed. Environmental Research Software, Hallowell, Maine.

26. **Silver, S., and J. L. Hobman.** 2007. Mercury Microbiology: Resistance Systems, Environmental Aspects, Methylation and Human Health. *In* D. H. Nies and S. Silver (ed.), Molecular Microbilogy of Heavy Metals. Springer-Verlag, Berlin.

27. **Zaslaver, A., A. Bren, M. Ronen, S. Itzkovitz, I. Kikoin, S. Shavit, W. Liebermeister, M. G. Surette, and U. Alon.** 2006. A comprehensive library of fluorescent transcriptional reporters for Escherichia coli. Nat Methods **3:**623-8.

APPENDIX 2

SUPPLEMENTARY INFORMATION FOR CHAPTER 2: FUNCTIONAL TOMOGRAPHIC FLUORESCENCE IMAGING OF pH MICROENVIRONMENTS IN MICROBIAL BIOFILMS WITH SILICA NANOPARTICLE SENSORS

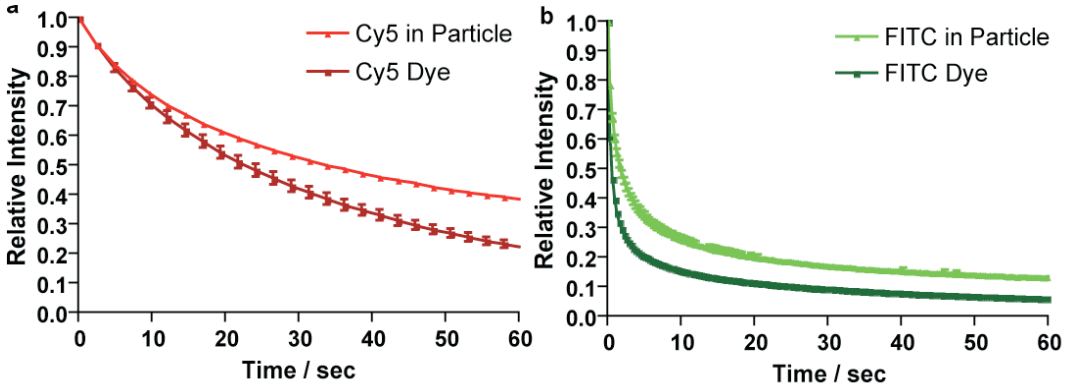

Supplementary Figure 1. Photobleaching characterization of C dot sensors compared to free dye. (a) A comparison of free Cy5 dye (dark red) to Cy5 in C dot sensor particles (light red) showing the increased photostability of the dye upon encapsulation in the silica matrix under illumination by a 4.5 mW excitation source. (b) A comparison of free fluorescein isothiocyanate dye (FITC, dark green) to FITC in C dot sensor particles (light green) showing the increased photostability of the dye upon encapsulation. In all imaging performed in this study, the excitation power and integration times were limited such that photobleaching did not affect pH quantitation in imaging.

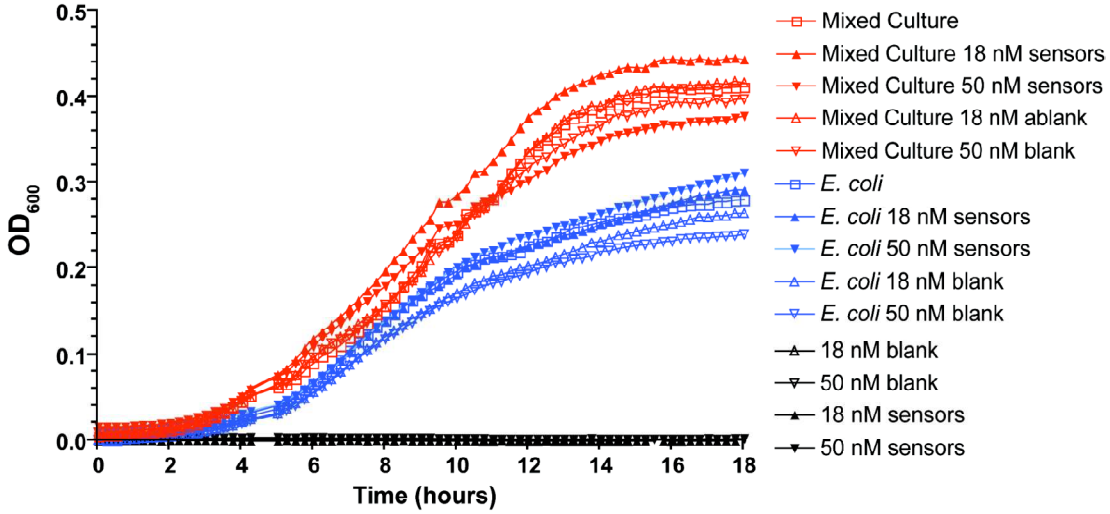

Supplementary Figure 2. Concentration-dependent growth curves for *E. coli* and mixed cultures. Demonstrates the minimal perturbations induced in the microbial environment by addition of 10 nm diameter bare silica sensors (filled) and 10 nm diameter bare silica particles without dye (outline) at 18 and 50 nM in *E. coli* (blue) and wastewater (red) cultures along with sterile controls (black).

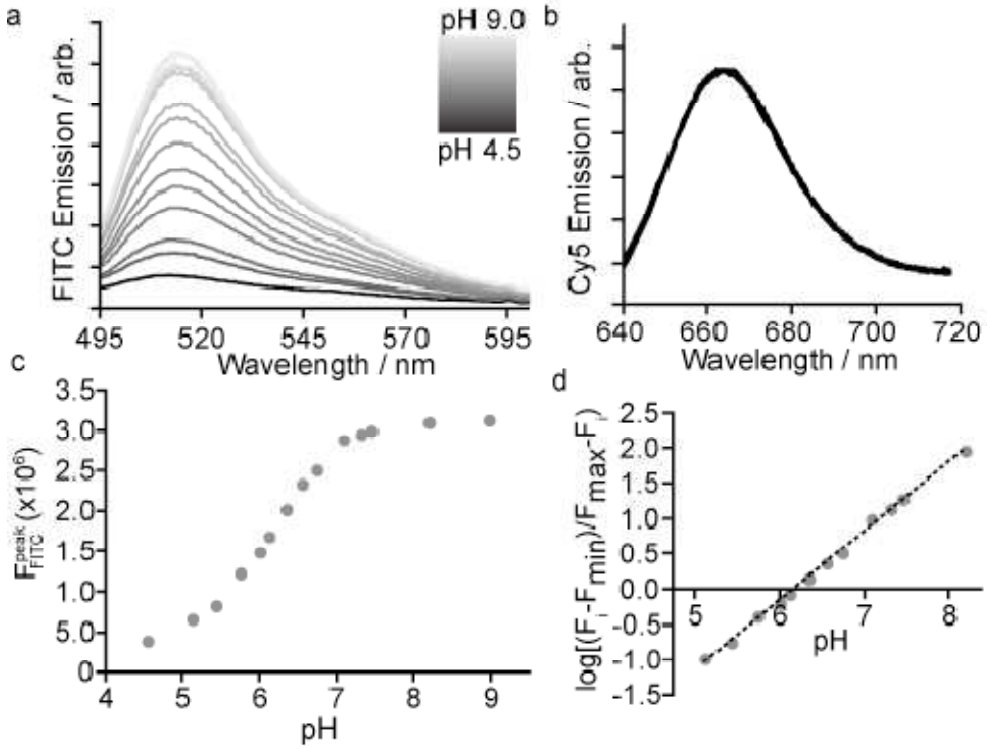

Supplementary Figure 3. Spectrofluorometric Calibration of C Dot Sensors. **(**a) sensor and (b) reference emission spectra upon excitation at 488 and 633 nm, respectively in calibration buffers of varying pH. (c) plot of pH versus peak intensity ratio ($F_i = I_{FITC}/I_{Cy5}$) and (d) a modified Henderson-Hasselbalch analysis (Eq. 1) of the data used to generate the calibration curve used in Figures 2 b and d.

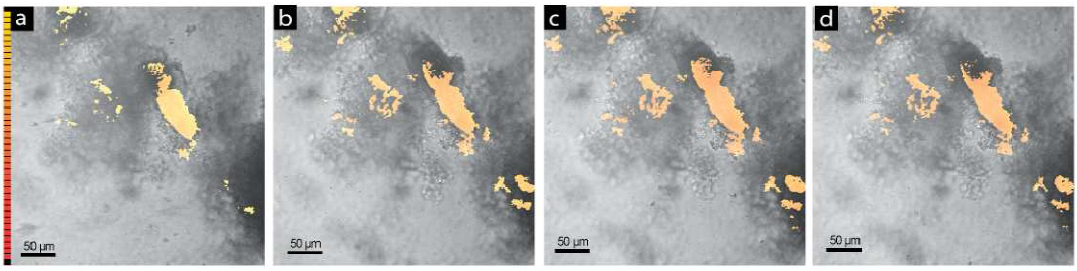

Supplementary Figure 4. Time-resolved *in situ* pH measurements in biofilms. pH imaging post injection of 90 mM glucose to biofilms to *E. coli* PHL628 at 0, 30, 60 and 90 minutes post injection. (Color scale corresponds to pH values from 4 to 8).

Polymer-Particle Size Calculations

Using dextran as a model extracellular polysaccharide, the root mean square (RMS) endto-end distance for a polymer chain can be calculated based on the relationship shown in Equation S1, where R_0 is the RMS end-to-end distance, a_k is the Kuhn length of the polymer and N_k is the number of Kuhn segments in a polymer of a given molecular weight.

$$R_O = a_K.\sqrt{N_K} \qquad \text{Eqn. S1}$$

The number of Kuhn segments can be determined from the contour length of the polymer divided by the Kuhn length as shown in Equation S2, where M is the molar mass of the polymer chain in question, M_0 is the monomer molar mass and L_0 is the length of a single monomer.

$$N_K = \frac{M.L_O}{M_O.a_K} \qquad \text{Eqn. S2}$$

Thus, R_0 can be determined for various molecular weight polymers by Equation S3.

$$R_O = a_k.\sqrt{\frac{M.L_O}{M_O.a_K}} \qquad \text{Eqn. S3}$$

Using literature values for the properties of dextran as a model system, assuming molecular weight values from 10kDa to 100kDa as representative of the highly polydisperse matrix material that forms a biofilm, the results are as follows:

$L_{O\ \text{Dextran}} = 0.41$ nm $\qquad R_{O\ 10\text{KDa}} = 3.9$ nm

$a_{K\ \text{Dextran}} = 0.60$ nm $\qquad R_{O\ 100\text{KDa}} = 12.4$ nm $\qquad$ Eqns. S4

$M_{O\ \text{Dextran}} = 162.14$ g/mol

Thus, sensor particles with ~10nm diameter would be much more likely to be well solubilized by the extracellular polymers of a biofilm than would 30-70nm particles, for which the entropic penalty would likely result in exclusion from the film.

Matlab Files

(background, calibration, volumetric and time-resolved m-codes)

```
%Background image analysis and averaging of WW Image Settings 041608
%for Leica Confocal Images 512x512 12-bit
%ww Image Settings => PMT2=X, PMT3 = X
%input = images
%output = averages & standard deviations of whole images
% averaged images

%read in filenames
filesg = dir('*backgd *00.tif');      % green images from ch00
filesr = dir('*backgd *01.tif');      % red images from ch01

%set zeros
cg=double(zeros(512,512));
cr=double(zeros(512,512));
c=double(zeros(512,512));
avg24=double(zeros(1,2));
stdev24=double(zeros(1,2));

%read in images
       for k=1:numel(filesg);
           c=double(imread(filesg(k).name)); %read in green image files
           cg=cg+medfilt2(c);                %add up pixel values after
                                             %median filtering (remove high
                                             %variance noise)
           c=double(imread(filesr(k).name));
           cr=cr+medfilt2(c);
       end
%divide sums by number of images
cr=cr/(numel(filesr));
cg=cg/(numel(filesg));

%compute averages & save
avg24(1,1)=mean(nonzeros(reshape(cg,262144,1)));
avg24(1,2)=mean(nonzeros(reshape(cr,262144,1)));
stdev24(1,1)=std(nonzeros(reshape(cg,262144,1)));
stdev24(1,2)=std(nonzeros(reshape(cr,262144,1)));

%upconvert and output images
imwrite(uint16(cg*16),'bgWW8g.tif');
imwrite(uint16(cr*16),'bgWW8r.tif');

%Calibration Analysis for WW8 Imaging Settings
%for Leica Confocal Images 512x512 12-bit
%WWImage Settings
%ww Image Settings => PMT2=X, PMT3 = X
%input = images
%output = averages & standard deviations of different pH calibration solns
%         averaged ratiometric images

%set zeros
cg=double(zeros(512,512));            %holder for green,
bg=double(zeros(512,512));            %background for green
cr=double(zeros(512,512));            %holder for red
br=double(zeros(512,512));            %background for red
c=double(zeros(512,512));             %intermediate result file
CavgWW8=double(zeros(1,19));          %average
CstdevWW8=double(zeros(1,19));        %stdev over average image
Cmax=double(zeros(1,19));     %max of each ratio image
Cmin=double(zeros(1,19));     %min of each ratio image
j=0;k=0;a=0;ratio=0;          %index counters & various variables

%Read in filenames
filesg=[dir('*phlow*ch00*.tif'),dir('*ph01*ch00*.tif')...dir('*phhi*ch00*.tif')];
%green files from ch00
filesr=[dir('*phlow*ch01*.tif'),dir('*ph01*ch01*.tif')...dir('*phhi*ch01*.tif')];
%red files from ch02
bg=double(imread('bgWW8g.tif'))/16; %read in background green
br=double(imread('bgWW8r.tif'))/16; %read in background red
```

```
%Read in images
       for a=1:19;
           j=20-a; j %show counter progress (adjust for # calib
points)
           cg=double(zeros(512,512)); %re-zero green before each image read sequence
           cr=double(zeros(512,512)); %re-zero red before each image read sequence
           c=double(zeros(512,512));
           for k=1:3
               c=double(imread(filesg(k,j).name)); % read in green images
               cg=cg+medfilt2(c)-br;        %add successive green images and
                                            %subtract avg background
               c=double(zeros(512,512));
               c=double(imread(filesr(k,j).name));
               cr=cr+medfilt2(c)-br;
               c=double(zeros(512,512));
           end
%Math on images
       cg=cg/3;       %divide by number of added images
       cr=cr/3;
       c=medfilt2(cg./cr); %determine pixel-wise ratio
       Cmax(1,j)=max(max(c)); Cmin(1,j)=min(min(c));
%Upconvert and export images
       ratio=Cmax(1,15)/64000; %upconversion ratio number calculated from max of
highest pH sample
       imwrite(uint16(c/ratio),sprintf('calWW8_ph%02d.tif',j)); %output calibration
images
       %Avg & Stdev
              c=c(isfinite(c));
              CavgWW8(1,j)=mean(reshape(c,numel(c),1)); %determine average value
                                                         across
                                                        %ratiometric image and add to
                                                        array
CstdevWW8(1,j)=std(reshape(c,numel(c),1)); %determine standard dev across rat.
                                           %image and add to array
end

%Volumetric Image Analysis for WW8 Imaging Settings
%for Leica Confocal Images 512x512 12-bit
%%ww Image Settings => PMT2=X, PMT3 = X
%input = images
%output = averages & standard deviations of different pH calibration solns
% averaged ratiometric images
%This file is for non-z-series data as it averages over all images (which
%are assumed to be coplanar)

%set zeros
cg=double(zeros(512,512));    %holder for green
bg=double(zeros(512,512));    %background for green
cr=double(zeros(512,512));    %holder for red
br=double(zeros(512,512));    %background for red
c=double(zeros(512,512));     %intermediate result file
j=0;k=0;a=0;ratio=0;          %index counters & variables

%Read in filenames
filesg = [dir('*ch00*.tif')];
%green files from ch00
filesr = [dir('*ch01*.tif')];
%red files from ch01
bg=double(imread('bgWW8g.tif'));
br=double(imread('bgWW8r.tif'));
threshold=median(median(br));
meansalt=double(zeros(numel(filesg),1));
bob = double(zeros(512,512));
avgg = double(zeros(numel(filesg),1));
avgr = double(zeros(numel(filesg),1));
ratio=X;                      %upconversion ratio number calculated
                              %from max of highest pH sample
%Generate pH scalebar
bob = double(zeros(512,10));
blank = bob;
       for i = 1:41
           for j=1:11
               bob((12*i+j),:) = (3.9+0.1*i);
           end
       end
```

```
%Read in images
    for a=1:numel(filesg);
        a %show counter progress
        cg=double(zeros(512,512)); %re-zero green before each image read sequence
        cr=double(zeros(512,512)); %re-zero red before each image read sequence
        c=double(zeros(512,512));
        c=double(imread(filesg(a).name));
        cg=medfilt2(c)-bg;            %add successive green images
                                      %and subtract avg background
        c=double(zeros(512,512));
        c=double(imread(filesr(a).name));
        cr=medfilt2(c)-br;            %add successive red images
                                      %and subtract avg background
        c=double(zeros(512,512));
        avgg(a,1)=mean(nonzeros(cg));
        avgr(a,1)=mean(nonzeros(cr));

        %Math on images
        for j=1:512
           for k=1:512
                g=cg(j,k);
                r=cr(j,k);
                b=((g/r-Fmin)/(Fmax-g/r));

                if (r > threshold) && (b>0)
                   % Analysis of green 1 channel vs red 1 channel gives:
                   %

                   c(j,k) = Slope*log(b) + Intercept;
                   %r
                else
                   c(j,k) = 0;
                   %k
                end
            end
        end

%Upconvert and export images including pH bar

        imwrite(uint16([bob,blank,c]/(ratio)),sprintf('WW%03d.tif',a));
end
```

```
%Time-resolved Image Analysis for WW8 Imaging Settings
%for Leica Confocal Images 512x512 12-bit
%WW8 Image Settings
%ww Image Settings => PMT2=X, PMT3 = X
%input = images
%output = averages & standard deviations of different pH calibration solns
%         averaged ratiometric images
%This file is for non-z-series data as it averages over all images (which
%are assumed to be coplanar)

%set zeros
cg=double(zeros(512,512));    %holder for green
bg=double(zeros(512,512));    %background for green
cr=double(zeros(512,512));    %holder for red
br=double(zeros(512,512));    %background for red
c=double(zeros(512,512));     %intermediate result file
j=0;k=0;a=0;ratio=0;          %index counters & variables
bob = double(zeros(512,10));
blank = bob;

%Read in filenames
filesg = [dir('*t00*ch00*.tif'), ... dir('*tfinal*ch00*.tif')];
%green files from ch00
filesr = [dir('*t00*ch01*.tif'), ... dir('*tfinal*ch01*.tif')];
%red files from ch01
bg=double(imread('bgWW8g.tif'));
br=double(imread('bgWW8r.tif'));
threshold=median(median(br))/5; %determine what background level to use
CmaxEC1=double(zeros(4,1));
CminEC1=double(zeros(4,1));

%Read in images
for j=1:numel(filesg(1,:));
   for a=1:numel(filesg(:,j));
        cg=double(zeros(512,512));
        cr=double(zeros(512,512));
        c=double(zeros(512,512));
        c=double(imread(filesg(a,j).name));
        cg=cg+medfilt2(c)-bg;
        c=double(zeros(512,512));
        c=double(imread(filesr(a,j).name));
        cr=cr+medfilt2(c)-br;
        c=double(zeros(512,512));
   end
%Math on images
        cg=cg/numel(filesg(:,j)); cr=cr/numel(filesg(:,j));
        for i=1:512
           for k=1:512
                g=cg(i,k);
                r=cr(i,k);
                b=((g/r-Fmin)/(Fmax-g/r));

                if (r > threshold/10) && (b>0)
                    % Analysis of green 1 channel vs red 1 channel gives:
                   c(i,k) = slope*log(b) + intercept;
                else
                   c(i,k) = 0;
                   %k
                end
           end
        end
         CmaxEC1(j)=max(max(c)); CminEC1(j)=min(min(c));
         %convert to pH

%Upconvert and export images
        ratio=X;
for l = 1:41
        for m=1:11
            bob((12*l+m),:) = (3.9+0.1*l);
        end
end
        imwrite(uint16([bob,blank,c]/(1.5*ratio)),sprintf('WWt%01d.tif',j));

%Avg & Stdev
        CmedianWW(j)=mean(nonzeros(c));
        stdevWW(j)=std(nonzeros(c));


end
```